Utrecht University

UNIS
The University Centre in Svalbard

MASTER'S THESIS

Reconstruction of the Late Glacial and Holocene deglacial history of Synndalen, Svalbard

Ymke Zoë LATHOUWERS

Department of Physical Geography
Utrecht University

In coorporation with:
Department of Arctic Geology
The University Centre in Svalbard

13 November 2022

Supervisors:

Dr. Wim HOEK
Department of Physical Geography, Faculty of Geosciences, Utrecht University

Dr. Mark FURZE
Department of Arctic Geology, The University Centre in Svalbard

Abstract

Due to their sensitivity to changes in climate and the imprints they leave behind in the landscape, glaciers are important for paleoclimate reconstructions. The distribution and ages of landforms in the modern landscape can provide understanding of patterns and processes of glaciation during the past. This study contributes to an enhanced understanding of Svalbard's deglaciation by investigating Synndalen, a deglaciated valley on Svalbard with two well constrained ice-marginal landforms. Here, the Late Glacial and Holocene deglacial history of Synndalen are reconstructed based on its geomorphological evolution. A detailed geomorphological map is presented based on in-field and remote geomorphological mapping and a spatiotemporal framework of glacial events is constructed based on absolute and relative dating methods. Radiocarbon ages of three marine bivalve molluscs are presented, ranging between 10251 and 10532 ^{14}C yrs BP, and have been calibrated to 11.3-11.7 cal. ka BP. These ages provide a minimum age constrain for the deglaciation of the Synndalen valley-mouth.

This study shows that Synndalen's deglaciation has been interrupted by two readvances. A minor retreat and advance cycle at the valley-mouth resulted in the formation of an end moraine and is considered to have been mainly dynamically driven. Very approximate age constraints constrain this advance to the Younger Dryas interstadial, although the importance of further research is emphasized. A readvance at the valley-head formed another moraine and adds to the increasing number of identified Early Holocene readvances on Svalbard.

As the climate on Svalbard during the Early Holocene was warmer than at present, reconstructions of cryospheric responses can serve as a potential analogue for future climate warming.

Acknowledgements

I never expected that finalizing this thesis would turn into one of the biggest challenges I have yet faced in my life, but I dare to say, even though it is quite a few months later than originally anticipated, I am relieved I finally made it to the point where I can write my acknowledgements to all the people that made it possible. I have been incredibly fortunate with the great number of people that contributed to different aspects of this thesis and therefore I would like to thank:

First and foremost, Mark Furze. For your enthusiasm after I first reached out to you, your perseverance when I was waiting for months for the borders to re-open, your guidance and supervision during my actual thesis and fieldwork and for your patience and thoughtfulness after Covid hit me hard and turned screens into my biggest enemy.

Wim Hoek, for believing in this project when all the restrictions made it seem unrealistic and for making clear that there was no pressure to finish this thesis when I physically couldn't.

My Synndalen sherpa's, Marjolein, Tomi and Florina, because I'm aware that without you it would all not have been possible. I know I exhausted you (and myself), but I will forever be grateful for your help, strength, dried food and of course party pills. Marjolein, I'm sorry I made you carry useless rocks!

Logistics, for the support when I was chaotically organizing my fieldwork last minute. In particular Audun Tholfsen, Charlotte Sandmo and Piera Guttorm, for the drop off and especially the pick up when conditions weren't easy. Sara Mollie Cohen, for helping me organise GPR fieldwork, even though I had to cancel to go down to Tromsø instead.

Lena Rubensdotter, for helping me make sense of the mapping process. Our meetings definitely increased the quality of my map and I'm so appreciative for the time you took to help me, even during a weekend.

Henriette Linge, for your attempt to date my rocks. I'm sorry I made you deal with 'the worst samples you ever saw'. Joe Licciardi, for giving these rocks a second chance. I am very curious to what future results may bring.

Rafael Kenji Horota, for your help with Agisoft Metashape and Sketchfab. Sönke Szidat from the Laboratory for the Analysis of Radiocarbon with AMS of the University of Bern, for radiocarbon-dating my shells. Rabecca Thiessen, for sharing your great knowledge on rock glaciers. Matthew Ellis for the stereo-microscope work and Maria Jensen for providing his funding.

Amélie, for joining on the Ming-recovery-mission and Sebastian, for lending me the sledge hammer – it came in handy.

Joe, Marjolein, Ellie and Anna for your valuable comments on my manuscript. Lotte, for the LaTeX support. Sebastian for your invaluable, late-night, help with preparing my presentation. In my first month at UNIS some of you already mentioned that you don't write a thesis on your own, it's a group effort. You all proved just that, and I'm immensely grateful to have such a system of support around me.

The Department of Arctic Geology of the University Centre in Svalbard (UNIS), for the funding without which

this project would not have been possible.

The many people in Longyearbyen and at UNIS that make Svalbard as magical as it is. Especially to all my friends here, for making this place a home. The great adventures, scooter, ski and cabin trips, near-daily swims and office yoga sessions are what made this one and a half year unforgettable. I can't wait for another spring season with all of you!

My mum and multiple friends, who offered to write my thesis for me, to sit down next to me while I'd dictate, or to type out text I could write by hand. This wasn't the solution, but the offer meant a lot.

Last, but absolutely not least, to my family and friends at home, for the unconditional support, no matter the distance or circumstances.

Contents

List of Figures

List of Tables

1 Introduction

Climate change is one of the biggest problems of our times and more accurate predictions are critical for policy makers to mitigate and adapt to future impacts of climate change on society (IPCC, 2013). An increased understanding of past climate fluctuations can serve as an important tool to predict the impact and extent of a future warming climate. Due to their sensitivity to changes in climate and the imprints they leave behind in the field, glaciers and ice caps are important for paleoclimate reconstructions and understanding (Oerlemans, 2005). Geomorphological records of past glacial extents are informative proxies for unravelling the interactions of ice-bodies with climate and the causes for change in their extent and dynamics. Empirical constraints on past glaciations can serve as an analogue for future cryospheric responses. Moreover, they can serve as essential independent inputs in numerical paleoclimatic and glaciological models, or for testing and validating outputs (e.g. Golledge et al., 2008; Seguinot et al., 2018).

The Svalbard Archipelago, situated in the High Arctic, is an ideal location to study past and present interactions between climate and glacial activity due to its relatively easy access, the strong climatic gradient across the Archipelago, and the wide range of topographic features (Humlum, 2005). Svalbard is particularly sensitive to changes in climate and currently experiences the fastest warming on Earth, which is more than twice the Arctic average and about seven times the global average for the same time period (Nordli et al., 2020; IPCC, 2013). Since the Last Glacial Maximum (LGM; 24-20 kilo annum Before Present (ka BP)), Svalbard's glacial extent has fluctuated considerably and glaciers have responded to a varying combination of climatic and dynamic driving forces. The Late Glacial interstadial and the abrupt onset of the Holocene (11.7 ka BP) mark a rapid transition from the full glacial mode of the LGM to warmer interglacial conditions. As Svalbard's temperatures during the Early Holocene were up to 7° C warmer than at present, this period is considered a potential analogue for future climate warming (van der Bilt et al., 2016; Farnsworth et al., 2020). Despite extensive ice-mass loss, some glaciers are known to have readvanced during this period (Farnsworth et al., 2020; Larsen et al., 2018; Lønne, 2005), although uncertainties remain about the extent and driving forces of these readvances, emphasizing the need for further studies.

Conceptual landsystem models are a useful tool for the reconstruction of former glacier environments and glacial dynamics as they connect specific sediment and landform assemblages to certain processes and environments. When viewed on the scale of an entire valley, the character and distribution of geomorphological 'fingerprints' in the modern landscape can provide understanding of patterns and processes of glaciation over complete glacial cycles. To contribute to an enhanced understanding of Svalbard's deglaciation this study investigates Synndalen, a deglaciated valley system on Svalbard. Synndalen serves as an ideal study site due to the preservation of ice marginal landforms and is, due to its proximity to Longyearbyen, relatively accessible. The aim of this study is to unravel the geomorphological evolution of Synndalen to present a reconstruction of its Late Glacial and Holocene glacial history. In order to achieve this, Synndalen is investigated according to a holistic, multi-proxy approach that integrates geomorphological mapping with dating techniques as follows:

1. A geomorphological map of Synndalen is created to establish a robust geomorphological framework of the landscape's evolution. This map focuses on landforms delineating previous ice margins and is based

on field investigations of sediment-landform assemblages and remote sensing analysis. Remote sensing analysis is primarily based on photogrammetric processing of drone imagery.

2. A spatiotemporal framework of glacial events is constructed based on absolute and relative dating techniques. Shells have been radiocarbon dated and cosmogenic-nuclide dating results are anticipated.

3. A conceptual model of Synndalen's deglaciation is developed, presenting the relative order of events such as glacial retreat and advances, sea level fall and isostatic rebound within the reconstructed timeframe.

This thesis is organized in six chapters. Chapter two describes the setting of Svalbard in general, and Synndalen in particular and provides information on Svalbard's glacial history. In the third chapter, the methods applied during the fieldwork and data processing and analysis are described, and the fourth chapter presents the results. Here, the observations and interpretations on which the geomorphological map is based are discussed before presentation of the map. Chapter five discusses the presented results, establishes conceptual models and provides an outlook for further research, before a final conclusion is given in chapter six.

2 | Setting

2.1 Physical Geography of Svalbard

Svalbard is situated in the European High Arctic between 74° and 81°N and 10° and 35°E and is bordered by the Arctic Ocean to the north, the Barents Sea to the south and east and the northern North Atlantic to the west. It is located at the northern extension of the North Atlantic Current and the southward extension of the Arctic sea-ice front (Rogers et al., 2005) (Fig. 2.1). It is a highly glaciated, mountainous archipelago consisting of six large and many smaller islands, covering a total of 66,667 km^2. The largest island of the archipelago is Spitsbergen, which has a coastline dominated by large glacially eroded fjords. High-Arctic tundra vegetation prevails at lower elevations, while the mountains-tops, the highest being Newtontoppen (1713m), are bare (Dallmann, 2015).

The general elevation of Svalbard was caused by tectonic forces in connection with the evolution of the Arctic and North Atlantic oceans and the type and structure of the bedrock influenced the shape and morphological characteristics of the mountains. Its current surface morphology, however, was largely shaped by ice movement during the successive Pleistocene glaciations in combination with on-going Arctic weathering, creating large valleys, fjords and submarine troughs (Dallmann, 2015).

The archipelago is highly glaciated, with a total glacier coverage of ca. 57% of the land area in the late 2000s, by glaciers of various types (Nuth et al., 2013). Most dominant are the huge, continuous ice masses divided into individual ice streams by mountain ridges and nunatak areas, called the Spitsbergen glacier type by Ahlmann (1933). The glacier distribution over Svalbard is controlled by a combination of topography and climate. The most continuous ice cover is found on the relatively flat eastern islands and eastern Spitsbergen, due to the relatively colder temperatures and moisture input from the Barents Sea. In the alpine mountain regions of western Spitsbergen, small cirque and valley glaciers are numerous (Hagen et al., 1993). Glaciers in the central region of Spitsbergen are smaller, mainly because of low precipitation, and many inland glaciers would probably not exist without the significant redistribution of snow by wind during winter (Humlum, 2002). The equilibrium-line altitude (ELA) increases on a transect from South-Eastern Spitsbergen, where there is more precipitation, to its Central-Northern part, reflecting a more continental type of climate ((Hagen et al., 1993; Humlum, 2002).

In temperate regions, such as the European Alps, the base of a glacier generally lies at pressure melting point except for the seasonally cooled surface layer. These glaciers are so-called warm-based glaciers and can slide at their bed. On Svalbard, the majority of the glaciers are polythermal; their margins and parts of the ablation area are below the freezing point and are partly frozen to the ground, while the accumulation area and the deeper part of the ablation area are at the pressure melting point (Hagen et al., 1993; Irvine-Fynn et al., 2011). Furthermore, many of the smaller cirque and valley glaciers tend to be entirely cold-based because their entire mass is below the pressure melting point. These glaciers are frozen to their beds and do not have any basal movement, they flow only by internal creep deformation (Hagen et al., 1993).

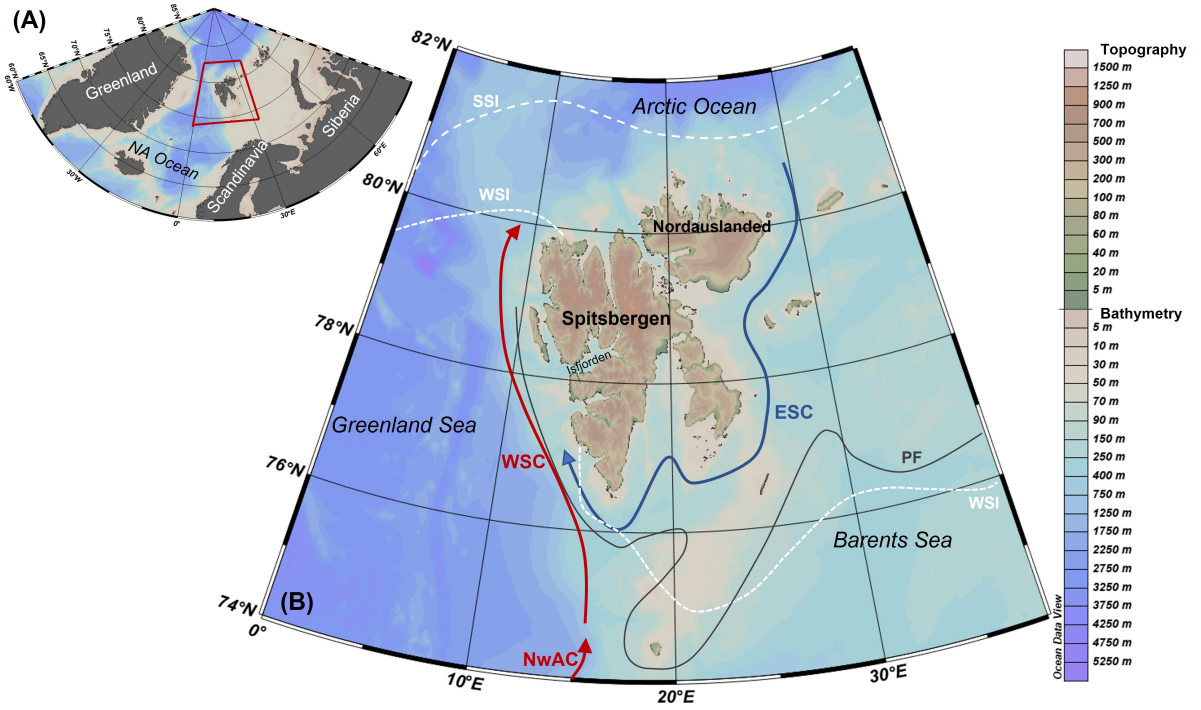

Figure 2.1: (A) Location map of the Svalbard Archipelago. (B) The Svalbard Archipelago, showing bathymetry, topography, general oceanographic circulation and sea-ice extent. Cold and warm currents denoted in blue and red arrows, respectively. NA Ocean: North Atlantic Ocean, WSC: West-Spitsbergen Current, NwAC: Norwegian Atlantic Current, ESC: Eastern Svalbard Current, PF: Polar Front, WSI: Winter Sea-Ice extent (average for 2000-2012 in March), SSI: Summer Sea-Ice extent (average for 2000-2012 in September). Base map created in Ocean Data View (Schlitzer, 2015). Oceanic currents after Ślubowska-Woldengen et al. (2007); polar front and sea-ice extent after Dallmann (2015).

Svalbard's glaciers are also well known for their surging behaviour. A surging glacier is distinguishable by its quasi-periodic oscillation of abnormally fast flow over a period of a few months to a few years, rapidly transferring mass down-glacier, followed by a period of slower flow rates during the quiescent phase, lasting tens to hundreds of years (Dallmann, 2015). During the quiescent periods, ice stagnates and builds up in the upper accumulation area, forming a reservoir of mass for the next surge (Sund, 2006). Surges occur on all types of polythermal or warm-based glaciers, from small inland ones to large calving tidewater glaciers. Estimates of the proportion of surge-type glaciers in Svalbard range from as low as 13% (Jiskoot et al., 1998) up to 90% (Lefauconnier and Hagen, 1991) of all glaciers.

The surface mass balance of glaciers has generally been negative since the beginning of the 20th century. This retreat has increased since the 1950s as a response to the sustained atmospheric warming. In the past few decades, glacier retreat has accelerated and the glacierized area over the entire archipelago has decreased by an average of 80 km^2 per year over the past ∼30 years, representing a reduction of 7% (Nuth et al., 2013; Hegerl et al., 2007).

The ice-free land areas of the archipelago are underlain by continuous permafrost to depths varying from about 100 m near sea level and under large riverbeds and up to 500 m thick in the higher mountains ((Humlum et al., 2003; Christiansen et al., 2010). Taliks, bodies of unfrozen ground, are found under most glaciers. Glacial and periglacial landforms related to permafrost are widespread and ground ice is present all over the archipelago in landforms such as rock glaciers, ice-cored moraines, pingos, buried glacial ice, ice wedges and patterned ground (Humlum et al., 2003). Due to solifluction and the melting of dead-ice, periglacial processes greatly alter landforms and surfaces over time (Schomacker and Kjær, 2008).

All Svalbard rivers are short-lived summer phenomena, but fluvial activity is important for transporting large amounts of sediments into the fjords. Especially during spring melt, but also during the rest of the summer,

large braided river systems, draining from glaciers, occur in most valleys. During autumn, the riverbeds dry up and wind erosion of fresh fine-grained sediments lead to deposition of eolian sediments downwind from the rivers, until winter snow cover is firmly established in October-November.

2.2 Current climate

Svalbard's climate is categorized as a 'High Arctic Maritime Snow Climate' (Eckerstorfer and Christiansen, 2011). Despite its High Arctic latitude, Svalbard currently experiences a relatively mild, wet and cloudy climate compared to other regions at the same latitude, for instance East Greenland. This difference is due to the major input of heat into the Arctic Ocean by the warm and saline West Spitsbergen Current (WSC), which flows along the western coast of Spitsbergen and is derived from a branch of the Norwegian Atlantic Current (NwAC), the northern end of the North Atlantic Current ((Aagaard et al., 1987; Ślubowska-Woldengen et al., 2007). Colder polar water from the Arctic Ocean, the East Svalbard Current (ESC), winds its way south past the east-coast of Svalbard, flowing around the southern and south-western coasts of Spitsbergen (Fig. 2.1). The meeting of the warmer WSC flowing along the continental shelf and the fresher and colder Arctic Water on the continental shelf in the ESC produces the Polar Front.

Precipitation on Svalbard falls predominantly in solid form (Eckerstorfer and Christiansen, 2011), with early summer being the driest and autumn the wettest seasons. The mean annual precipitation (1971-2000) measured at weather stations in Svalbard varied from 196 mm at Svalbard Airport to 581 mm in Barentsburg and is estimated to be around 720 mm on average for all Svalbard land areas (Hanssen-Bauer et al., 2019). Due to its location in the transit zone between cold Arctic air in the north and mild maritime air in the south, Svalbard can experience strong winds, leading to a high cyclonic activity, especially in winter. North-easterly winds are predominant, although local wind directions are dependent on topographic effects. The effect of wind is highly significant for redistributing snow all over Svalbard (Humlum, 2002).

Svalbard is considered to have a high climatic sensitivity. In recent decades, temperatures in the Arctic have increased at an amplified rate compared to the global mean, a process referred to as Arctic Amplification (IPCC, 2013; Humlum, 2005). It is currently warming at approximately 1.7°C per decade, which is more than double the Arctic average of 0.8°C per decade and about seven times the global average for the same period (Nordli et al., 2020).

2.3 Svalbard's climate and glacial history

There are two end-member modes of glacierization on Svalbard: a full glacial mode and an interglacial mode (Ingólfsson, 2011). During full glacial modes, Svalbard and the Barents Sea were extensively covered by a large marine-based ice sheet, the Svalbard Barents Sea Ice Sheet (SBSIS). The current glacial situation on Svalbard represents the interglacial mode, when the glacial system is dominated by highland ice fields, ice caps and numerous valley and cirque glaciers (Ingólfsson, 2011). During the Last Glacial Maximum (LGM), around 24-20 ka BP[1], Svalbard was in full glacial mode (Svendsen et al., 2004), and covered by the Late Weichselian SBSIS. Since then, throughout the late Pleistocene and the Holocene, glacial extent has fluctuated considerably, and glaciers have responded to a varying combination of climatic, environmental and dynamic driving factors. These Quaternary glaciations have left pronounced 'fingerprints' in the landscape, both in terrestrial and marine environments, which, in combination with geochronological data, such as radiocarbon,

[1]BP: calendar years Before Present. This refers to the standardized commencement date of the 'present' in January 1950, the time before nuclear weapons testing artificially drastically increased the proportion of carbon isotopes in the atmosphere, leading to unreliable carbon dating results. Furthermore, referring to a fixed year prevents ages to increase by one every year. Within this report, ka BP refers to calender (cal.) years. If radiocarbon ages are cited, this will be specified.

terrestrial cosmogenic nuclide and optically stimulated luminescence ages, have been used to reconstruct the glacial history of Svalbard.

2.3.1 Quaternary glaciations in the Cenozoic context

Although sea-ice cover existed in the central Arctic basin by the middle Miocene (13 Ma) (Krylov et al., 2008), ice-sheet build-up over the Svalbard and Barents Sea regions likely did not commence until the Pliocene-Pleistocene, 3.6-2.4 Ma (Knies et al., 2009). The first indications of large-scale glaciations in the northern Barents Sea are from about 2.7 Ma (Knies et al., 2002) , while repeated ice advances to the shelf break may have occurred since 1.6 – 1.3 Ma along the western Barents Sea and Svalbard margins (Solheim et al., 1998; Sejrup et al., 2005). The number of full-scale ice-sheet glaciations over the Svalbard-Barents Sea area is unknown, but the seismic structure of the north-western margin suggests at least sixteen glacial advances during the last ∼1 Ma (Solheim et al., 1996).

2.3.2 Late Pleistocene to Holocene transition

Towards the end of the Late Pleistocene, around 24-20 ka, the SBSIS reached its maximum extent, broadly coincident with the global Last Glacial Maximum (LGM). It appears to have maintained a size close to its peak for several thousand years (Hughes et al., 2016). Svalbard was entirely covered by ice, except for several nunataks on the west coast. The SBSIS reached the shelf edge, with fast flowing ice-streams draining the ice-sheet through fjords and cross-shelf troughs and less active ice covering the inter-fjord areas (Landvik et al., 2005, 2014; Ottesen et al., 2007). The continental-shelf edge posed a major limit on the ice sheet's growth towards the north and west, and expansion was only possible on the continued shelf towards the east and southeast (Hughes et al., 2016). At a 1000-year resolution, the rate of ice-sheet build-up (40-21 ka) was almost as fast as the rate of retreat (21-10 ka). Ice-marginal retreat initiated from the outer shelf around the western margin of Svalbard around 20.5 ka BP (Jessen et al., 2010) and was coincident with and followed by ice sheet thinning (Hormes et al., 2013). Deglaciation continued and the ice sheet retreated from the western shelf towards the fjord mouths and the present coastline (Jessen et al., 2010; Hormes et al., 2013). By 14 ka BP most of the Barents Sea was completely deglaciated, the former SBSIS was reduced to ice caps centered over Svalbard and Franz Josef Land (Hughes et al., 2016). During the Younger Dryas interstadial (12.7-11.5 ka BP), there does not appear to have been a net total ice-sheet growth. Ice still filled the inner parts of Isfjorden, Storfjorden and Wijdefjorden and it remains under debate whether there was a climatic cooling on the archipelago (Hormes et al., 2013; Gjermundsen et al., 2013). According to Salvigsen and Elgersma (1993) and Mangerud and Landvik (2007), the ice was close to the coast in southern Svalbard by 13 ka and by 12 ka, the outer fjords of Svalbard were ice free (Forman et al., 1996; Landvik et al., 2013), although Farnsworth et al. (2020) suggests that this extent of glacier cover during the transition from the Late Pleistocene to the Early Holocene is probably overestimated and that, while there is minimal evidence of ice loss between 12.0 - 11.7 ka BP, by 11.0 ka BP, most fjords were likely ice free.

The extensive deglaciation since the Last Glacial Maximum led to a pronounced glacio-isostatic rebound, visible as series of raised marine shorelines along Svalbard's present-day coastline. These raised beaches indicate previous shorelines that have subsequently been uplifted relative to current-day sea level. The elevation and age of these raised-beach deposits can serve as a critical field observation to determine the magnitude and distribution of past-glacier loads and the timing of deglaciation. The formation age of these raised shorelines can be constrained by determining the radiocarbon age of preserved shells, whale bones and/or driftwood found on or within them. When combining age and altitude, relative sea level curves quantifying the postglacial uplift rates through time can be established (Forman et al., 2004) (Fig. 2.2). These relative sea level curves depict that the greatest uplift rates occurred during the Late Pleistocene and the Early Holocene (Forman

et al., 2004; Farnsworth et al., 2020). The great variability in uplift observed over Svalbard can be explained by spatially differential ice-cover thickness, duration and timing of deglaciation (Fjeldskaar et al., 2018).

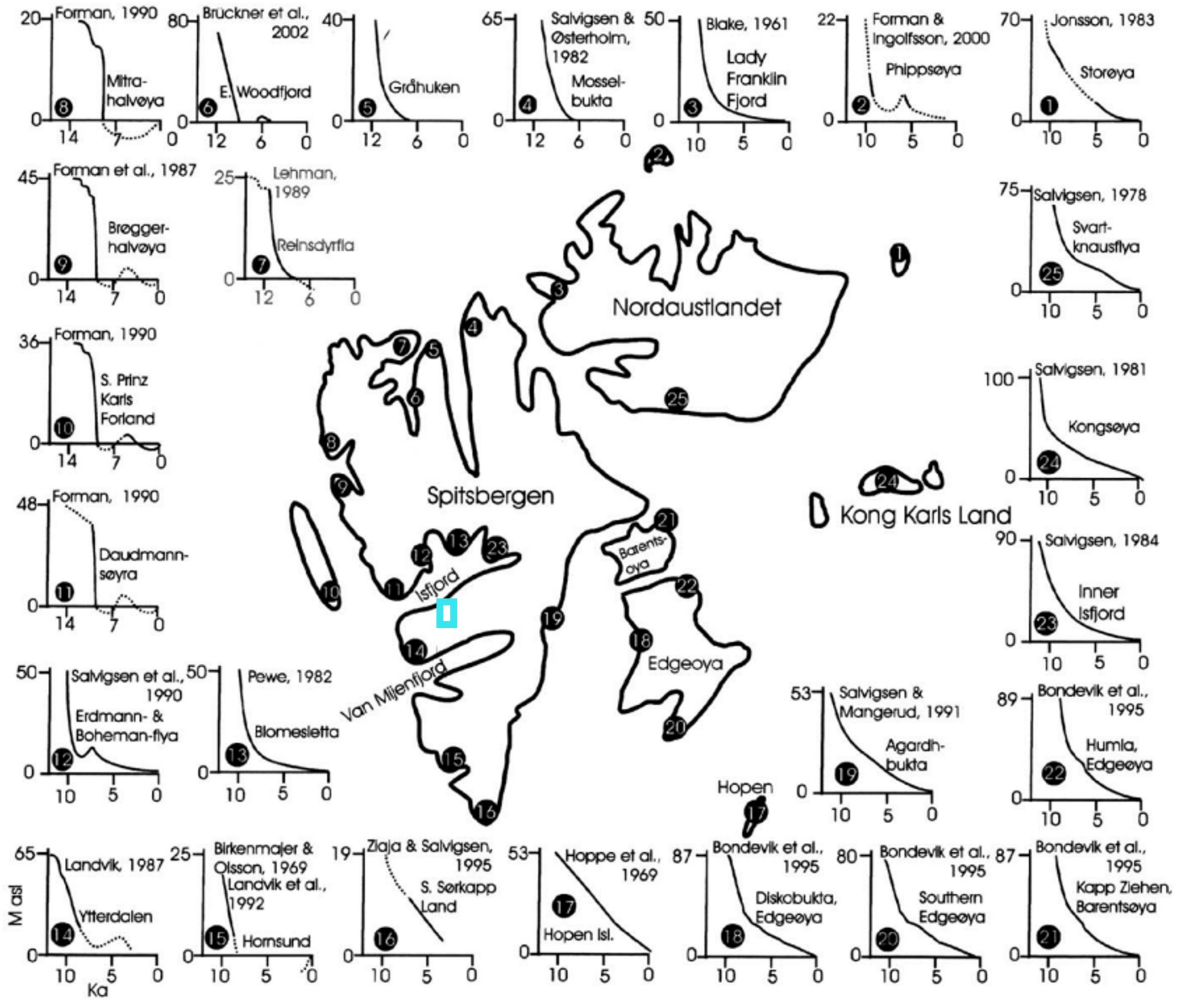

Fig. 2. Majority of post-glacial emergence curves for Svalbard, Norway (modified from Forman, 1990).

Figure 2.2: Relative sea level curves from Svalbard. Blue box marks the approximate location of Synndalen. Modified from Forman (1990) and Forman et al. (2004).

2.3.3 Early Holocene (11.7 - 8.2 ka BP)

Climate

Throughout the Early Holocene, Svalbard experienced summer temperatures both warmer and colder than today. Dating of thermophilous molluscan species (e.g. *Mytilus edulis*) indicate that the temperature along the west coast of Svalbard had reached the present-day[2] values around 11 ka BP (Mangerud and Landvik, 2007). A peak in summer insolation culminated between 9.7 and 7.5 ka BP (Laskar et al., 2004). As a result of early inflow of warm Atlantic Water prior to 11 ka BP, and the strong influence of sea surface temperatures on terrestrial temperatures, the peak in Holocene terrestrial summer temperature is observed earlier, at around 10 ka BP. Around 10.6 ka BP, *Mytilus edulis* had reached the north coast of Svalbard, suggesting summer temperatures there were about 2°C warmer than at present. From around 10.5 ka BP, Temperatures up to 7°C warmer than at present were found by van der Bilt et al. (2016), in their study on temperature reconstructions

[2]All comparisons in this study to present-day climate or temperatures refer to the old 1960-1990 climate-normal, used by the Norwegian Meteorological Institute until the end of 2020 (MeteorologiskInstitutt, 2020)

based on alkenones (U^{K}_{37}) extracted from lake sediments. Extensive studies of a marine core collected on the continental slope west of Isfjorden furthermore show that Atlantic Water along west Spitsbergen was warmer than at present from 10.8 to 8.8 ka BP (Ebbesen et al., 2007; Hald et al., 2004).

Shorter cooling intervals interrupted the warming trend during the early stages of the Holocene. These periods of declined temperatures are related to one or several factors such as internal feedback mechanisms in the Earth's climate system, increased explosive volcanism, changes in solar activity and sudden fresh-water outburst during the deglaciation of the Fennoscandian, Laurentide and Greenland ice sheets (Nesje et al., 2004, 2005; Rohling and Pälike, 2005). *Mytilus edulis* seems to have disappeared from eastern Svalbard around 9 ka BP, suggesting climatic cooling at this time (Mangerud and Svendsen, 2018), which has also been recorded in lake records (van der Bilt et al., 2016). A significant short-lived cold temperature anomaly occurred around 8.2 ka BP, known as the 8.2 ka event (Hald and Korsun, 2008). The sudden decrease in global temperatures is attributed to a large meltwater pulse into the North Atlantic Ocean from the final collapse of the Laurentide Ice Sheet and a slowdown of North Atlantic Deep-Water formation (Rohling and Pälike, 2005).

Glacial history

Glaciers on Svalbard underwent further extensive ice-mass-loss during the Early Holocene and deglaciation is observed across marine, terrestrial and lacustrine records (Farnsworth et al., 2020). Ice retreated initially through fjords, subsequently fjord-valleys and terrestrial realms (Ingólfsson and Landvik, 2013). Fjords, lake basins and shorelines become ice-free, allowing for the deposition of datable material. Marine sediment cores from fjords in northern and western Svalbard show high but diminishing sedimentation rates, including ice-rafted-debris (IRD) from retreating marine ice margins (Forwick and Vorren, 2009; Allaart et al., 2020). From 10.1 ka, IRD became nearly absent in marine cores from Svalbard's western margin, which has been interpreted as the onset of the Holocene Thermal Maximum (Jessen et al., 2010), when the Svalbard archipelago reached glacier coverage similar to or even less than today (Hormes et al., 2013). Records show that most marine-terminating glaciers retreated onto land, while cirque glaciers greatly diminished in size and in some cases disappeared completely (Svendsen and Mangerud, 1997; Forwick and Vorren, 2009). Most tidewater glacier margins were located well inside of their late Holocene extents (Blake Jr, 1989; Farnsworth et al., 2020).

Nevertheless, glacier activity during the Early Holocene is complex. Despite progressive deglaciation, evidence from glaciers of varying size found across the archipelago suggests asynchronous ice margin readvance(s) (Mangerud et al., 1992; Forwick and Vorren, 2010; Farnsworth et al., 2017). For example, at least six Late Glacial and Early-Holocene readvances have been identified at the west coast of Spitsbergen and the highest frequency of Early Holocene glacier readvances occurred between 11-10 ka BP (Farnsworth et al., 2020). Often, the ice margin extent of these readvances is several kilometres distal to Late Holocene glacier maxima, although the exact magnitudes of most readvances are unknown (Farnsworth et al., 2018). The earliest readvances have been identified near the mouths of the fjords, while younger Early Holocene readvances are found in the inner tributaries and heads of fjord systems (Larsen et al., 2018).

2.3.4 Middle Holocene (8.2 - 4.2 ka BP)

Climate

The temperatures during the Middle Holocene are considered to have been slightly warmer than present, but had cooled down since the Early Holocene. Around 8.2 ka BP warm Atlantic Water is thought to have extended around almost the entire Svalbard Achipelago (Mangerud and Svendsen, 2017). The persistence of *Mytilus* suggests that ocean temperatures were c. 4°C warmer than present between 8.0 - 6.5 ka BP. From 6.2 ka BP onwards a gradual cooling started. As the flow of Atlantic waters progressively decreased, surface and

subsurface sea temperatures cooled down and around 5 ka BP the climate was close to the present climate. From then on, the climate has been colder than the present until a warmer interlude in the medieval age around 0.9 ka BP (AD 1050) (Mangerud and Svendsen, 2017).

Glacial history

Based on glacial lake sediment records, it is assumed that Svalbard glaciers and ice caps retreated back to their Holocene minimum during the beginning of the Middle Holocene (Farnsworth et al., 2020; Mangerud and Landvik, 2007). Despite the survival of some tide-water glaciers fed by bigger ice caps, it is assumed that most glaciers disappeared from the archipelago (Hald et al., 2004). A modeling study based on Holocene relative sea level concludes that some Svalbard glaciers survived the Holocene Thermal Maximum and suggests that Nordaustlandet and eastern Spitsbergen were the main regions where ice remained throughout the Middle Holocene (Fjeldskaar et al., 2018). As these regions are also at present characterized by a cooler climate, this suggests a strong E-W temperature gradient across Spitsbergen, similar to modern conditions, existed through the Holocene (Forwick and Vorren, 2009).

As modern ice covers any geomorphological evidence associated to this Holocene Glacial Minimum (HGM), such as landforms (e.g. end moraines) and sediment, no exact spatial constraints exist on any Svalbard ice margins, stand-stills or readvances during the Middle Holocene (Farnsworth et al., 2020). Hence, it remains difficult to determine the Holocene minimum ice extent, or to prove its absence. Presumably however, the Holocene glacial minimum occurred in the Middle Holocene, sometime between 8.0 - 6.0 ka BP (Farnsworth et al., 2020).

2.3.5 Late Holocene (4.2 ka BP - Present day)

Climate

From about 4 ka BP, cooling intensified due to the combination of decreasing summer insolation (Berger and Loutre, 1991; Laskar et al., 2004) and the progressive cooling of regional waters (Svendsen and Mangerud, 1997; Rasmussen and Thomsen, 2014). This long-lived cooling trend during the Late Holocene led to an extensive period of glacier growth, which is referred to as the Neoglacial period (Bradley and Bakke, 2019). The coldest oceanographic conditions around Svalbard during the Holocene are assumed to have occurred during the period from 4.0 - 2.0 ka BP (Rasmussen et al., 2012). Between 950 and 700 BP (1000 and 1250 Anno Domini (AD)), the warmest period of the Late Holocene (excluding the present) took place, referred to as the Medieval Climate Anomaly (MCA). The re-occurrence of *Mytilus edulis* at 0.9 ka BP coincides with the MCA and may suggest warm Atlantic waters were more widespread around Svalbard (Mangerud and Svendsen, 2018). Following the MWP, a late phase in the Neoglacial cooling occurred during the Little Ice Age (LIA). The LIA is believed to have been brought about by the coincidence of gradually decreasing summer insolation driven by orbital forcing, with unusually low solar activity and a high number of major volcanic events (Wanner et al., 2008). Furthermore, analysis of a deep-sea core in the South Iceland Basin suggests a reduced deep-water flow (Bianchi and McCave, 1999). The warming observed at the very beginning of Svalbard's historical temperature record (Førland et al., 2011; Nordli et al., 2014) indicates that the LIA on Svalbard ended around 1900 AD.

Glacial history

Svalbard glaciers readvanced throughout the Late Holocene, during the Neoglacial and the LIA (Furrer et al., 1991; Svendsen and Mangerud, 1997; Humlum, 2005; van der Bilt et al., 2016; Philipps et al., 2017), often as the result of surge events (Schomacker and Kjær, 2008). Enhanced glacial activity is interpreted from increasing sedimentation rate and IRD flux in regional waters (Rasmussen and Thomsen, 2014; Bartels et al., 2018) and from lacustrine sedimentary archives (Svendsen and Mangerud, 1997; Røthe et al., 2015; van der

Bilt et al., 2016). Prominent terminal moraines are often observed in front of present day glaciers (Svendsen and Mangerud, 1997), constraining the glacier forefields that are exposed since the retreat after the LIA. It has long been the consensus that the end of the LIA coincides with the (Late) Holocene glacial maximum (Svendsen and Mangerud, 1997; Snyder et al., 2000), however, this theory is increasingly being challenged, as evidences of earlier advances are being identified outside of the LIA moraines in some glacier forefields. Studies based on inter alia radiocarbon dates (Dzierzek et al., 1990; Humlum, 2005; Lovell et al., 2018), lichenometry (Werner, 1993) and cosmogenic exposure dating of moraine ridges (Reusche et al., 2014; Philipps et al., 2017) imply that there have been numerous phases of glacial readvances during the Late Holocene and conclude that the LIA is not the largest glacial event in most locations. Since the end of the LIA, glaciers have retreated, coinciding with the increase in global atmospheric temperatures since the middle of the 19th century, although glacier retreat on Svalbard is often punctuated by short-lived surge events (Farnsworth et al., 2016, 2017).

2.4 Study area

The land area in between the two largest fjords of the archipelago, Isfjorden and van Mijenfjorden, is called Nordenskiöld Land, located at about 78°N (Institute, 2014) and named after Finnish-Swedish explorer and geologist Nils Adolf Erik Nordenskiöld. As opposed to alpine mountains in other regions of Svalbard, the mountains on Nordenskiöld Land are characterised by large plateaus. This study investigates Synndalen, a deglaciated valley situated on Nordenskiöld Land (Fig. 2.3). Synndalen is roughly orientated north-south and has a total length of approximately 6.5km. The valley drains as a tributary valley to the large valley Colesdalen in the north and the smaller Istjørndalen in the south, breaching the watersheds between Isfjorden (via Colesdalen) and Van Mijenfjorden (via Istjørndalen and Semmeldalen). At the valley head, there is a non-glacially fed lake, Istjørna, draining into Istjørndalen. Istjørna is oval-shaped, located at 235 m above sea level (a.s.l.), has a maximum depth of 29 m, a lake area of 0.37 km^2 and an catchment area of 1.76 km^2 (Holmgren et al., 2010).

Due to the low amount of precipitation in Central Spitsbergen (191 mm per year at Svalbard Airport, Førland et al. (2011)), Nordenskiöld Land is less extensively glaciated than other areas of the Svalbard Archipelago (Humlum, 2002). Glaciers are less frequent and smaller, but nevertheless many relatively small cirque, valley and alpine glaciers are found in the area. One of them is located at the western limit of Istjørndalen, the glacier Passfjellbreen. Passfjellbreen currently drains into Istjørndalen and Hollendardalen.

Aside from the characteristic glacial U-shape, the Synndalen area in general shows few traces of glaciation, with only a sparse till cover. Extensive postglacial colluvium, such as talus and rock glaciers, occupies the valley sides. Vegetation in the area is scarce, in part due to pronounced solifluction, and has a typical high-arctic tundra nature. Areas with continuous plant cover, consisting mainly of mosses, grasses and lichens, are restricted to valleys and other sheltered places. The mountains are generally bare, except for small patches of lichens, mosses, and some vascular plants (Holmgren et al., 2010).

Only one previously published study is available for Synndalen, focussing on lake sediments from Istjørna by means of a 34.5 cm long core (Holmgren et al., 2010). As this study focuses on the 20^{th} century Holocene-Anthropocene transition, it is not of relevance for the current study.

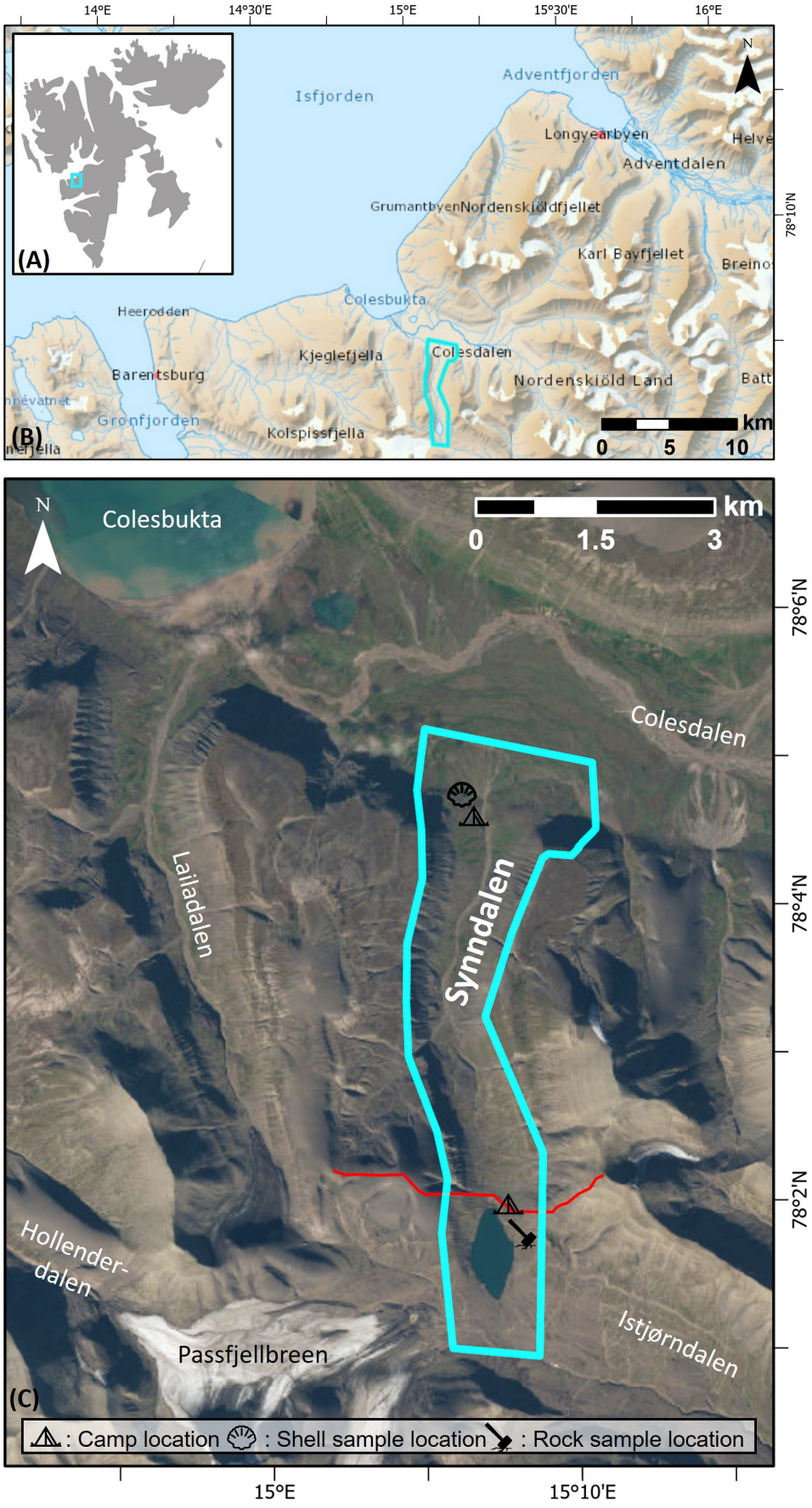

Figure 2.3: Location of the study area, Synndalen within; (A) the Svalbard archipelago and (B) the Isfjorden fjord system. Basemap: NPI (2014). (C) The study area Synndalen and its surroundings. Blue polygon: delineation of the presented geomorphological map. Red line: watershed boundary between the Synndalen and Istjørndalen catchments (see section 3.2.3). Basemap: NPI (2020).

2.4.1 Bedrock geology

The Synndalen catchment is part of the Svalbard Central Basin (SCB), a broad NNW - SSE-trending syncline that covers a great part of the area south of Isfjorden, and formed during the Early Paleocene along the strike-slip boundary between the Greenland and Eurasian plates (Müller and Spielhagen, 1990). The near horizontal Paleogene succession consists of alternating sandstone and shale formations that all belong to the Van Mijenfjorden Group (Major and Nagy, 1972). Up to approximately 450m a.s.l., the bedrock in Synndalen belongs to the Grumantbyen and Hollenderdalen Formations (Fig. 2.4), previously referred to together as the Sarkofagen Formation ((Major and Nagy, 1972; Müller and Spielhagen, 1990)). The Grumantbyen Formation mainly consists of silt or fine-grained, matrix-rich sandstones, most probably deposited in a lower shoreface environment. The Hollenderdalen Formation consists of a sequence of shales, overlain by alternating fine- to medium-grained sandstones, siltstones and subordinate shales, reflecting a prograding, wave-dominated delta system with tidal influences in shallow, protected parts (Müller and Spielhagen, 1990). Around 400-450m a.s.l., the transition to the Gilsonryggen Formation, also referred to as the Frysjaodden Formation, is observed as a sharp lithological transition from silt/sandstones to a rather monotonous sequence of black and dark-grey shales, which do not contain coarse-grained material in the lower part, indicating a rapid transgression. Upwards towards the boundary of the overlying Battfjellet Formation, the content of silt and fine-grained sand increases, mainly deposited in an offshore or lower shoreface environment (Müller and Spielhagen, 1990) (Fig. 2.4).

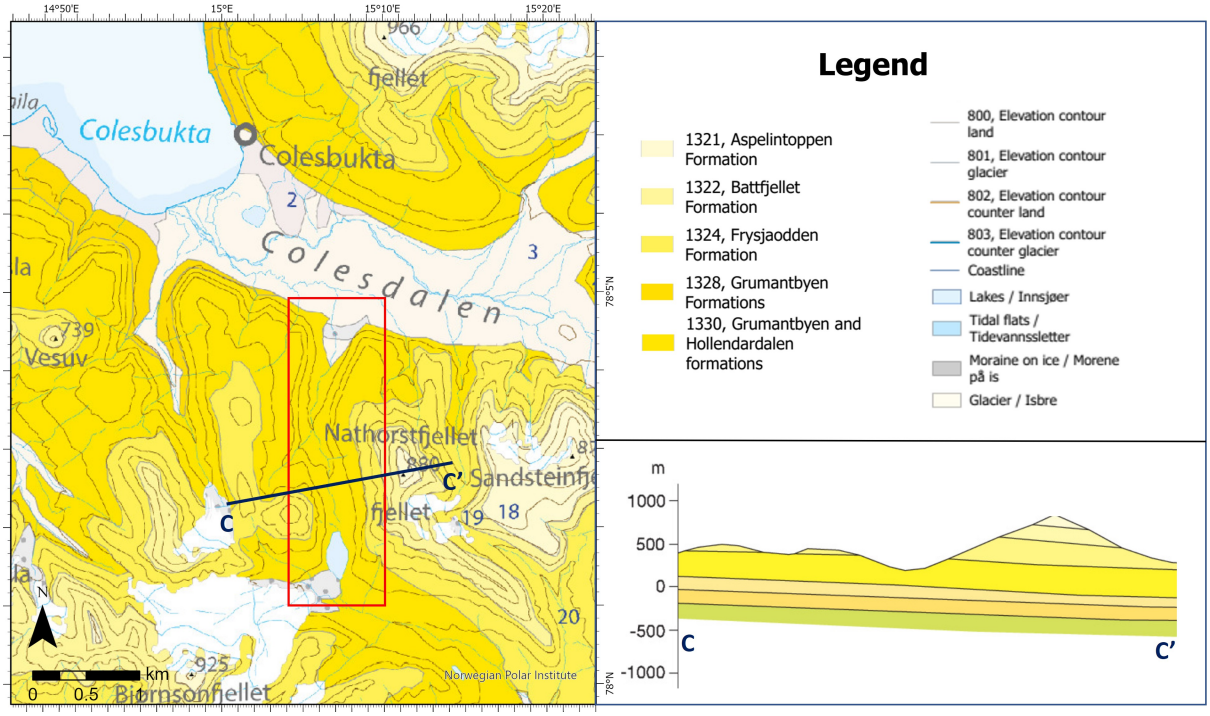

Figure 2.4: (A) Geologic map of the field area. Blue C - C' line marks location of the depicted cross-section. Red square marks Synndalen field area. Legend shows youngest to oldest bedrock Formations. Map and cross-section from Major et al. (2020), NPI.

3 | Methodology

This chapter provides a description of the various methods used for this study. Fieldwork methods are described in section 3.1 and the methodology for photogrammetry, remote sensing and the mapping process in section 3.2. Sections 3.3 and 3.4 describe the dating techniques, whereas sections 3.5 presents the work on a lacustrine core and section 3.6 the data archiving.

3.1 Fieldwork

Fieldwork was carried out in Synndalen from July the 22nd to the 29th, 2021. A field log is presented in Appendix A. The field party consisted of five persons. The first two nights were spend in 'Camp 1', located at the valley mouth of Synndalen, the subsequent three nights in 'Camp 2' at the north side of lake Istjørna and the last two nights back in Camp 1. Camp locations are marked on Fig. 2.3. The goals of the fieldwork were threefold:

1. To obtain aerial imagery using a drone, for later photogrammetric analysis.
2. To conduct in-field geomorphological mapping of landforms.
3. To collect samples for absolute dating of landforms, namely shells for radiocarbon age determinations and rock samples for cosmogenic nuclide dating.

3.1.1 Drone imagery acquisition

A DJI Mavic 2 Pro drone was used to obtain aerial imagery of the valley. To assure that sufficient and evenly spaced pictures were acquired, predefined flight-plans were used. The drone settings were kept constant throughout the droning campaign, with a forward speed of 10 m/s, a resolution of 6.33 cm/pixel, a side overlap of 60%, a frontal overlap of 80% and a margin of 50m.

Due to battery constraints, it turned out to be impossible to fly the drone over the entire surface area of Synndalen. Therefore, areas that were considered most important were given priority. As a result, no drone imagery of the central area of Synndalen was obtained.

3.1.2 In-field geomorphological mapping

Field mapping was carried out to identify different geomorphological landforms and sedimentary deposits throughout the valley. To achieve this, landforms were described, documented and photographed, with special emphasis on geometry, distribution, ground cover and internal structures. Sediment types were described,

focusing on grainsize, roundness and lithology. If sediment characteristics were unclear at the surface, shovels were used to dig out sections to assess internal structures. A handheld Garmin GPS 64s, with an accuracy of 15 m 95% of the time, was used to save the coordinates of points of interest.

3.1.3 Sampling

3.1.3.1 Shells for radiocarbon age determination

In a sedimentary deposit near Camp 1, shells and shell fragments were found and subsequently sampled, to be used for radiocarbon age determination. Besides shells from the riverbed, special attention was paid to sample the shell fragments found highest in the stratigraphy (Fig. 3.1). In total, 5 samples were collected, two intact shells and three shell fragments (Appendix B).

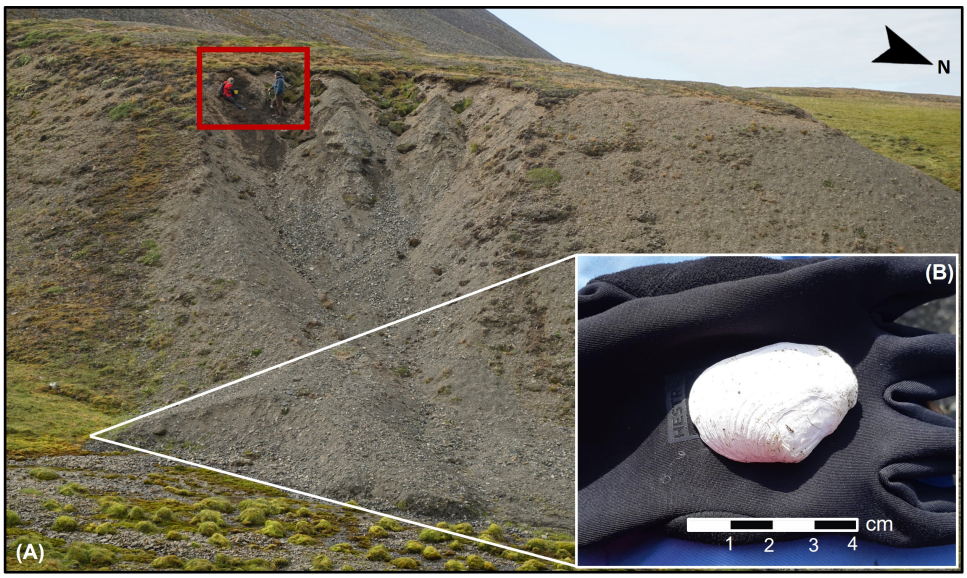

Figure 3.1: (A) Sample location for the five shell samples, location marked on Fig. 2.3. Field team on picture (within red square) marks location in the stratigraphy where the shell fragments were collected. White lines mark the location within the riverbed where the intact shells were collected. (B) Shell sample Synn-1-S2. Pictures by Florina Schalamon

3.1.3.2 Rocks for Beryllium dating

From both a landform next to Camp 2 and one halfway up the valley (locations marked on Fig. 2.3), rock samples have been collected with the aim to perform Beryllium dating on them, to constrain the ages of these landforms. Beryllium dating is a form of cosmogenic nuclide dating and involves the measurement of ^{10}Be isotopes, which build-up in rock minerals predictably over time when rocks are exposed to sunlight, due to bombardment of the upper few metres of the earth's surface by cosmic rays (Darvill, 2013). These rock samples were collected from the biggest boulders that were found on these landforms that were laying in a stable position, meaning away from slopes and showing as little sign of solifluction as possible. The samples were collected from flat areas on top of these boulders on locations where physical weathering visually seemed least extensive. Due to material problems with the rock saw, the samples were collected with hammer and chisel. Physical characteristics of the boulders were measured, described, sketched and photographed. The strike and dip of the sample was measured with a geological compass. This compass was further used to record the topographic shielding of the boulders, by recording the angular elevation of the horizon at regular intervals of 30° for a full 360°. In total, 3 samples were collected from the landform next to Camp 2, from 3

different boulders, and 4 samples from the location halfway up the valley, from 3 different boulders (Appendix B).

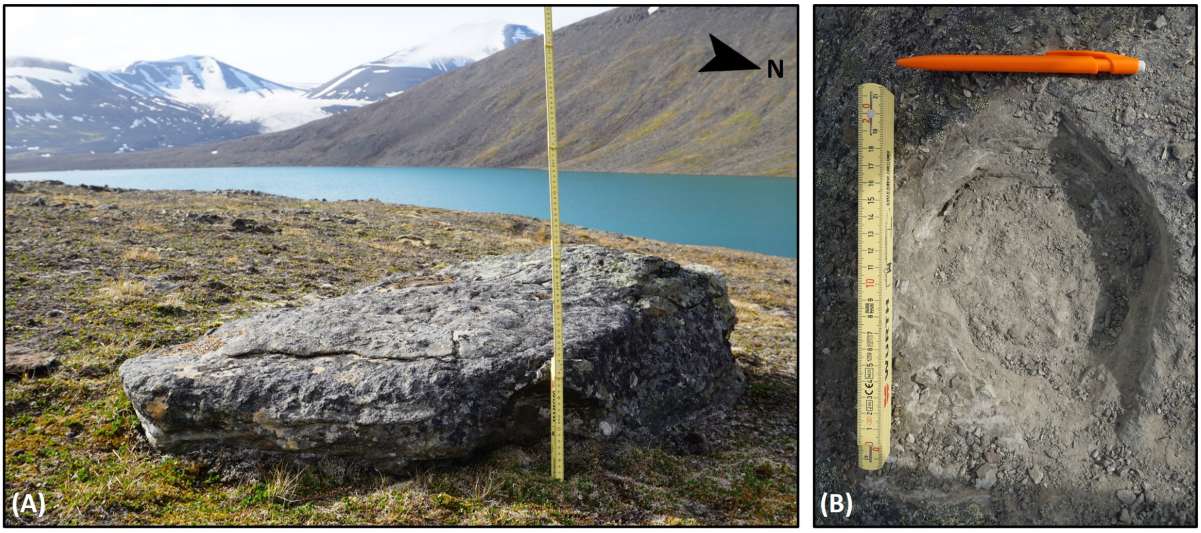

Figure 3.2: (A) One of the boulders sampled near Camp 2 (Synn-2-R2). (B) Imprint of taken rock sample in boulder (Synn-2-R3).

3.2 Remote geomorphological mapping

3.2.1 Photogrammetry

The aerial photos obtained with the droning campaign were used to create orthophotos and Digital Elevation Models (DEMs) of both the area around Camp 1 and Camp 2. An orthophoto is an aerial photograph that has been geometrically corrected for distortions caused by terrain relief and camera tilts such that the scale of the photograph is uniform and utilised in the same manner as a map (Thrower and Jensen, 1976). DEMs are raster-based models of topography that record absolute elevation, with each grid cell in a DEM representing the average height for the area it covers (Smith et al., 2006). To produce the orthophotos and DEMs, the survey was processed in Agisoft Metashape 1.8.4., a stand-alone software product that performs photogrammetric processing of digital images and generates 3D spatial data to be used in GIS applications. First, all the photos were added to Agisoft and aligned to build a dense cloud, with an alignment quality of 'high' (full resolution) and a dense cloud quality of 'ultra high' (full resolution). This Dense Cloud was subsequently used to create the DEMs and orthomosaics, which were then exported, saved and imported in ArcGIS Pro (Fig. 4.1). Small errors associated with model acquisition and processing should have been so minute as to not affect geomorphological interpretations based on the orthophotos and DEM and are therefore regarded as insignificant.

3.2.2 3D-models

Two 3D-models, one from the area around Camp 1 and one from Camp 2, were produced in Sketchfab. Sketchfab is an online platform to form, publish and share 3D models. For this purpose, a mesh-file was created in Agisoft Metashape. As a model could only be maximum 100 MB in size, the mesh file was reduced to 700K, with a texture size/count of 4096x4.

3.2.3 Analysis in ArcGIS Pro

ESRI's ArcGIS Pro 2.8.2 software was used for further analysis of landforms and for the creation of the geomorphological map. All geographical data presented are projected to the WGS84 datum, UTM zone 33N coordinate system. The mapping process was based on a variety of different maps (Table 3.1, both produced during the by photogrammetry, or available online. Based on these maps, different further analysis have been performed in ArcGIS Pro, which are discussed below.

The imported DEMs were used to create hillshade maps. To further aid remote landform identification, hillshade maps with a vertical exaggeration of five times were also produced. The ArcticDEM, courtesy of the Polar Geospatial Center (Porter et al., 2018), was used to generate a contour line map with an isoline interval of 20 m, by means of the contour raster function. This contour map served as the base layer for the produced geomorphological map. Slope maps were produced with the spatial analyst slope tool and the average slope of specific areas was acquired by the 'Zonal Statistics as Table' Spatial Analyst function. The profile tool was used to create elevation profiles, which were subsequently plotted as a profile graph chart. To obtain a better understanding of current-day flow behaviour in the valley, and to aid with delineation of the valley boundaries, watersheds were delineated from the ArcticDEM using the Hydrology toolset from the Spatial Analyst toolbox. To acquire this watershed model, consecutively a fill map, a flow direction map, and a flow accumulation map were created. After assigning a pour point; an outlet point where all the water flows out of the area, the Watershed tool was run to create a raster of the different watersheds, which was subsequently converted into a polygon. The border between the Istjørna and Synndalen watersheds is depicted on Fig. 2.3.

Table 3.1: List of maps used for geomorphological mapping of Synndalen

Type of map	Map Name	Year	Reference
Orthophotos Synndalen	Ortho_Camp1	2021	this study
	Ortho_Camp2	2021	this study
DEMs Synndalen	DEM_Camp1	2021	this study
	DEM_Camp2	2021	this study
Svalbard Topography	NP_Basiskart_Svalbard_WMTS_25833	2014	NPI (2014)
Svalbard Satellite Imagery	NP_Satellitt_Svalbard_WMTS_25833	2020	NPI (2020)
Orthophoto Svalbard	NP_Ortofoto_Svalbard_WMTS_25833		NPI (2011)
	Layer: GSD20_NordenskioeldLandVest_2011.tif	2011	
Raster map	S100_Svalbard_Raster_10m	1990	NPI (1990)
ArcticDEM	ArcticDEM	2018	Porter et al. (2018)
Geologic map	Temadata/G_Geologi_Svalbard_S250_S750	2000	Major et al. (2020)

3.2.4 Mapping in ArcGIS Pro

The geomorphological map was produced based on the analysis of the produced orthophotos and DEMs, satellite imagery, the 3D-models, field observations, pictures, the different available maps (Table 3.1) and the descibed further analysis in ArcGIS Pro. Mapping was performed at a scale of approximately 1:1000 and the final scale of the presented map is 1:30,000. To facilitate a more detailed overview, this map is further split up in two, and a close-up map of the northern and southern part are presented separately, at a scale of 1:15,000.

During the mapping process, polygons were created by drawing lines around interpreted landforms or sediment units. Within these polygons, a code point was added to refer to the code chart of the SOSI-standard layerfile. SOSI, a Norwegian acronym for 'Coordinated Approach for Geospatial Information', is the standard for exchanging geospatial data in Norwegian government institutions (Bergstrøm et al., 2001). Subsequently, the 'feature to polygon' tool was used to create a polygon file. The symbology of this polygon file was changed

to the SOSI layerfile to colour the polygons according to the SOSI-standard.

3.3 Radiocarbon age determination

To obtain absolute age controls, the retrieved shells have been dated by determining their radiocarbon age. Radiocarbon age determination is a widely used dating method of organic material and one of the most common methods for dating Quaternary landforms and deposits. Below, the principles of radiocarbon age determination, the assumptions on which they are based and the different error sources are discussed further.

3.3.1 Formation of ^{14}C

The natural carbon present in the Earth's atmosphere is composed of three naturally occurring isotopes, the two stable isotopes, ^{12}C (98.9%) and ^{13}C (1.1%), and traces of the unstable and radioactive ^{14}C (c. 1ppm) (Bowman, 1990). ^{14}C is continually being formed in the upper atmosphere due to the collision of neutrons, which are produced by cosmic rays and constantly stream into Earth's atmosphere from space, with nitrogen atoms, ^{14}N. These ^{14}C atoms rapidly oxidize into carbon dioxide (CO_2). Carbon dioxide has an average residence time in the atmosphere of around 4 to 5 years (Starr, 1993) and newly produced ^{14}C mixes throughout the atmosphere, dissolves in the oceans and, through photosynthesis processes and the food chain, enters all plant and animal life on earth (Bowman, 1990). Once an organism dies, the carbon exchange with the atmosphere ceases, meaning that no new ^{14}C is incorporated to replace decaying radiocarbon; 'the clock starts ticking'.

3.3.2 Principle of ^{14}C age determination

Over time, the ^{14}C parent decays back to the ^{14}N daughter, a gas that escapes to the atmosphere, and β^- rays. The level of ^{14}C falls at a rate that is determined by the law of radioactive decay, according to its half life of 5730 ± 40 years. This law relates the number of atoms left after a time t to the initial numbers of atoms at time zero (t=0). The principle according to which radiocarbon age determination works is therefore that when measuring the ratio of $^{14}C/^{12}C$ or $^{14}C/^{13}C$ in the dead organism and comparing it to the present day $^{14}C/^{12}C$ ratio, the time elapsed since the organisms dead can be inferred. This is represented by the following equation:

$$(^{14}C/^{12}C)_t = (^{14}C/^{12}C)_{t=0}e^{-\lambda t} \tag{3.1}$$

where λ is the reciprocal of the mean life, representing the decay rate, related to the half-life $t_{\frac{1}{2}}$ by the relation $\lambda=(\ln 2)/t_{\frac{1}{2}}$ (Libby, 1946; Arnold and Libby, 1949, 1951). The calculation of the age thus requires knowing the ratio of $^{14}C/^{12}C$ at the time of death of the organism. Through analysis of the radiocarbon content of known-age tree rings from the last 9 ka, it has become clear that there have been variations of this ratio throughout history (de Vries, 1958). Therefore, the obtained ^{14}C age is expressed as ^{14}C years BP, which does not equal calendar equivalent years. For radiocarbon dates to be used as true ages, they must first be calibrated and converted to calendar years using a calibration curve, such as IntCal20, describing the variations in the atmospheric $^{14}C/^{12}C$ ratio in the past (Reimer et al., 2020). Most intervals are older than the radiocarbon dates by a few thousand years (Stuiver and Reimer, 1993). For consistency, this conversion is done according to an internationally agreed upon reference value for the current ratio ($^{14}C/^{12}C)_{t=0}$) and the ^{14}C half-life determined by Libby (1946) $t_{\frac{1}{2}} = 5568 \pm 30$ years (Godwin, 1962). The radiocarbon age

determination method allows to date material of up to about 50 ka in age, which is about ten half lives (Linick et al., 1989).

3.3.3 Marine reservoir age

The situation is more complex for samples which obtained their ^{14}C in the marine environment, as these samples reflect the $^{14}C/^{12}C$ ratio of the water in which they formed. Reservoirs of ^{14}C within the ocean are systematically depleted compared to the atmosphere, due to the time it takes for atmospheric ^{14}C to exchange with the surface ocean and the interior storage of large amounts of old carbon in the ocean, resulting in older apparent radiocarbon ages (Törnqvist et al., 2015). Therefore, to calibrate marine radiocarbon samples accurately, this global marine-terrestrial offset must be accounted for and is known as the marine radiocarbon reservoir age, denoted as R, which represents the difference between the apparent age and the real age of the water body. Present day R values are quite well constrained in the modern ocean and amount to 400-600 ^{14}C years (Key et al., 2004; Heaton et al., 2020; Pieńkowski et al., 2022). R varies both spatially and temporally, in accordance to ^{14}C production and varying ocean circulation, the location of deep-water formation and the kinetics of air-sea gas exchange (Waelbroeck et al., 2001). To incorporate R and its time-variant nature, different calibration curves are used for marine samples, Marine20 (Heaton et al., 2020) being the most recent iteration.

To further complicate marine calibration, an additional correction is required as the apparent ages of marine samples are also influenced by spatially varying factors that determine the exchange of carbon between the atmosphere and the ocean, called ventilation, such as sea-ice cover, upwelling and freshwater inflow (Bard, 1988; Pieńkowski et al., 2022). This additional offset is known as ΔR and is defined as the difference between the age of the local marine reservoir and the modelled age of the global ocean surface mixed layer (Stuiver et al., 1986). Due to the impact of the nuclear bomb-peak around the 1950s, which resulted in a drastic increase in ^{14}C in the atmosphere (and subsequently ocean), a straightforward determination of modern ΔR_R is not possible. Therefore, to estimate ΔR_R, pre-bomb, live-collected molluscs and cetaceans can be used (Mangerud et al., 2006; Pieńkowski et al., 2022). Both Mangerud and Svendsen (2017) and Pieńkowski et al. (2022) present mollusc-based ΔR_R value for Western Svalbard, in conjunction with Marine13 (Reimer et al., 2013) and Marine20 (Heaton et al., 2020) respectively. As the ΔR_R value from Pieńkowski et al. (2022) is based on the most recent marine calibration curve, which is said to better capture the time-variant nature of R, radiocarbon ages in this study are calibrated according to this ΔR_R value, -61 ± 37 ^{14}C years for Western Svalbard. In theory, these ΔR_R values apply only for the period and oceanographic conditions for which they were calculated. Nevertheless, both Pieńkowski et al. (2022) and Mangerud et al. (2006) assert that these values are broadly applicable in the study area for the entire Holocene, due to the relative continuity in oceanographic conditions and sea-ice cover throughout this time.

3.3.4 Synndalen shells

To obtain absolute age controls, three shell samples were selected for radiocarbon age determinations, one intact shell and two shell fragments. The intact shell was selected based on its quality and identifiability, the two shell fragments were selected because they were found highest in the stratigraphy (Fig. 3.1). These samples were cleaned with deionized water in an ultrasonic bath and shipped to Switzerland, where they were analysed in the 'Laboratory for the Analysis of Radiocarbon with AMS' (LARA) at the University of Bern. There ^{14}C content was measured in an accelerator mass spectrometer (AMS), which measures the actual number of ^{14}C atoms in the sample relative to ^{12}C or ^{13}C atoms.

3.3.5 Calibration and reservoir age

The resulting radiocarbon dates were calibrated to calendar years by using the calibration software OxCal 4.4 (Ramsey, 2009). The software returns the different intercepts of the given radiocarbon ages with the calibration curve and calculates the median calibrated age for 1σ and 2σ confidence intervals, which are reported in the following chapter. For 1σ, there is a 68% chance that the age is in the indicated range, which constricts the age range and consequently increases the precision. Using results in the 2σ range results in a 95% probability of the actual age to be in the indicated range, resulting in a larger age span and decreased precision. For the calibration, ΔR values from Pieńkowski et al. (2022) (-61 ± 37 ^{14}C years) was used, in conjunction with Marine20.

3.4 Beryllium dating

The rock samples that were taken near Camp 2; Synn-2-R1, Synn-2-R2 and Synn-2-R3, were brought to Bergen University for Beryllium dating. Unfortunately, the grain size of these siltstones turned out to be too fine for quartz separation to be successful. As of October 2022, a new attempt for Cosmogenic Dating has been made: the rock samples have been shipped to the University of New Hampshire, USA, where Chlorine dating will be attempted.

3.5 Complementary: Lacustrine core from Istjørna

A lacustrine core from Istjørna (Ist-R-1-21) has served as a complementary resource to this study. The core has a length of 170 cm and has been collected with a reasoner coring system from the middle of the lake in spring 2021. The objective of integrating this core within this study is to obtain the age of the base of the core by obtaining radiocarbon ages of the deepest found organic material. To achieve this, the core has been split, logged and sub-sampled. These sub-samples were taken from the lowermost part of the core where organic material was visible with the naked eye in pronounced black layers (at 165 cm, 155 cm and 146 cm; Appendix B). These sub-samples were sieved under running water through a 63 μ sieve and analysed under stereo-microscope, to enable picking of macro-organics. The isolated organic material was oven-dried at 40°C and sent to Switzerland for radiocarbon age determination in November 2022. There results were still anticipated to return from the lab when finalizing this study.

As not all top material was retrieved, the top of Ist-R-1-21 does not represent the lake bottom. It was attempted to correlate this core to a second, shorter percussion core, ISTP-1-21, that does contain the upper sediments. However, no tie-points for correlation were distinguished so this correlation was not achieved.

3.6 Data archiving

The drone imagery and 3D-models will be archived in Svalbox, a primarily open-access repository of digital models from Svalbard, accessible at `www.svalbox.no` (Senger et al., 2021).

4 | Results and interpretations

This chapter presents the results obtained during this study. First, the photogrammetry results are presented in section 4.1. Subsequently, different landform-sediment assemblages that occur in the valley are described and interpreted in section 4.2, often illustrated by pictures or maps. A geomorphological map is presented afterwards in section 4.3. Hereafter, radiocarbon age results are presented in section 4.4 and, lastly, a log of the lacustrine core is described in section 4.5.

4.1 Photogrammetry

4.1.1 Orthophotos and Digital Elevation Models

Orthophotos of both the area around Camp 1 and Camp 2 were created in AgiSoft (Fig. 4.1A. Due to battery constraints, no aerial photos were obtained from the central area of Synndalen. Hence, instead of a single orthophoto of the entire valley, two separate ones were created, one from the northern part (around Camp 1) and one from the southern part (around Camp 2). The difference in colour tones between Ortho_Camp1 and Ortho_Camp2 is caused by the different weather conditions at times of aerial imagery collection, the day of acquisition around Camp 1 being more cloudy. A DEM was created from both these areas (4.1B) and these DEMs were thereafter used to create hillshade maps (4.1C). Furthermore, hillshade maps with a vertical exaggeration, slope maps, contour maps and fluvial maps delineating watersheds were produced.

4.1.2 Sketchfab

3D models were created in Sketchfab for both the area around Camp 1 and Camp 2. These models are available online at:

- **Camp 1:** `https://sketchfab.com/3d-models/synndalen-camp-1-ab4f6d9e7ee445c0a216d3901c3f1575`.
- **Camp 2:** `https://sketchfab.com/3d-models/synndalen-camp-2-352f6b4b22c549849384157dba657b6f`.

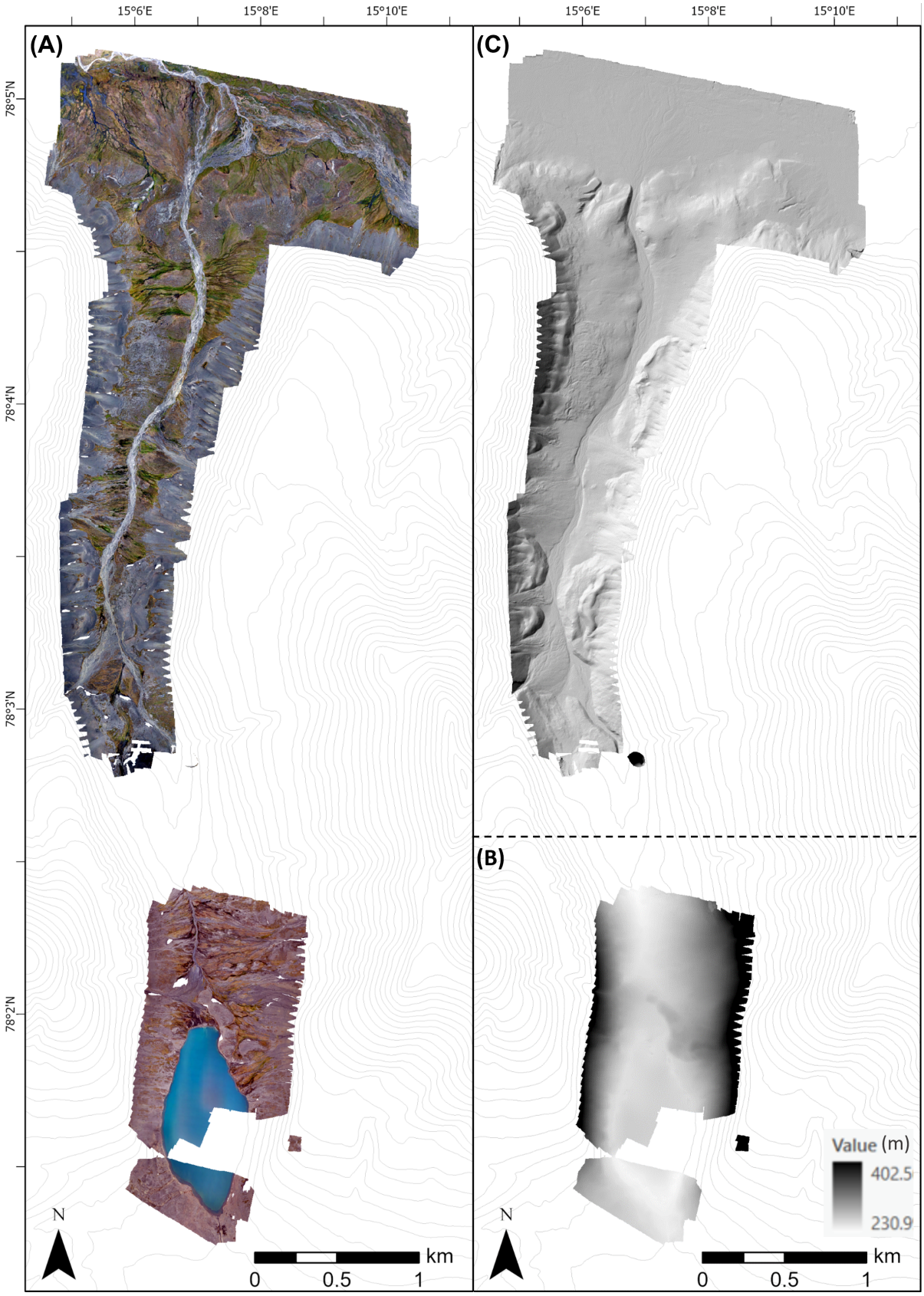

Figure 4.1: (A) The produced orthophotos of both the northern (Ortho_Camp1) and southern (Ortho_Camp2) part of Synndalen. (B) DEM of the southern part of Synndalen (DEM_Camp2). (C) Hillshade map of the northern part of Synndalen. Scale: 1:30.000. Base map: Contour map based on ArcticDEM, courtesy of the Polar Geospatial Center (Porter et al., 2018)

.

4.2 Landform descriptions and interpretations

The creation of the geomorphological map of Synndalen is based on observations and interpretations, made both in the field and remotely, of the landforms and sedimentary structures present in the valley. To prepare for a better understanding of this map, and to understand some of the choices made, the section below describes and interprets the majority of the mapped landforms, before the presentation of the geomorphological map of Synndalen in the following section. First, landforms that are common throughout the entire valley are discussed. Afterwards, two key locations within the valley; the landforms at the valley-mouth and the valley-head, are discussed separately. To underline the importance of integrating information on both surface form and internal composition, this report often refers to the term 'sediment-landform assemblage', as opposed to only 'landform', as different glacial landform systems are characterized by different assemblages of glacial sediment and landforms (Chandler et al., 2018; Benn and Evans, 2014).

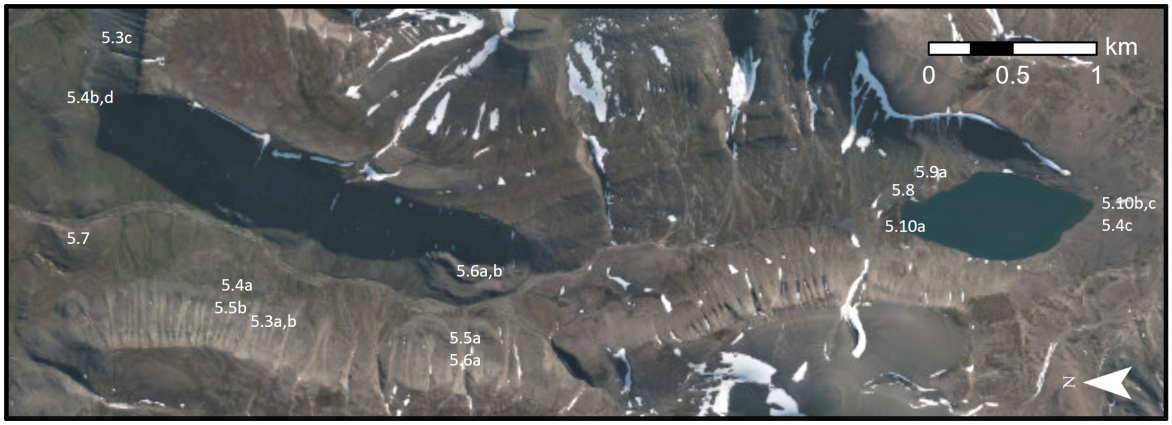

Figure 4.2: Overview of the locations of presented pictures within Synndalen. Basemap: NPI (2011).

4.2.1 Slope process deposits

Amongst the most widespread landforms in Synndalen are the talus slope deposits that cover the lower parts of the steep, rocky slopes. These slope systems consist of multi-stepped erosion, transport and sedimentation systems (Eckerstorfer et al., 2013) with a vertical relief of approximately 250 m. A prominent periglacial landform that is important for all the slope deposits considered below, is the highly weathered plateau edge, which in most places gradually transitions into vertical rock faces covered by thin layers of sediment. A clear connection exists between erosional and depositional areas, in the form of transport couloirs between protruding rock noses. These couloirs are primarily erosional landforms, with only a thin sediment cover, and lead down to a range of different distinctive slope process deposits that are described below.

4.2.1.1 Debris flow deposits

Description

One of the slope deposits found in Synndalen on the lower parts of the slopes, are fan shaped lobe deposits (Fig. 4.3.D). On most of these deposits, multiple channels can be distinguished, sometimes with incised tracks bordered by elongated ridges. Often, the channels reach until the end, or just past the end, of the fan deposit, but in some cases the channels nearly reach the valley floor. Especially on the northern flank on the west side of Synndalen, the deposits sometimes consist of only a single channel. The fan and channel deposits have a long run-out, a gentle surface gradient ranging between 20-25° and a concave surface profile (Fig. 4.3.A).

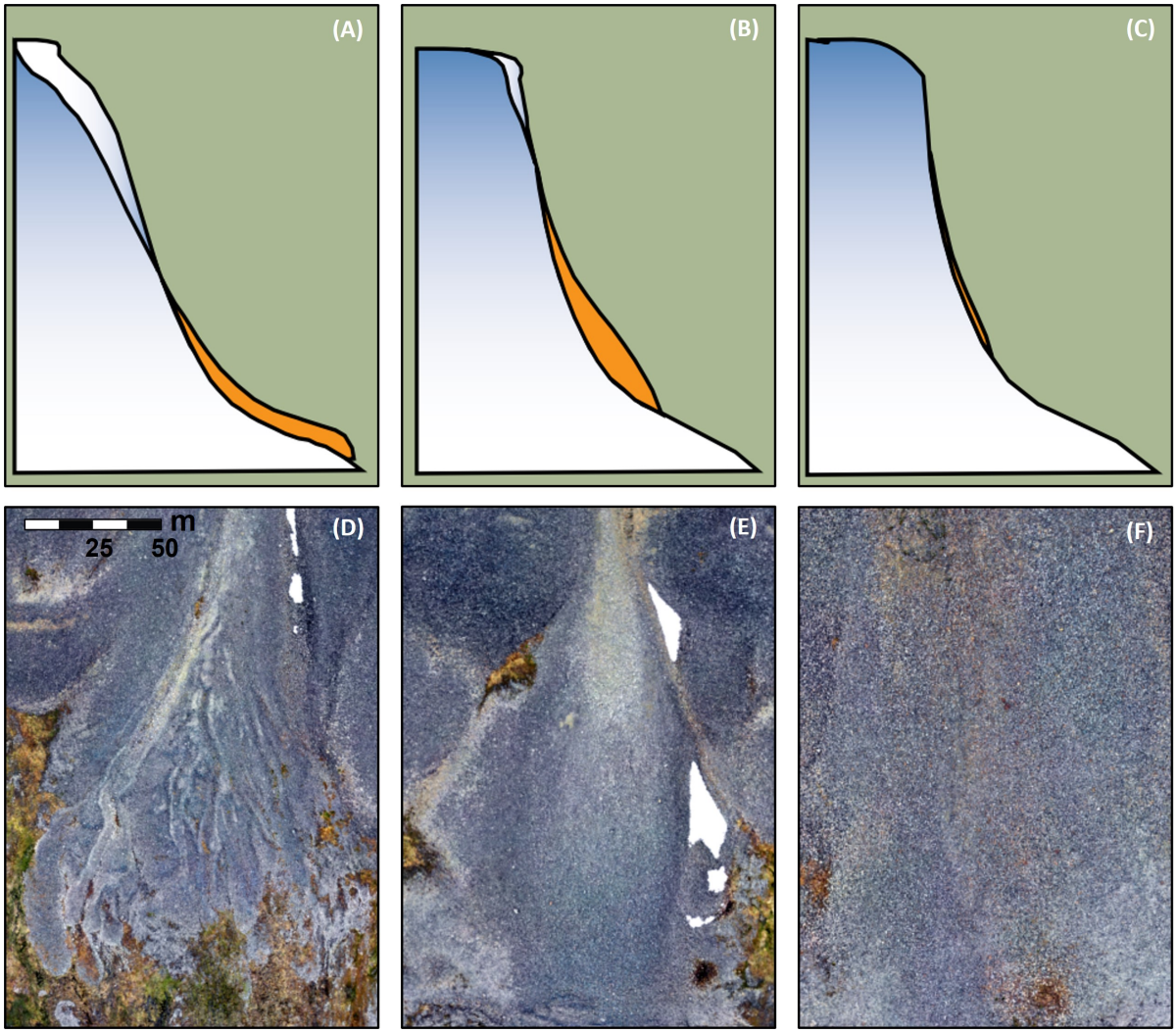

Figure 4.3: Slope process deposits in Synndalen. (A) and (D), conceptual model and example of debris flow deposit respectively, showing a long run-out, a gentle surface gradient and a concave surface profile with erosion tracks; (B) and (E), conceptual model and example of snow avalanche deposit, with a medium length of the run-out zone and a convex surface profile; (C) and (F), conceptual model and example of rockfall deposit, with a short run-out zone and a steep surface gradient. Figures (A), (B) and (C) from Rubensdotter et al. (2015), (E), (F) and (G) from Ortho_Camp1, al at similar scales.

Their width typically ranges between 80-200 m and their length between 150-300 m. The deposits contain a mix of sediments, ranging from sand to boulders, and are generally composed of sandstone and siltstone.

Interpretations

Based on their shape and position, these slope deposits are interpreted as debris flow or debris flood deposits. Both of these terms describe the failure and collapse of material on a slope, that often start in gullies, channels or other drainage paths. The different terms primarily relate to varying water content in the moving mass. If the volume of water is high, it is called a debris flood (Rubensdotter et al., 2015). Debris flows can occur if a slope is steep enough, there are enough loose sediments available on the slope and these sediments are unstable enough for the flow to initiate, for example due to elevated pore water pressure after large precipitation events or due to snow melt (Eckerstorfer and Christiansen, 2011). Usually, the starting point of debris flows is on inclinations over 30°, but in Synndalen they also appear on more gentle slopes, indicating higher percentages of water (Eckerstorfer et al., 2015). The more water or snow in the mass movement, the farther downslope the flow will reach before it stops. At the locations where the debris flow gullies reach farther down-stream, until almost the valley floor, the debris flow is interpreted to have originated as a slush avalanche, released in over-saturated snow. As opposed to most avalanches, slush flows also occur on

slopes with low gradients (5°-25°). When these flows of over-saturated snow have eroded into the slope and incorporate boulders and sediments, they become debris flows. In general, most of the debris is deposited in the lobes or tongues at the bottom of the slope, but also a significant amount of sediment is deposited alongside the debris flow paths and forms elongated ridges on the flanks of the tracks; levees. In general, debris flows are recurring events, where the continued process of erosion and deposition over time has lead to the development of well-established debris flow gullies and debris flow fans. At the locations with only a single channel however, it seems like a single debris flow event has occurred. At some locations, debris flows have occurred on slopes that were already covered with other types of slope process deposits, such as snow avalanche or rockfall deposits, acting as a secondary transport agent bringing the material farther out into the valley (Rubensdotter et al., 2015).

4.2.1.2 Snow avalanche deposit

Description

Much of the western slope of Synndalen, but also other parts of the slopes in the valley, are covered by cone shaped talus deposits (Fig. 4.3.F). As opposed to the previously described debris flow deposits, these deposits do not have a concave, but a convex surface profile, clearly bulging forward and their run-out is less far downslope (Fig. 4.3.B). At some locations, individual cones seem to have merged laterally to coalescing cones. The gradient of these deposits range between 23° to 34° degrees, there length between 100 to 200 m and their width between 50 to 150 m. When travelling through Synndalen on snowmobile in spring 2022, it was noted that on the cliffs above many of these deposits, cornices were present. Cornices are snow masses deposited by wind, often overhanging and usually near sharp terrain breaks such as ridges or, as on Svalbard, plateau edges.

Interpretations

These concave, cone shaped slope deposits have been deposited by avalanches. Avalanches are a common slope process in snow covered mountains. A special type of snow avalanche that is frequently occurring in Svalbard are cornice fall avalanches, as cornices frequently collapse and produce large snow avalanches. These avalanches transport rockfall deposits from the rock-face downslope during the entire winter. Towards late spring, full depth avalanches incorporate rock debris of different origin in the transport couloirs, sweeping away the sediments (Eckerstorfer et al., 2013). The geological setting in Synndalen, with the extensive plateau mountain topography in combination with snow transport by prevailing winds from the SE, is favourable for the formation of cornices, especially on lee sides (Eckerstorfer et al., 2013). Eckerstorfer et al. (2013) found that cornice fall avalanches are the most dominant type of avalanche in the Longyearbyen area and assumes that they are likely to be the dominant mode of sediment transport of any leeward slope on Svalbard. Due to the high abundance of avalanche deposits in Synndalen compared to debris flow deposits or rockfall deposits, this assumption is assumed to be correct for the Synndalen slope systems.

4.2.1.3 Rockfall deposit

Description

On some of the steeper slopes, with a gradient of up to 42°, steep talus fans and extensive sheets have formed on the slopes (Fig. 4.3.F). They have a shorter run-out, and consequently are deposited slightly higher up-slope than the previously described debris flow and avalanche deposits (Fig. 4.3.C). These fans and sheets are generally thinner and much less pronounced than the other slope deposits.

Interpretations

These steep talus sheets or cones are formed due to rockfall processes. Rockfall deposits can occur under all rock scarps that are steeper than 40° and have a short run-out. Rockfalls are caused by rocks that detach from the bedrock through weathering processes and subsequently fall, jump and/or roll down the slope. Larger rocks will reach locations farther away from the cliff than smaller rocks (Eckerstorfer et al., 2015). Rockfall talus deposits take three forms: as talus sheets, where rockfall has been fairly uniform across slopes; as talus cones, resulting from a concentration of rockfall downslope of gullies or coulouirs; and as coalescing talus cones, formed by the lateral merging of individual cones (Ballantyne, 2018). In Synndalen, talus sheets are the most prevalent form of rockfall slope deposits.

4.2.2 Permafrost related landforms

The geomorphology in areas associated with permafrost is dominated, or significantly influenced, by the presence of perennially frozen ground and the cyclic ground freezing and thawing over timescales ranging from diurnal to millennial (Ballantyne, 2018). Periglacial processes have left their signature in the landscape of Synndalen, and associated landforms are discussed below.

4.2.2.1 Solifluction

Description

On many of the slopes in Synndalen, lobes, stripes and large sheets are visible. Often, these structures can be found draped over other landforms, complicating their identification. In many of the places these features appear in ordered stripes and lobes, although in some locations the pattern is quite chaotic (Fig. 4.4.A). The lobes mostly do not exceed a width of a few metres and a length of tens to hundreds of metres. The sediments that make up the stripes and lobes are better sorted than most of their surroundings. Vegetation is often absent or minimal on the stipes and lobes, but more extensive in between them, also enhancing their distinguishability. Near most of these features, there are no signs of (past) running water, excluding the possibilities that these stripes on slopes are fluvially deposited. Some of the features, especially within the 'chaotic' part of Fig. 4.4.A, are defined by steep frontal parts that mark their downslope extent.

Interpretations

These lobes, stripes and 'chaotic' sheets are interpreted as being the result of solifluction. Solifluction is the slow downslope movement of soil or rocks due to the cyclic freezing and thawing of the ground. This downslope movement occurs without the aid of running water and can even occur on very gentle slopes of only 2°. Solifluction encompasses different components of mass movement. The process called *frost creep* will move soil and rocks downslope due to repeated cycles of volumetric expansion (frost heave) during freezing and contraction (settling) during thaw. Another process, *gelifluction*, is the slow gravity-induced shear deformation of soil associated with the generation of high pore-water pressure during thaw of ice-rich soils (Ballantyne, 2018). A key feature defining solifluction lobes is the frontal riser, which is indeed present at some of the solifluction locations in Synndalen.

4.2.2.2 Patterned ground

Description

Some of the solifluction stripes described above contain sorted sediments. Away from slopes, on flatter areas,

features that contain sorted sediments range from circles to polygons. These circles and polygons, with a diameter of approximately 1.5-2 m, and a width of 2-3 dm, border each other and are regularly spaced. In between these features, soil can be found consisting of finer material and including unsorted clasts. In general, the clasts at the outside are coarser than the clasts on the inside of the circles or polygons. No ice has been observed in any of the polygons.

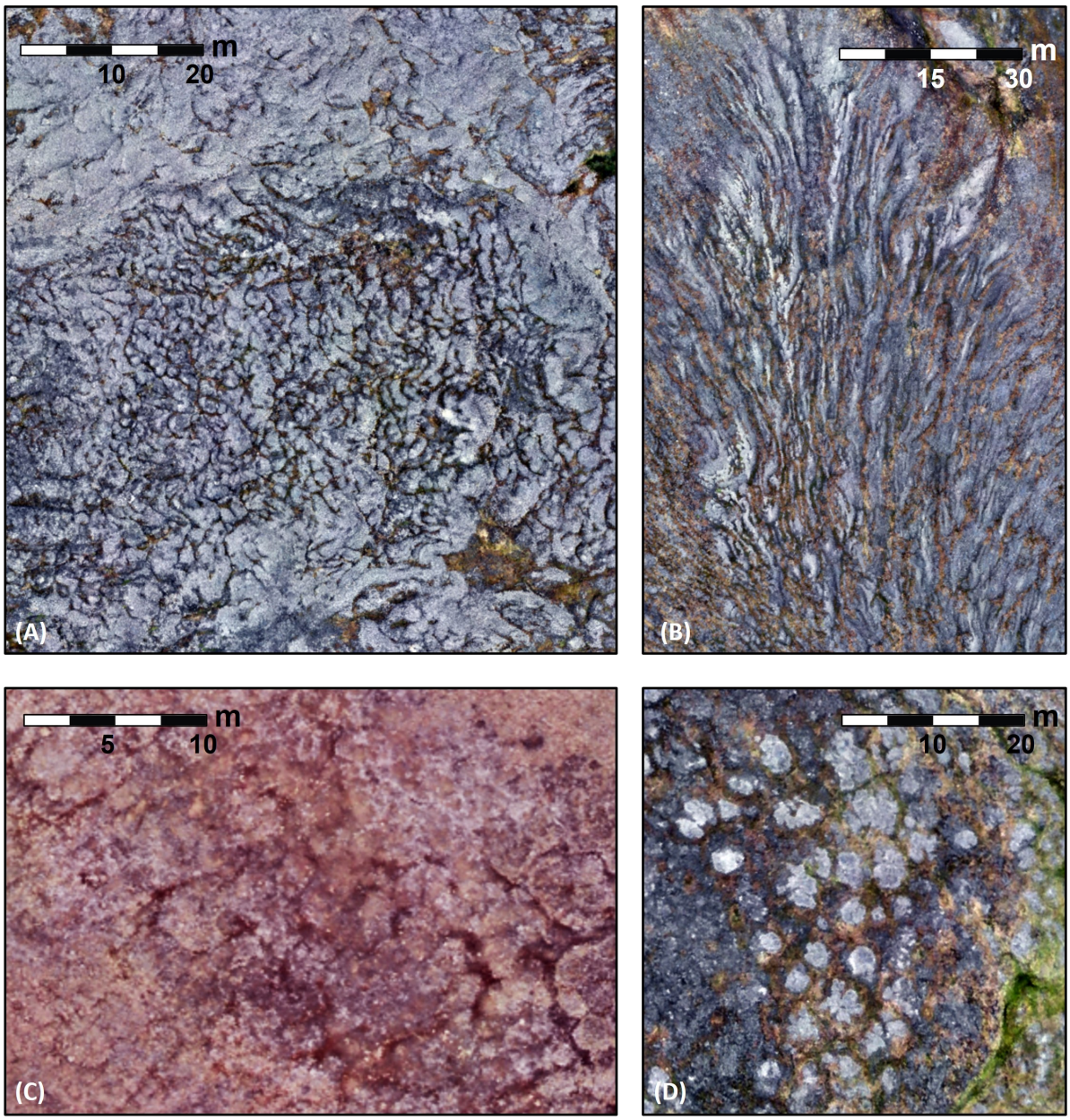

Figure 4.4: Permafrost related landforms. (A) Solifluction lobes/sheets with a chaotic pattern. (B) Solifluction lobes. (C) Patterned ground. (D) Frost boils. (A), (B) and (D) from Ortho_Camp1, (C) from Ortho_Camp2.

Interpretations

These sorted surface patterns are referred to as 'patterned ground' and occur most commonly in the form of circles, polygons and stripes. Particles of different sizes move differently in the soil column and repeated freezing and thawing of the active layer, year after year, will cause sorting of particles on the surface, in alternation with soil. Sediment moving outwards towards the borders is coarser than that moving towards the centers of circles or polygons, resulting in lateral sorting (Ballantyne, 2018). These patterns gradually

evolve, and over time, if freeze-thaw processes would continue, the patterned circles might progress into polygons.

On slopes, the same processes are responsible for the formation of sorted stripes, but the gravity-driven downslope component that adds to the component of soil movement causes downslope-oriented movement.

4.2.2.3 Frost boils

Description

Small piles of unsorted rocks are abundant in Synndalen, especially very pronounced in the area around Camp 1. These piles have a diameter of 0.5-1.5 m, a height of 2-3 dm and often occur in groups with 1-2 m in between them.

Interpretations

A distinction can be made between sorted and unsorted patterned ground. Unsorted patterned ground is defined by micro-relief, in the form of hummocks or ridges and furrows, or alternating vegetated and unvegetated ground. The observed non-sorted circles are often described as *mud boils* or *frost boils*. Still some uncertainty exists, but the nature of patterning (sorted or unsorted), seems to be mainly determined by initial boundary conditions, such as the abundance of clasts, the soil texture, moisture content and the extent of vegetation cover (Ballantyne, 2018).

4.2.3 Rock Glaciers

Description

Along different locations on the valley sides, both on the eastern and western flank and near the valley entrance in the north, multiple lobate or terrace-like talus landforms are distinguished (4.5.A). These landforms are mostly cone shaped in their upper part, with bulging forward flatter lower parts that are sometimes almost horizontal on top. These lower parts are delimited by steep frontal slope inclinations, at some places approaching 50°, but on average around 36° - 39°. Some of these landforms have ridges, furrows and sometimes lobes in front of them, convex in a down-slope direction (Fig. 4.5B). These landforms consist of angular debris, mostly greyish fine grained sandstone, ranging in size from clasts of a few cm to boulders with a diameter of up to 2 m. There is little matrix infill; much open space between the debris is not filled in by sediment or smaller sized boulders. This landform occurs in different sizes, ranging from a single lobe (Fig. 4.5.B), to a more concave crescent shape (Fig. 4.5.A) to features with a length of several hundred metres. Many of the larger features have a depression in their surface just behind the front and seem to have moved farther away from the slopes than the smaller ones. In these cases, the individual, longitudinal features are often connected to individual talus cones, but longitudinal furrows, in front of these inter-cone depressions, separate the ridges (Fig. 4.5.A).

Most of these landforms seem to consist of two distinct layers (Fig. 4.5.C). In the lower layer, some vegetation is present, boulders are covered with lichens and mosses and some grasses can be found between the debris. In the upper layer on the other hand, vegetation is basically absent.

Interpretations

These landforms are interpreted to be rock glaciers. A rock glacier is a glacier whose motion and behaviour is characterized by a large amount of embedded and/or overlying rock material. They are characteristic landforms associated with mountain periglacial landscapes, and are common in Svalbard; most of them occur

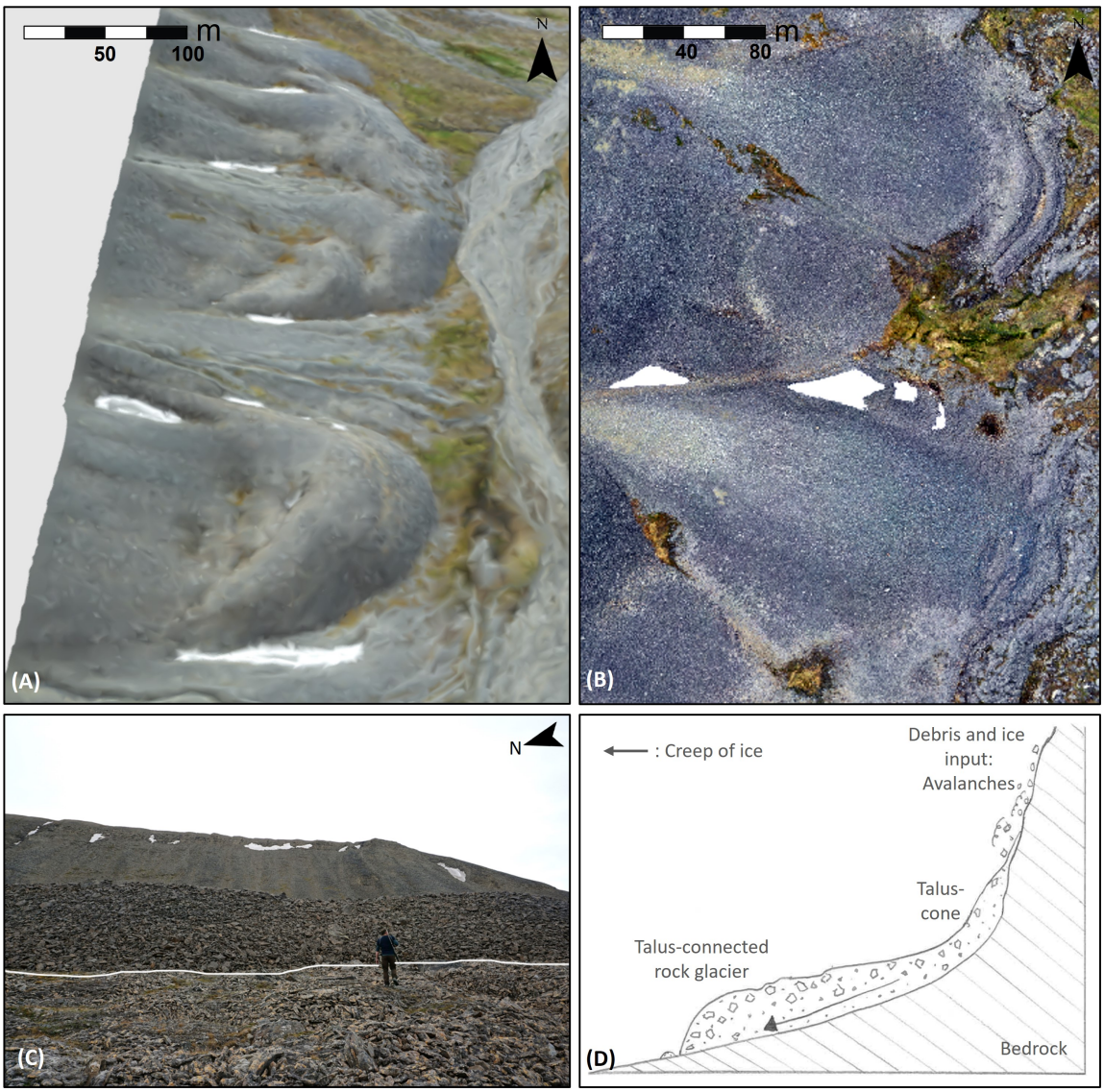

Figure 4.5: (A) Rock glaciers on the western flank of Synndalen, clearly showing the lobate form, lateral margins and steep fronts. Screenshot from Sketchfab Synndalen Camp 1 3D-model. (B) Rock glaciers clearly showing the convex-downslope ridge-and-furrow topography associated with compressive flow. Screenshot from Ortho_Camp1. (C). Picture taken on top of first generation rock glacier, with the second generation of rock glacier in front, delineated by white line. (D) Schematic talus-connected rock glacier, also called 'avalanche derived' rock glacier. Based on (Ballantyne, 2018).

on the western coast and are located at altitudes just above sea level (Sollid and Sørbel, 1992), which is in line with our observations. Rock glaciers may be composed of ice-cemented debris formed in talus that is subject to permafrost, ice-cemented rock fractions formed from avalanching snow and rock, or rock debris that has a core of ice; either a debris-covered glacier or a remnant ice-cored end moraine (Sollid and Sørbel, 1992). Rock glaciers are landforms that convey debris from an up-slope area, called the rooting zone, towards their moving front, from which debris slides and tumbles, to be overridden by the advancing mass. They move downslope as a consequence of the deformation and creep of internal ice lenses or frozen sediments, typically with a few centimetres per year. To allow for the identification of rock glaciers in the landscape, RGIK (2022) provides a standard guideline for inventory of rock glaciers. Cited from their definition, rock glaciers are detectable in the landscape with the following morphologies (RGIK, 2022):

- **Front** (mandatory criterion): Discernable talus delimiting the terminus of a (formerly) moving part of the rock glacier and usually displaying a convex morphology perpendicular to the principal (former) flow direction. For a rock glacier developing on a steep slope, the front may be difficult to recognize.

- **Lateral margins** (mandatory criterion): Discernible lateral continuation of the front. Lateral margins may be absent, particularly in the upper part of the landform.

- **Ridge-and-furrow topography** (optional criterion): Pronounced convex-downslope or longitudinal-surface undulations associated with current or former compressive flow.

Rock glaciers can be derived from different origins and it is especially the geomorphological unit located directly up-slope of a rock glacier that holds implications for the characterization, internal structure and composition, ice origin and ice content of rock glaciers. For a better inventory of rock glaciers, RGIK (2022) presents a list of various geomorphological units that can exist up-slope of rock glaciers. The rock glaciers in Synndalen are interpreted to be talus-connected rock glaciers. These rock glaciers are part of a downslope sequence that includes headwall, a talus slope and the rock glacier (Fig. 4.5.D). The rock glacier is subjacent and connected to talus slopes, which can be fed by rockfall activity from the headwall, surface runoff, or debris flow, but most most dominantly by avalanches, as the talus cones above most of the rock glaciers in Synndalen are avalanche deposits. Therefore, Humlum et al. (2007) refers to these rock glaciers as 'avalanche-derived rock glaciers'. Avalanches are in this case not only an important supplier of fresh rock debris, but they also add significant amounts of new ice to the rock glacier interior. Thus, over time and depending on factors such as the thickness, slope, relative ice content and temperature, deformation of thickening avalanche deposits can gradually lead to the formation of a rock glacier in permafrost regions (Humlum et al., 2007).

On Svalbard, both active and inactive rock glaciers exist. Active, or functional, rock glaciers currently convey sediment from a rooting zone towards its front and are characterized by a steep, frontal slope without vegetation cover due to slope processes, where debris is transported forward to the sharp break at the top of the slope and then falls or slides down the frontal scree slope. Inactive rock glaciers are landforms that today no longer convey sediment, have no movement in their frontal parts, yet still contain ice. They are characterized by vegetation cover on the frontal slope and more subdued topography. Compared with active rock glaciers, inactive features have a less distinct break between the frontal slope and the upper surface (Sollid and Sørbel, 1992). In many regions, inactive rock glaciers can serve as a proxy for permafrost exhaustion or other climatic conditions. On Svalbard however, active and inactive rock glaciers can be found side by side along the same escarpment, indicating that their activity is independent of the contemporary climatic conditions and may be due to changes in for example the source area and debris production (Sollid and Sørbel, 1992). The best way to distinguish between active and inactive rock glaciers would be to obtain kinematic data do determine if the rock glacier is moving or not. As no kinematic data is available in this study, the distinction between active or inactive rock glaciers is made based on geomorphological evidence, such as the steepness of the slope and the vegetation cover. Based on these criteria, all rock glaciers in Synndalen are interpreted to be (at least partly) active rock glaciers.

The depressions in the surface of the rock glaciers behind the front is a characteristic that occurs regularly for rock glaciers on Svalbard. Sollid and Sørbel (1992) mention that this might be due to erosion by melting permafrost, for instance caused by thermal erosion from running water. These depressions are not restricted to inactive rock glaciers, but are also common on many active ones, which is the case in Synndalen (Fig. 4.5.A). Due to these depressions and the continuous movement forward of the rock glaciers, parts of these rock glaciers are not in direct contact anymore with their source area, the steep wall above the rock glacier. Therefore, parts of these rock glaciers are detached from their source, but as their sides are still connected by talus cones that receive debris material, these rock glaciers are still interpreted as active rock glaciers.

Rock glaciers can have a complex morphology that consists of multiple generations, one on top of the other, which is called a multi-unit (Fig. 4.5.C). The interpretation of the apparent two layers of rock glaciers observed in Synndalen is that these rock glaciers represent two phases of rock glacier formation.

4.2.3.1 Landslide connected rock glacier

Description

One of the features mapped as rock glacier on the presented geomorphological map has a different morphology than the other described rock glaciers. Similar to the other rock glaciers, it exists of two layers, interpreted as two generations. However, the front of the lower layer is significantly less steep than that of the other rock glaciers, ranging between only 18° to approximately 35°. Furthermore, it has a more subdued topography, is covered by solifluction lobes and the vegetation cover is more extensive. The lithology is different than that of the other rock glaciers and of the layer on top and consists of fine grained siltstone and shales. One of the largest differences however, is found in the headwall behind the rock glacier. Both the couloirs in the headwall, and the associated talus cones, are much less pronounced than those of the other rock glaciers. Furthermore, on the contour map in Fig. 4.6, there seems to be a scar visible in the upper part of the cliff above the rock glacier. This figure also shows the headwall above the talus-connected rock glaciers of Fig. 4.5.A, to emphasize the difference.

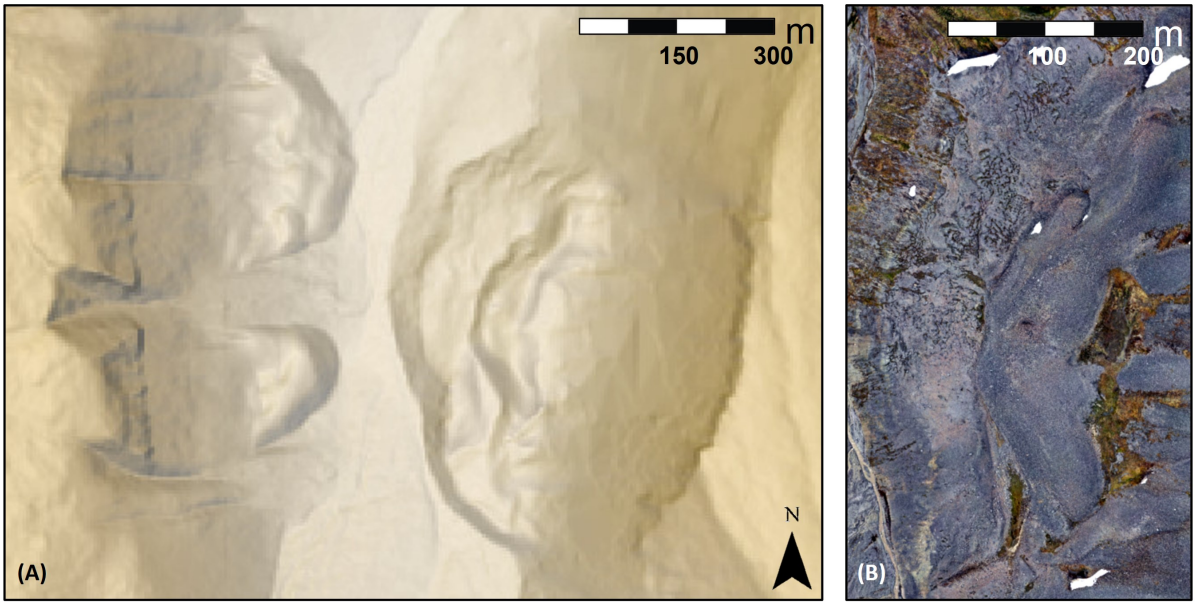

Figure 4.6: (A) Terrain map of the landslide connected rock glacier, showing the scar in the upper hanging wall. Note the difference with the hanging walls of the two talus-connected rock glaciers, with distinct couloirs (same rock glaciers as in figure 4.5) on the west side of the valley. Screenshot of the terrain map of TopoSvalbard (Institute, 2014). (B) Screenshot from the rock glacier from Ortho_Camp1. Note the clear distinction in surface morphology between the lower and upper generation rock glacier.

Interpretations

As opposed to the talus-connected rock glaciers in the rest of the valley, the older generation of this rock glacier is interpreted to be a landslide-connected rock glacier located in direct down-slope spatial connection to a landslide or deep-seated gravitational slope deformation (DSGSD) (RGIK, 2022). A DSGSD, also called a 'slow moving landslide', is the deformation of steep mountain slopes that often involves entire valley flanks and can reach beyond the slope crests. These slope deformations are manifested by sharp scars and cracks, but normally lack a defined rupture surface (Teshebaeva et al., 2019), which would be in line with the geomorphology of this specific rock glacier. The described scar that is visible in Fig. 4.6.A is interpreted as the detachment scar of a landslide or rock failure. As this would also mean that the lower generation of this rock glacier is not dominantly fed by rockfall activity or avalanches, this explains the less pronounced formation of couloirs and debris cones. A hypothesis explaining the occurrence of the different lithologies on this rock glacier compared to the other rock glaciers, is that this landslide originated from a different part of the rock face, there where it consists of shales and siltstone, than the head walls that feed the other rock glaciers with

predominantly sandstones.

The lower part of this rock glaciers is interpreted to be less active to inactive, in comparison with the other active rock glaciers, as indicated by the solifluction lobes, pronounced vegetation cover and more subdued topography.

The boulders on this rock glacier were sampled for performing cosmogenic nuclide dating. It has been decided however to not try to date the rocks from this rock glacier, as there are too many associated uncertainties. DSGSD's are generally characterized by slow deformation rates over long periods, of several cm per year (Teshebaeva et al., 2019), which would complicate the dating. Another scenario would be that the concerning rock was already exposed in the rock cliff, meaning there would not be a complete reset before exposure to sunlight on the rock glacier, which would result in a over-represented age.

4.2.4 Fluvial deposits

As in any glacial environment, sediments deposited by flowing water are widely present, due to the seasonal abundance of meltwater. The main river of Synndalen is a braided river - its width ranges from only about 10 m in the headwaters, up to 100 m farther downstream. The river is fed by multiple smaller side streams flowing down through gullies, either continuously during the meltwater season, or temporarily after peak-events. The main river originates just to the north of Camp 2. The stream directly above Camp 2, on the west side, is situated exactly on the watershed, as it changed draining direction from north to south during the fieldwork in 2021. Approximately halfway down the valley, the addition of stream draining from a small cirque on the west side of the valley significantly increases the width of the main river.

The lowest half of the valley, up to around 75 m a.s.l., has less relief than its upper counterpart and has likely been filled in by sediments over time. The riverbed has less deep incisions than the upper part of the valley, approximately 1 m. Higher up in the valley, this ranges up to a few metres. Mostly, the river moves freely, although at some locations the river is more constrained, by bedrock or other landforms. Where it flows through the elevated terrain in the north of the valley for example, with a width of 20-35 m, the river plain is significantly narrower than at the flatter part more southwards.

Some of the steeper slopes contain some very shallow 'water tracks', especially many of the slopes around the lake. This is interpreted as slopewash; the downslope transfer of sediment by flowing water on hillslopes (Ballantyne, 2018).

As Passfjellbreen currently drains into Istjørndalen, river deposits in Synndalen have been mapped as fluvial, as opposed to glaciofluvial, as they are mainly fed by snow melt and precipitation. It is acknowledged that Passfjellbreen has drained into Synndalen in the past, however, it is assumed that all the resulting glaciofluvial deposits from this time period have now been covered or eroded away by more recent processes.

The small cirque basin draining into Synndalen on the west side, approximately halfway down the valley, is assumed to have contained a small cirque glacier in the past. As this cirque glacier does not exist anymore, and it cannot be determined when it disappeared, the deposits downstream of this cirque have also been mapped as fluvial deposits. As part of the fan deposits downstream of the cirque currently seem inactive, it is possible however that for part of this fan the term glaciofluvial would better describe the deposit, but no data is available to clarify, hence the choice for the described approach.

4.2.5 End moraine system valley-mouth

The northern part of Synndalen is characterized by elevated terrain up to 60 m a.s.l. (Fig. 4.7). Currently, the river is flowing through the landform, dividing it into western and eastern parts. This landform-sediment assemblage system is formed by the interplay of multiple processes, that are discussed below.

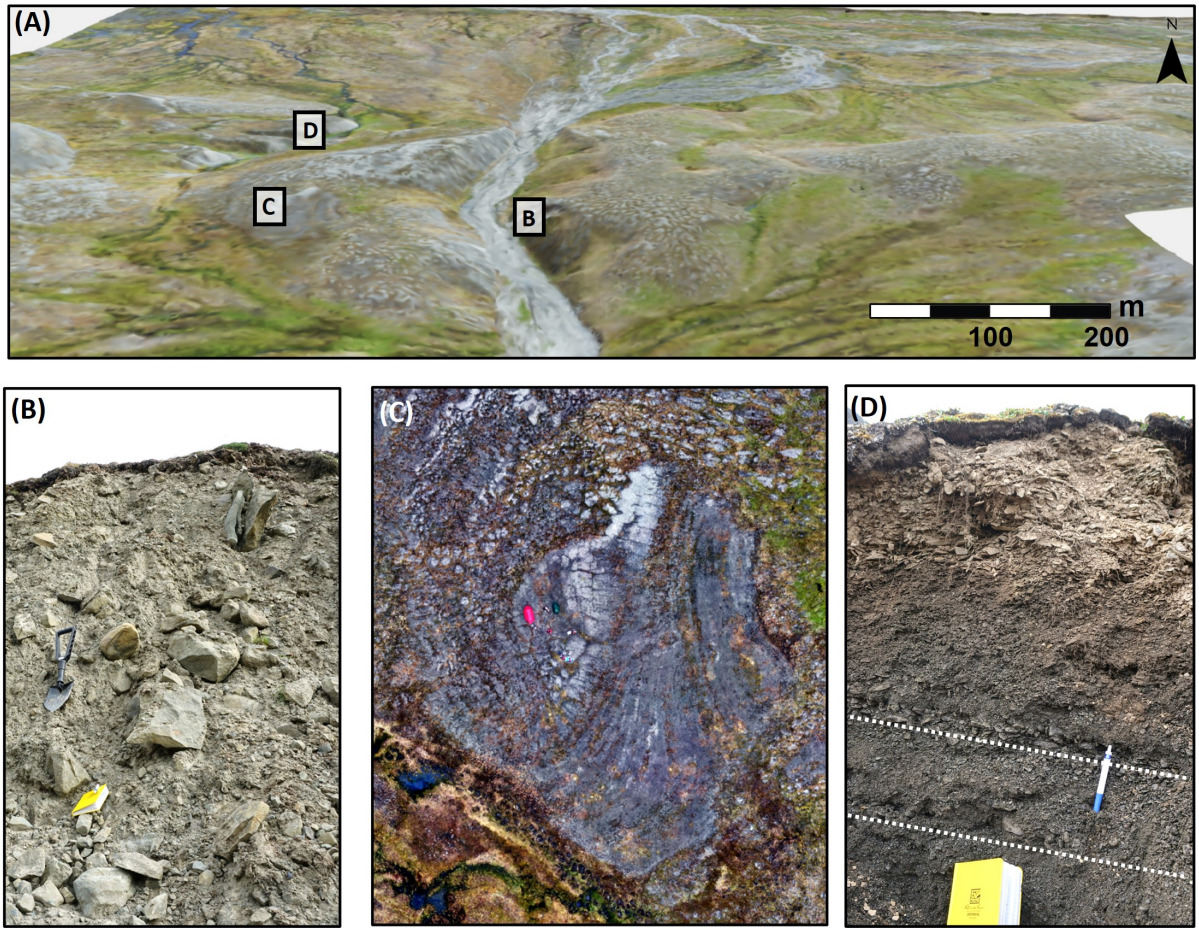

Figure 4.7: (A) Overview of the elevated terrain at the entrance of the valley (screenshot from Sketchfab Camp 1). Locations of (B), (C) and (D) marked in black squares. (B) Sandy gravel section, interpreted as longshore drift deposits. The white dashed lines mark the dipping layers; (C) the location of Camp 1, on top of multiple levels of traceable lines, interpreted as beach deposits; (D) Outcrop formed by slumping, showing the angular, very poorly sorted till deposit constitute the end moraine.

4.2.5.1 End moraine

Description

Most of the elevated terrain consists of an angular, very poorly sorted diamict, composed of (dark) grey, loose material. The diamict consistst of different lithologies, sandstone, siltstone and shales. All these lithologies are local to the valley. On the east side of the river, two slumps leading down to the river have created outcrops into this landform (Fig. 4.7.B), allowing for the internal structures to be assessed. The deposit does not contain sedimentary structures or stratigraphy or preferred clast orientation. Clast size ranges from fine sandy grains to large boulders, up to ca. 70 cm in diameter. Some of these clasts are striated, with striations in different directions. In general, all the clasts are angular, although some of the sandstones are sub-angular. Other slumps in the deposit, on the east and west side of the river, show the same characteristics.

The landform is sloping down on both sides; towards Synndalen in the south and Colesdalen in the north, but

has a relatively flat top. The northern slope is steeper than the southern slope (8°-12° vs 4°-6°). Both on all the sides and on the top of the landform, significant parts of the surfaces have been reworked by solifluction. Solifluction lobes and sheets are clearly distinguishable on the slopes. Many of the flatter areas are covered by frost boils.

Interpretations

The unsorted, angular diamict is interpreted to be an unconsolidated, unstructured till. This till landform is interpreted to be a moraine. Due to the location of the landform at the mouth of the tributary valley, this moraine is interpreted to be a end moraine.

Due to its shape and the general geometry of the valleys, the location of current-day Passfjellbreen, and previous research on the glacial history of Svalbard (section 2.3), this moraine is interpreted to be an end moraine that constrained a glacier that came from the south, and thus covered the entirety of Synndalen with ice. The observation that all the lithologies that are present within the till are local lithologies also does not contradict the hypothesis of a glacier flowing through Synndalen. The slightly more rounded sandstones are likely to have originated from farther inward in the valley, increasing their transported distance. The morphology of the moraine, with a flat top and no signs of the existence of burried ice, suggests deposition in a submarine environment.

Ice dynamics can also be deduced from the existence of this landform. As the glacier must have been flowing significantly to form such a pronounced end moraine, the glacier must have been warm-based or polythermal (Hagen et al., 1993).

4.2.5.2 Beach deposits

Description

On the northern side of the moraine, at several locations near the top, the sediment assemblage is different from the sediments that constitute the till deposit. It generally consists of smaller clasts (up to 2 cm in diameter), that are sub-rounded, better sorted, lighter brown, contain a higher proportion of sandstone and less matrix. The locations where these deposits can be found are traceable as lines in the landscape (Fig. 4.7.C). Multiple of these lines run parallel to each other, with several metres of slightly sloping ground in between. On many locations, these deposits are only very thinly deposited right over the previous described till. On the east side of the river, these deposits have also been found on the south side of the end moraine.

Interpretations

These deposits are interpreted as beach deposits. The different lines traceable on top of the moraine are paleo-beachlines. They exist at multiple levels of elevation along the moraine due to the lowering of the relative sea level as a result of glacio-isostatic rebound. The thin beach deposit of reworked till on top of the moraine serves as a cross cutting relationship, proving the moraine already existed during the formation of the beach deposit, hence proving the beach deposits are younger than the end moraine. It furthermore proves that the moraine has been formed under water. If the sea level had already fallen while the moraine was still continuously being formed, the beach deposits would have been incorporated into the moraine deposits, or at the very least, not have been preserved as they are now.

As the south side of the moraine is also beach washed, water must have been present on the inner, Synndalen side, of the moraine. Once the glacier had retreated farther towards the south, an incision at the location of the current-day river valley, that cuts through the moraine, could have served as an entrance point for the sea. This would have resulted in some form of sheltered lagoon between the retreated glacier and the end moraine, where these beach deposits could form in the intertidal zone.

4.2.5.3 Ice-proximal glacio-marine deposits

Description

Both on the east and west side of the river, the lower parts of the northern slopes of the moraine, an unconsolidated, poorly stratified deposit is identiefied at several locations. This deposit consists of fine grained material, mostly silt and clay. Within this deposit, larger (1-5 cm) angular clasts occur. Most of these deposits are buried under current day soil and frost boils.

Interpretations

This deposit is interpreted as an ice-proximal glacio-marine deposit. The fine grained, muddy deposit is expected to be glacial sediment, transported into the sea by meltwater channels and slowly settling down to be deposited on the distal side of the moraine. The larger clasts are expected to be ice rafted debris, transported by glacial ice bergs or sea-ice and, after melting out, deposited within this ice-proximal deposit.

4.2.5.4 Lateral melt-water channel

Description

On the east side of the river, on the outer side of the valley, faint traces of an ancient river channel are distinguishable at an elevation of ca. 80 m. Downwards from the moraine, into Colesdalen, a fan can be distinguished, now greatly covered by solifluction lobes.

Interpretations

This is interpreted to be an ancient lateral channel, formed above sea level, and corresponding submarine fan.

4.2.5.5 Longshore drift deposit

Description

The section where the sampled shells were found is exposed due to the incision of a small creek (Fig. 3.1. The section consists of a sandy gravel, that consists of medium-sorted, sub-rounded, coarse grained sand and in general small (ca. 1-4 cm), platy, sub rounded gravel, although sub-rounded clasts of up to 15 cm occur (Fig. 4.7.D). The deposit also contains some angular clasts with a size up to a few centimetres, but their occurrence is rare. After digging out parts of the section, it could be distinguished that the sequence generally consists of planar, horizontal layers with a gentle dip of ca. 8° in north-east direction. No cross-beddings or other sedimentary structures were distinguished. Different layers consist of different grainsizes. In general, these layers show a coarsening upwards pattern, although in some parts of the stratigraphy, there are short episodes of fining upwards. The coarsening upwards sequences start with layers consisting of mostly medium-sorted coarse-grained sand, although an ca. 4 cm thick layer of fine grained sand also exists. The coarsening upwards sequence ranges to layers with mostly pebbles of 2 cm in diameter, but also contains clasts of up to 5-15 cm. Higher up in the sequence, there is gradually less sand that acts as matrix infill. The deposit that covers this section, at an elevation of 42 m, is of a different composition and consists of small, (1-3 cm), flat pebbles, with no matrix. This sequence is a continuous deposit, no erosional surfaces have been distinguished.

Within this section, and in the creek running below it, shells and shell fragments of marine bivalve molluscs were found. In the creek and in the lowest part of the section, whole valves were found. Higher up in the section, above an elevation of ca. 40 m, only shell fragments were found. Their occurrence decreased with

increasing elevation; the higher in the section the smaller and less common the fragments. In the deposit on top of this section, no shell fragments were found.

Interpretations

As the sediments and shells in this deposit have been influenced by wave action, this sediment sequence is interpreted to have been deposited in the (sub)littoral zone, with tidal influences. The sorted, general coarsening upward trend in the sequence is thought to represent shallowing up. This is in line with the presence of whole shell valves in the lower part of the section, deposited in a deeper marine environment with much less reworking. The shell fragments, higher up in the section, have been prone to more reworking forces and wave action. The thin deposit on top of the section is similar to the deposits previously described; a beach deposit, in line with further shallowing up.

The dipping of the layering is not directly away from the moraine, which would be expected if the main sediment source would come directly from the Synndalen hinterland. As the layers dip towards the north-east, a different process is expected to be at play, and these sediments are interpreted to have been transported and deposited by a longshore drift, which moved parallel to the coast, originating from the west. This also means that the fossil shells were not necessarily local, but could have been transported in by the longshore current from different locations, either close or farther away.

This longshore drift prograding facies is not expected to have been deposited in an ice-proximal environment, due to the lack of ice rafted debris. If the glacier had still been at its maximum extent during the formation of this sequence, angular clasts in different sizes are expected to be more abundant, as is the case in the previously described glacio-marine deposits. The sparse amount of angular clasts that do occur within the deposit could indeed have been transported in from ice-bergs that have floated in, from sea-ice, or might have been brought in from the valley due to frost weathering and solifluction.

4.2.6 Bedrock features

Description

Halfway up the valley, the valley floor quickly gains in elevation over the course of three different ‘steps’, with a few metres of a steeper slope in between. These steps show some bedrock features in them and are covered with an unsorted, angular diamict. After the highest step, the valley floor flattens out again, with relatively little relief all the way until the lake.

Interpretations

These different steps in elevation are interpreted to be bedrock influenced features, covered by till. The bedrock outcrops on the valley slopes can be traced to the bedrock structures within this landform and are therefore likely to consist of the same bedrock layer. The diamict that covers them is interpreted to be a glacial till. The bedrock is brittle, but must have been resistant enough to withstand glacial erosion. Likely, the glacier retreated relatively fast on the steeper parts of this feature, whereas the flatter top could have been an ideal place for the glacier to stabilize for some time, while till was deposited on top of the bedrock. The till could therefore represent a retreating moraine. The deposition of a retreating moraine would imply that the glacier was flowing and was thus still polythermal or warm-based (Hagen et al., 1993).

4.2.7 Moraine System at valley-head

Description

The large landform on the north-east side of the lake, next to the location of Camp 2, is one of the most pronounced landforms that exists in Synndalen (Fig. 4.8). It consists of two parts. The longest part is roughly NW-SE trending, with a length of approximately 500 m and an elevation above the valley floor of approximately 20 m. In the north, approximately 150 m away from the lake shore, the feature starts approximately mid-valley and extends farther in south-east direction. The southern part borders the lake, the northern part borders paleo-lacustrine deposits, so has likely bordered the lake in the past. The second part of the feature is trending in E-W direction, has an arcuate form and a length of approximately 150 m. Both features consists of a diamict with angular, poorly sorted material, ranging from fines to boulders with a diameter of up to 2 m. The space between all these different clasts and boulders is in-filled, without open spaces (Fig. 3.2.A). Grasses, mosses and other vegetation is quite well spread and the boulders are extensively covered with lichens. Both parts have a considerably steeper slope on the south side (up to 32°) than on the north side (8°-15°).

Figure 4.8: The moraine at the valley-head. (A) Picture taken from west side of valley; (B) Aerial view of the moraine (from Ortho_Camp2).

Interpretations

Due to its shape, location within the valley and sedimentology, this feature is interpreted as a moraine. This is also in line with the large boulders on top of the feature. As the slopes in this part of the valley almost purely consist of finer grained, black shale, the large siltstone boulders have likely been transported in from elsewhere.

This moraine is considered to have formed during an ice-advance from the glacier flowing through Istjørndalen, spilling over into Synndalen. It is therefore interpreted as an end moraine of a glacial readvance. This is in line with the asymmetry in slope angle, although the southern slope might also have been influenced by erosion due to its proximity to the lake. Much of the variation in topography of the moraine has likely formed due to melt out of buried ice. The moraine has not been preserved in its entirety, but is assumed to have extended farther to the western side of the valley during formation. On the west slope of the valley however, some till patches still exist, and could have been connected to the moraine in the past.

The different, E-W trending part of the moraine in the east seems to have been formed by ice with a different flow direction than the first described part. One hypothesis that could explain the orientation of this feature, is that it marks the margin of a small glacier on the valley slope to the south of the moraine.

A different hypothesis for the origin of this moraine could be that it marks the margin of a glacier on the valley slope to the north-east of the moraine. This is unlikely however because of the following reasons: quite an extensive glacier must have been able to from on this valley side, while the rest of Synndalen was not glaciated. This glacier would have had to fan out significantly for it to reach the location of the moraine.

This fanning out would have had to be up-stream, into the valley. No signs of any previous moraine have been recognized at the downstream part of this supposed glacial fan. Furthermore, this hypothesis would not be in line with the steep side of the moraine being in the south, as the steepest parts of moraines generally are on the ice-proximal side.

4.2.7.1 Protalus rampart

Description

The E-W trending part of the moraine is connected to another landform-sediment assemblage higher up the slope, with a different morphology and consisting of different material (Fig. 4.9.A). The material is much finer and better sorted than the till constituting the moraine. It consists mostly of black shale, although some larger boulders exist. The feature forms a 'ramp', is N-S trending and curves to the NE in the northern part. Its length is approximately 180 m. Its upper and lower slopes are covered by grass. The slope below the head-wall above this feature is covered by talus and, in summer, a small snowfield persists above it on the plateau-edge and slope.

Interpretations

This landform is interpreted as a relict protalus rampart. A protalus rampart is a ridge or ramp of debris that is formed by the accumulation of sediment at the foot of a perennial firn or ice bed (Fig. 4.9.B). After falling from the cliff above, clasts fall, roll, bounce or slide to the foot of the firn field where they can accumulate and form arcuate, straight or sinuous ramps (Ballantyne, 2018). These ramps can further be fed by supranival debris flows and sediment-rich snow avalanches, depositing fine-grained sediments. In modern times, a snowpatch still exists throughout the season, but it does not extent all the way to the ramp, meaning the protalus rampart is not actively fed today. In the past however, a more extensive perennial snowpatch likely existed. The observation that the clasts are of the same lithology as the rockwall source, black shales, is in line with the hypothesis that this landform consists of local sediments, as opposed to the large boulders on top of the moraine. It is likely that the original formation of the rampart at this location is bedrock influenced.

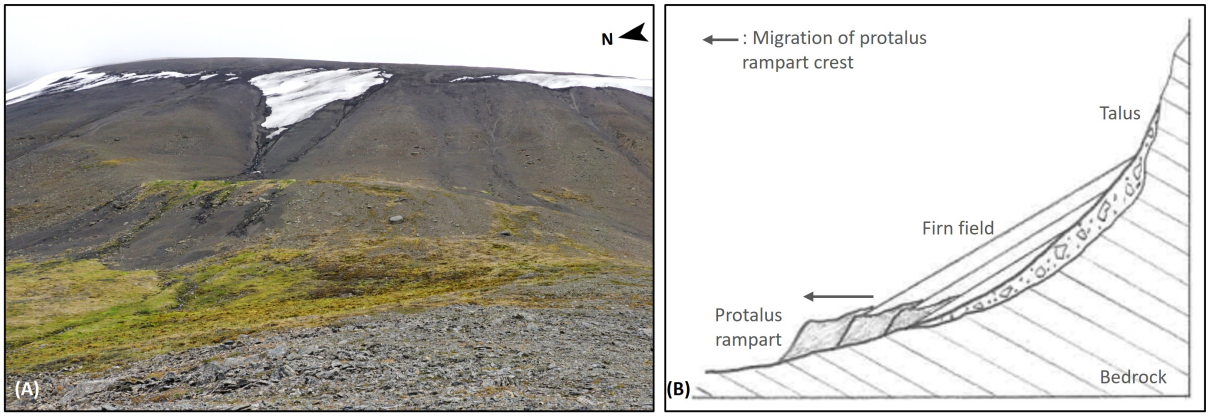

Figure 4.9: (A): The ramp interpreted as a protalus rampart. Picture taken on top of the moraine; note the difference in composition between the morain and the protalus rampart. (B) Sketch of the formation of a protatlus rampart, based on Ballantyne (2018).

4.2.7.2 Istjørna

Istjørna drains into Istjørndalen. On the east and west side, the lake is bordered by talus slopes and in the north-east by the previously described moraine. In the north, up to approximately 80 horizontal metre and 7 vertical metre away from the current shoreline, a flatter area exists with very fine-grained, sorted material,

on which multiple lines parallel to the lake shore can be distinguished, covered by patterned ground (Fig. 4.10.A). These lines are interpreted as paleo-shorelines, which were formed at times of higher water levels. In the south, the lake drains into Istjørndalen. The outlet of the lake is not very pronounced, the water first flows partly under ground, through boulders (Fig. 4.10.B), before incising into bedrock, forming a small canyon with a depth of a ca. 5-7 m and a width of ca. 10 m (Fig. 4.10.C). The depth of this canyon seems to correlate with the elevation of the paleo-shorelines in the north. It is therefore considered that as this river cut into the bedrock, the water-level of Istjørna dropped.

Istjørna's basin must have been scoured out by a glacier flowing through the valley, but is assumed to today be confined by bedrock. In the south, the incision of the outlet river into bedrock proves the occurrence of resistent bedrock. In the north, the previous described bedrock features are on approximately the same elevation as the lake. On top of this, the moraine probably contributes to damming the river.

As Passfjellbreen does not currently drain into Istjørna, deposits are mapped as lacustrine, as opposed to glacio-lacustrine.

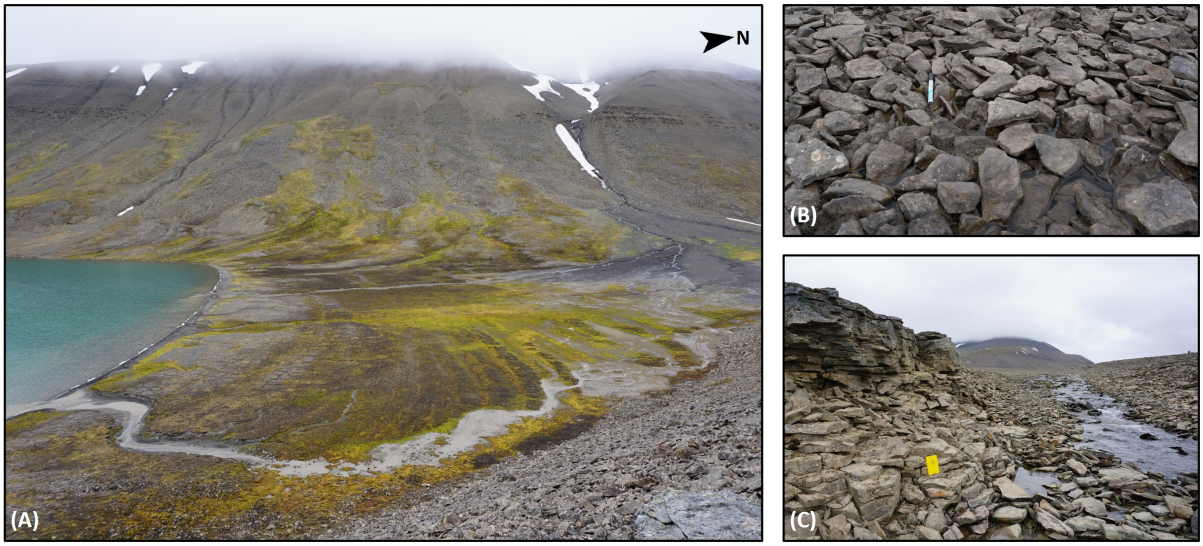

Figure 4.10: (A) the paleo-shorelines in the north of lake Istjørna, as seen from on top of the moraine. (B) The indistinct lake outlet in the south, where the water drains in between the boulders. (C) The incision of the river into the bedrock south of lake Istjørna.

4.3 Geomorphological map of Synndalen

Below, the geomorphological map of Synndalen is presented. The first map presents Synndalen in its entirity, the two following maps show a close-up of the northern and southern part of Synndalen respectively.

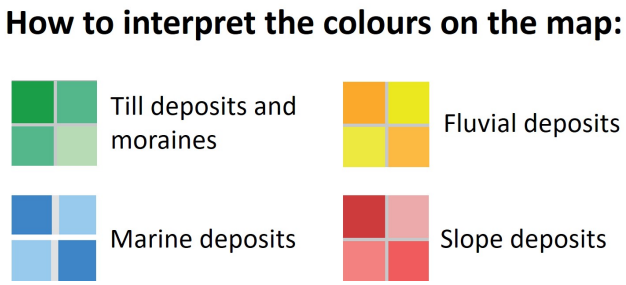

Figure 4.11: General overview of the colours used on the geomorphological map. Based on Eckerstorfer et al. (2013) and Rubensdotter et al. (2015).

Figure 4.12: Legend for the geomorphological map

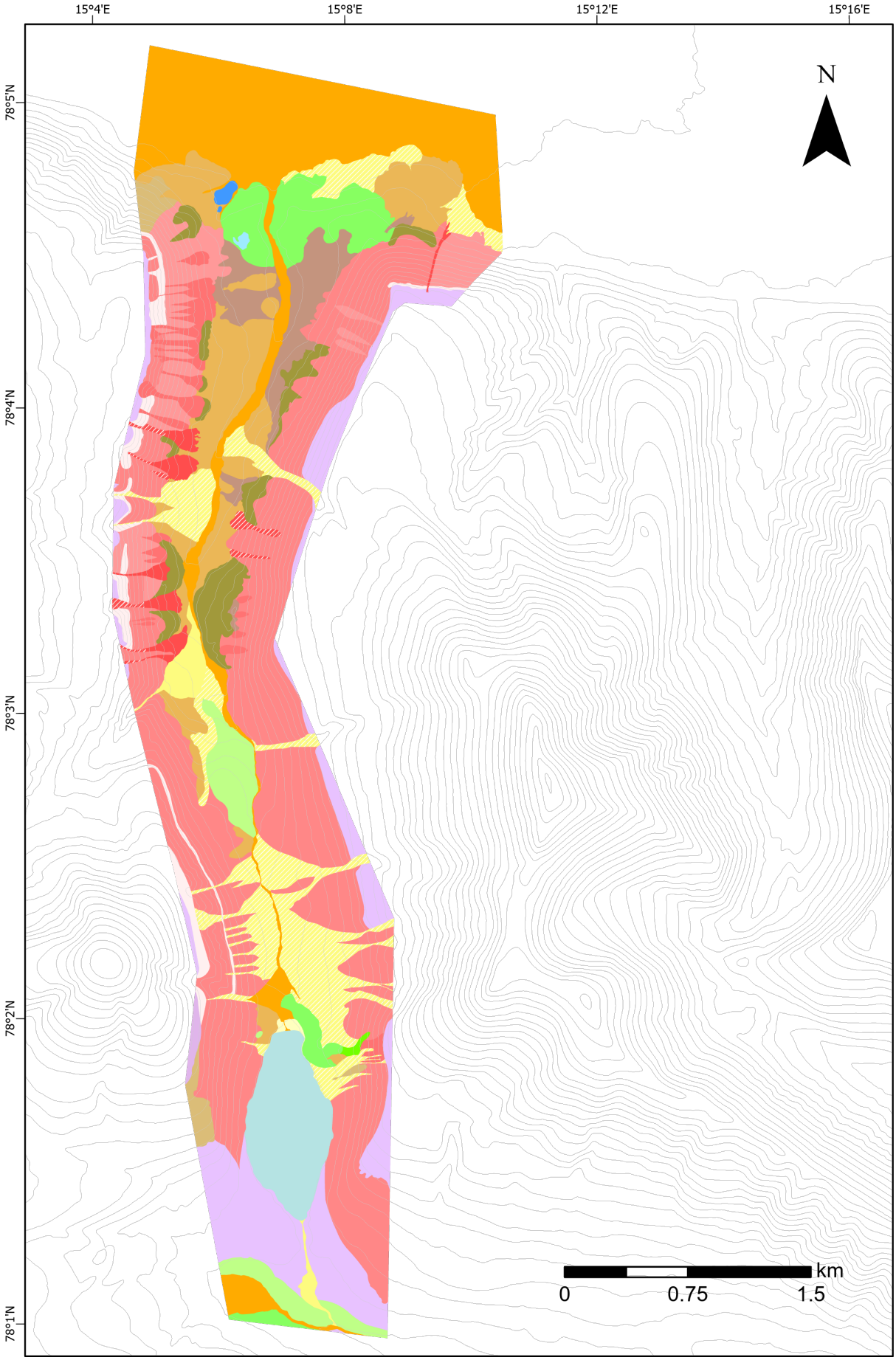

Figure 4.13: Geomorphological map of Synndalen. Scale: 1:30.000. Base map: Contour map with 20 m interval, based on ArcticDEM (Porter et al., 2018)

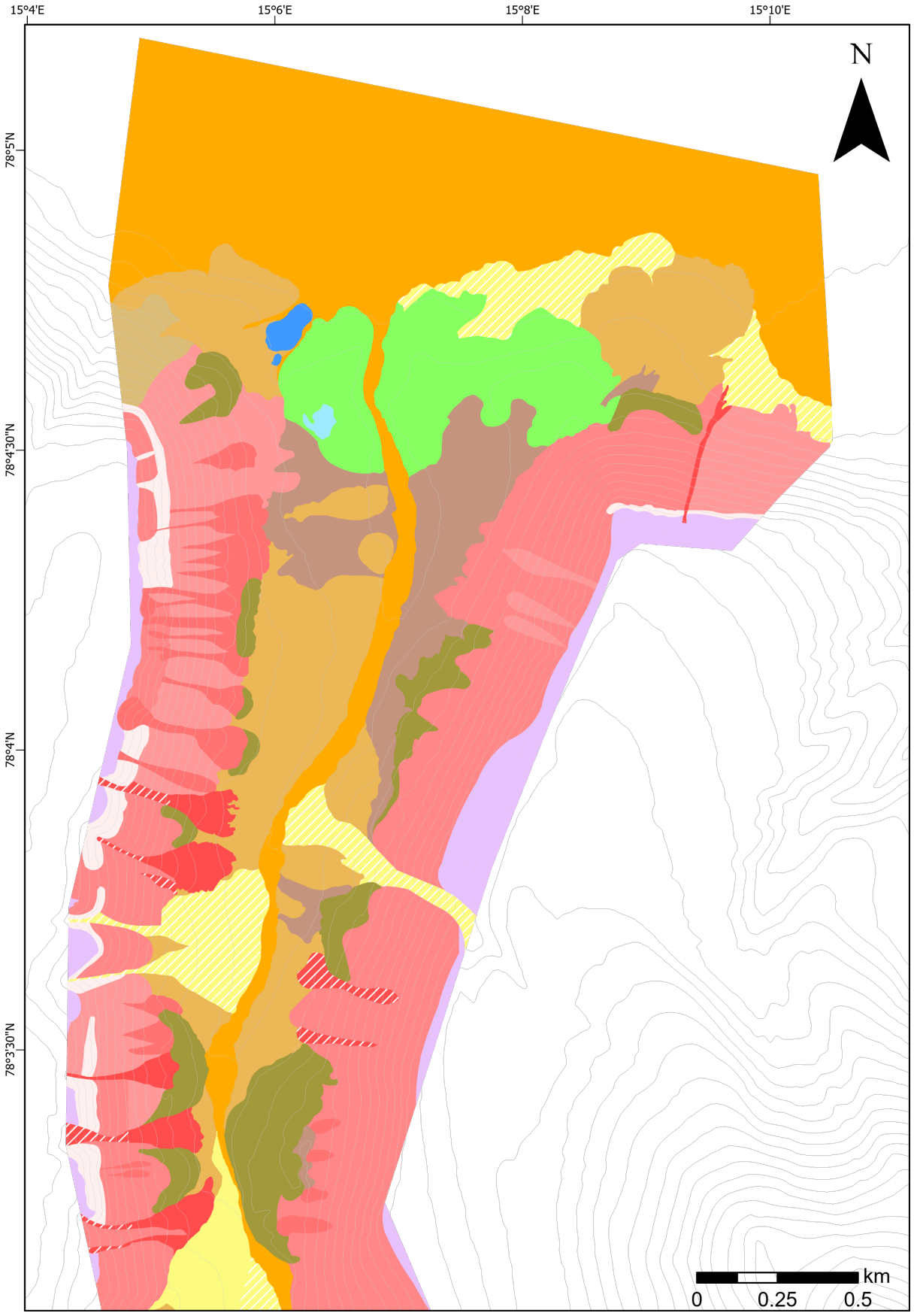

Figure 4.14: Geomorphological map of north part of Synndalen. Scale: 1:15.000. Base map: Contour map with 20 m interval, based on ArcticDEM (Porter et al., 2018)

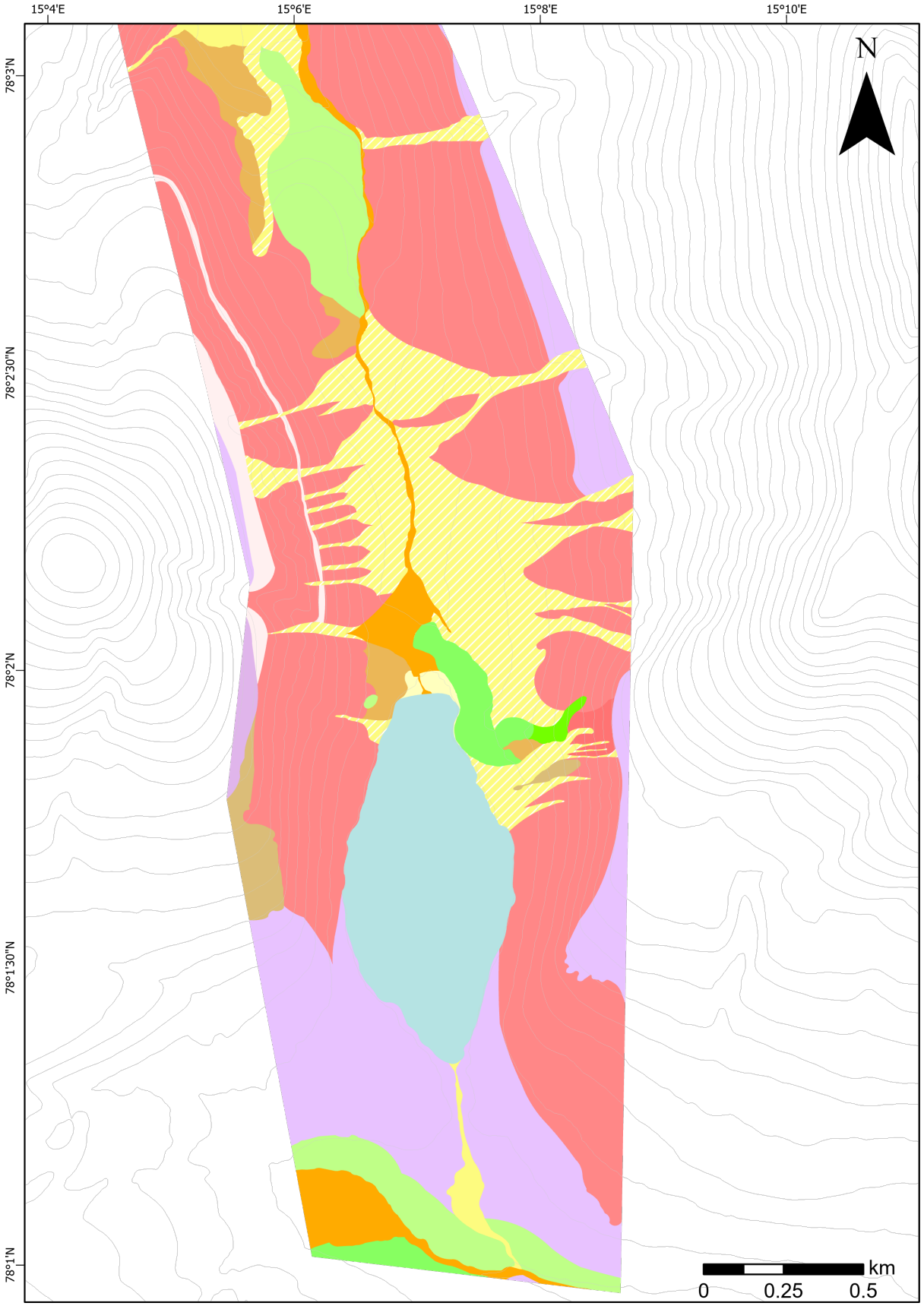

Figure 4.15: Geomorphological map of south part of Synndalen. Scale: 1:15.000. Base map: Contour map with 20 m interval, based on ArcticDEM (Porter et al., 2018)

4.4 Radiocarbon age determination

Within the river bed of a small stream, intact shells of the species *Mya truncata* and *Hiatella arctica*, marine bivalve molluscs, were found. *M. truncata*, with its common name the 'blunt gaper', or 'truncate softshell', is a marine bivalve mollusc from the family Myidae. Their shells can reach a size of about 2 - 7 cm. They are widespread throughout the Arctic and live from the lower shore down to depths of 70 m, burrowed in sand or sandy mud (de Kluijver et al., 2018). *H. arctica*, also known as the 'wrinkled rock-borer' or the 'Arctic Saxicave' is a marine bivalve mollusc in the family Hiatellidae. The shells can be up to 4 cm long and they are widespread throughout all oceans, ranging from the Arctic and Antarctic to subtropical and tropical waters. They occur from the lower shore well out onto the continental shelf, to depths down to 800 m (de Kluijver et al., 2018). Higher up in the section shell fragments were widespread, but it was not possible to identify the species to which these shell fragments belong.

Both the intact shells from the river bed and the shell fragments found highest in the stratigraphy were sampled. A total of three samples, one intact shell and two shell fragments, were sent to Bern for radiocarbon age determination (Table 4.1 *'Sample'*). The resulting radiocarbon ages issued by the LARA laboratory in Bern and corresponding 1σ intervals are presented in Table 4.1 under '*lab results*'. These ages are calibrated to calendar years by using the calibration software OxCal 4.4 (Ramsey, 2009). Despite the study area being localised in the High Arctic and as discussed in section **??**, the Marine20 calibration curve (Heaton et al., 2020) has been used to calibrate the radiocarbon ages. Table 4.1 '*Age Calibration*' presents the results after calibration according to Pieńkowski et al. (2022), using Marine20 and a ΔR value of -67 ± 37 years and presents the 1σ (68% probability range), 2σ (95% probability range) and median probability age.

The shell fragment found at the highest elevation in the stratigraphy (Synn-1-S3) does not have the youngest date, even though the deposit must be younger than the lower deposits from which Synn-1-S2 has been sampled. Within the 2σ ranges, all three ages overlap however. Furthermore, it is important to keep in mind that these shells have been reworked and not deposited in-situ. They have been eroded from previously deposited marine sediments, transported and redeposited. Hence, their ages do not strictly represent the age of the longshore drift deposit; it provides a maximum age.

Table 4.1: Radiocarbon age results and calibrated ages. ΔR value based on Pieńkowski et al. (2022)

		Parameter	**Synn-1-S2**	**Synn-1-S3**	**Synn-1-S5**
Sample		Description	Intact *Myatruncata* shell	Shell fragment	Shell fragment
		Sampling year	2021	2021	2021
		Latitude N.	78.077468	78.077342	78.077333
		Longitude E.	15.098083	15.099599	15.099426
		Elevation (m)	35	40.5	40
Lab results		Lab ID	BE-16699.1.1	BE-16700.1.1	BE-16701.1.1
		^{14}C age (yrs BP)	10251	10272	10532
		1σ (yrs)	35.45	35.56	35.02
		δ^{13}C	6.4	3.1	3.2
Age Calibration		Calibration curve	Marine20	Marine20	Marine20
		ΔR (^{14}C years)	-61 ± 37	-61 ± 37	-61 ± 37
	1σ {	Area enclosed (%)	68.3	68.3	68.3
		Cal. yrs BP age range	11189 - 11379	11198 - 11400	11592 - 11841
	2σ {	Area enclosed (%)	95.4	95.4	95.4
		Cal. yrs BP age range	11109 - 11533	11143 - 11572	11442 - 11954
		Median probability	11290	11317	11714

4.5 Complementary: Lacustrine core

Description

The core consists of a grey, unconsolidated mud, alternated by laminations of a 2-5 mm thick. In the first 37 cm, these laminations are reddish-yellow mud, although at 22 cm one dark grey layer with a thickness of approximately 3 mm exists that contains some medium grained clasts. In the rest of the core, the laminations are generally either dark grey or black, containing organic material. Only a 4 mm thick lamination at 53 cm and a 1.5 cm thick lamination at 57 cm are greenish grey. From 46 cm all the way to the base of the core, the organic material consists of very fibrous material; very thin and with a length of up to 2 cm. This organic material mostly aggregates within the black laminations, but also exists within the grey mud in lower densities. Especially in the lowest part of the core, three layers with a very high content of these organic fibres exist, almost consisting solely of organics. The lowest two of these layers (at 155 and 145 cm) have been sampled. The third sample is taken from the lowestmost part of the core in which still some organic material was observed, at 165 cm.

Interpretation

The anticipated radiocarbon dates will hopefully clarify if the different laminations within the core are yearly varves or if they represent multi-year events. None of these preserved lacustrine sediments are interpreted to originate from a pro-glacial environment, as larger clasts and coarser material are lacking. Therefore, the core is not expected to be long enough to aid with dating the most recent time the glacier drained into Synndalen, which could also constrain the age of the moraine next to the lake. However, obtaining dates on the deepest organic material in the core can hopefully provide an idea of the lacustrine sedimentation rate throughout its deposition time. This could give an idea of the (very) approximate length a future core would need to be to reach back to glaciolacustrine sediments.

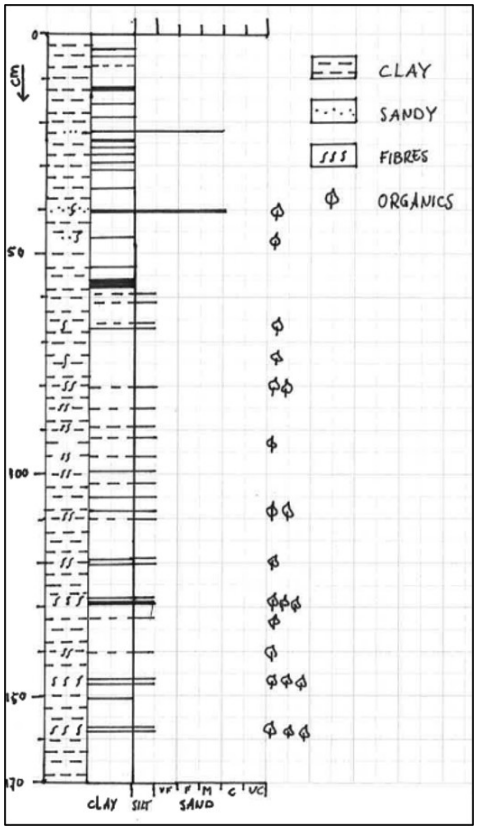

Figure 4.16: Log of core. VF: very fine grained; F: fine grained; M; medium grained; C: coarse grained; VC: very coarse grained.

5 Discussion

In this chapter the radiocarbon ages and their calibration are discussed in section 5.1. Discussion of the deglacial history, and presentation of a conceptual model of the valley-mouth and valley-head are found in section 5.2 and 5.3 respectively. Section 5.4 discusses the implications of the results in a wider, Quaternary - Holocene context and section 5.6 briefly discusses the post-glacial valley evolution. Finally, pitfalls of geomorphological mapping and suggestions for further research are discussed in section 5.6 and 5.7.

5.1 Radiocarbon ages

Several factors may influence the radiocarbon results of marine samples in general and molluscan shells in particular. The influence of different carbon sources on mollusc shells, fluctuations of reservoir ages through time and space and the limitations of available calibration curves all may result in extra uncertainties or can cause errors towards younger or older ages. Awareness of these uncertainties and error sources are therefore important, hence the following discussion.

5.1.1 Filter feeders

Marine bivalve molluscs are sessile, and should therefore in theory monitor the ^{14}C content of the sea water passing their dwelling site during their life time (Mangerud et al., 2006). Nevertheless, radiocarbon age determination of molluscs does come with some complications, which will be discussed below.

Molluscs are filter-feeders, meaning they consume particles suspended in the water (Allen, 2017). They build their carbonate shells with carbon from two sources; dissolved inorganic carbon (DIC), mainly bicarbonate, from the sea water and respired metabolic carbon. Metabolic carbon contribution is species, growth stage, and food availability dependent (Lartaud et al., 2010). Whereas carbonate derived from DIC has a radiocarbon signature matching that of the surrounding waters, this is not necessarily the case for metabolic derived carbon. Therefore, it would be useful to distinguish between carbon derived from particulate food and water, although identification of the carbon source is often impossible (Mangerud et al., 2006). The apparent ^{14}C age of particulate food is called the *food reservoir age* and may be both older and younger than the marine water reservoir age (Mangerud et al., 2006). As long as filter feeders feed on recently produced marine food, the food reservoir age should be negligible and not pose any problems for the determination of radiocarbon ages. It is therefore favourable that, when considering shells for dating, these filter-feeding species normally filter and digest particles, normally phytoplankton, suspended in sea water. However, also organic detritus on the sea bottom, including remnants of other marine organisms, may be re-suspended and thus be ingested by the filtering shells, 'contaminating' the food with old carbon (Mangerud et al., 2006). For this study however, this exposure of 'old' food is regarded to be of minor importance, as Colesdalen was filled in by ice until relatively recently before deposition of the sampled shells, leading to the expectation that the amount of old

marine organic detritus on the sea bottom was likely not of significant importance.

Another concern can be carbon derived from ambient sediment-pore-water or ground water, which, stemming from bedrock, sediments or oil and gas seepage, may have a different carbon sources than seawater and hence a different composition. Solution of carbonate rocks in this water can bring dissolved, depleted carbon into the sea water, resulting in too old apparent ages. The influx of runoff on the other hand, with negligible reservoir ages, can yield the opposite effect. Both of these two factors could play a role at our sample location. The bedrock in the hinterland consists of shale, silt-, and sandstone in which carbonate, although not predominant, is likely not absent. The shells were, however, also deposited right in front of a glacier front, with a corresponding fresh water influx. Nevertheless, Mangerud et al. (2006) did not find higher ΔR values for molluscs from locations where carbonate rocks or other old carbon were to be expected at the collection site compared to molluscs from areas without old carbon. Likely, these filter feeders did not digest much carbon derived from sediment. As the Svalbard samples from Mangerud et al. (2006) come from comparable locations as the ones in this study, it is assumed that the influence of old carbon will also not have been significant on the shells collected at our study site. This effect will therefore not be taken into account further, although it has to be kept in mind that no further proof is available to substantiate this hypothesis and uncertainties remain.

A last factor to take into account when dealing with molluscs, is that they build their shells during their entire life, fixing carbon during the shell building process. This means that the umbo of the molluscs will have a slightly higher radiocarbon age than the shell margins (Mangerud et al., 2006). Given the relatively short lifespan of many Arctic molluscs of 5 to 20 years and in the light of a significantly bigger error range than this life span, this 'mollusc reservoir age' is considered negligible for the purpose of this study.

5.1.2 The use of Marine20

The relatively small surface water ages that are currently observed in the North Atlantic did not prevail throughout the past. At present, the relatively constant reservoir ages over the North Atlantic are principally due to the North Atlantic Drift, which brings low-latitude surface waters into the Norwegian Sea. The cooling of these warm and saline surface waters at high latitudes induces active deep-water formation in these areas, which is associated with a large flux of atmospheric ^{14}C to the surface waters. In the past however, for example during the Younger Dryas stadial and during the LGM, the presence of large continental ice caps, the southward shifted polar front and the associated shift in deep-water-formation areas likely resulted in an important decrease in ventilation and, as a result, an increase in surface-water reservoir age, north of the polar front (Bard, 1988; Waelbroeck et al., 2001). Detailed sea-ice histories, and thus also ventilation, remain poorly constrained and are difficult to model in four dimensions. Hence, like earlier iterations of the marine calibration curve (eg. Reimer et al. (2013)), Marine20 is intended to be used in subtropical to temperate regions with no sea ice and not for calibration of samples from polar regions. Consequently, Heaton et al. (2020) explicitly advices against the use of their marine radiocarbon calibration curve in regions north of 50°N.

Although these concerns are valid, there are simply no better alternatives at hand. The alternative approach recommended by Heaton et al. (2020) of using regional 3D Large Scale Geostrophic Ocean General Circulation Models (LSG OGCM) for northern latitudes is problematic as these simulations only consider single climate scenarios, generate time-invariant ΔR_R values, are very complex and result in highly overestimated simulated reservoir ages (Pieńkowski et al., 2022; Butzin et al., 2017). Of course, it would be desired to solve the problem by developing a detailed sea-ice history based on robust chronologies. However, as such reconstructions are often based on radiocarbon age determinations, this approach is in danger of becoming circular (Pieńkowski et al., 2022). Hence, the strict application of Marine20 calibration to latitudes south

of 50°N excludes extensive areas of high latitude coasts, shelf seas and ocean for which no better dating alternatives are available, but which are of utter importance for the reconstruction of detailed Late Quaternary climate histories. Therefore, due to the lack of practical alternatives and in line with the recommendation of Pieńkowski et al. (2022), the technical limitations of calibrating the radiocarbon ages of the shell samples with Marine20 are accepted in this study.

5.1.3 Further considerations

Radiocarbon results with calibrations based on Pieńkowski et al. (2022) have been presented in table 4.1. Although these presented ΔR_R values apply, in the strictest sense, only for the period and oceanographic conditions for which they were calculated, they are assumed to be broadly applicable for the entire Holocene due to the relative continuity in oceanographic conditions and sea-ice cover throughout this time Pieńkowski et al. (2022); Mangerud et al. (2006); Mangerud and Svendsen (2017). Important to emphasize however, is that the calibrated shell ages in this study, ranging between ca. 11.3 to 11.7 cal ka BP, are from very early in the Holocene, and possibly even from the end of the YD. The YD was characterized by the presence of larger ice caps, more sea ice and an associated shift in deep-water-formation and hence residence times. Furthermore, the YD is characterized by a plateau in radiocarbon ages. The evolution of atmospheric ^{14}C concentration over time is not linear, but reveals variations with numerous distinct jumps (i.e., rapid change) and plateau-shaped (slow or no change, or even an inversion) structures, which are indicative of fluctuations in atmospheric ^{14}C concentrations (Sarnthein et al., 2020). These plateaus can further complicate age calibration. Therefore, as the calibrated ages are from very early in the Holocene, on the border with the Younger Dryas, this is potentially another factor that increases the uncertainties of the presented age calibrations. As no ΔR_R values are available that are specifically applicable to the YD on Svalbard, there are again no practical alternatives than to use the ΔR_R value constrained by Pieńkowski et al. (2022).

5.1.4 Inferences and implications

The calibration of radiocarbon ages is important as, by doing so, dates can be presented in a universally understood manner. Furthermore, the conversion of radiocarbon years into calendar-equivalent years is essential for meaningful comparisons to ages derived from different dating techniques. Consequently, despite the many associated uncertainties discussed, calibration, and the utilization of ΔR_R in the calibration process, is eminently preferable over no calibration (Pieńkowski et al., 2022). Therefore, the technical limitations that come with high-latitude marine radiocarbon age calibration, and the uncertainties related to dating of filter-feeders, have been acknowledged, but also accepted for the calibration of the acquired radiocarbon ages.

After calibration, the rounded median probability ages of the shells found in Synndalen are therefore: 11.3 cal. ka BP for Synn-1-S2 and Synn-1-S3 and 11.7 cal. ka BP for Synn-1-S5.

5.2 Deglaciation of the Synndalen valley-mouth

Based on the presented observations, interpretations, radiocarbon ages and cross-cutting relationships, the deglaciation of Synndalen is discussed. This section first focuses on the deglaciation of the valley-mouth, whereas the following section will discuss the glacial history of the head of the valley. For both locations, a conceptual model has been developed en is presented. Furthermore, time constraints and their implications are discussed.

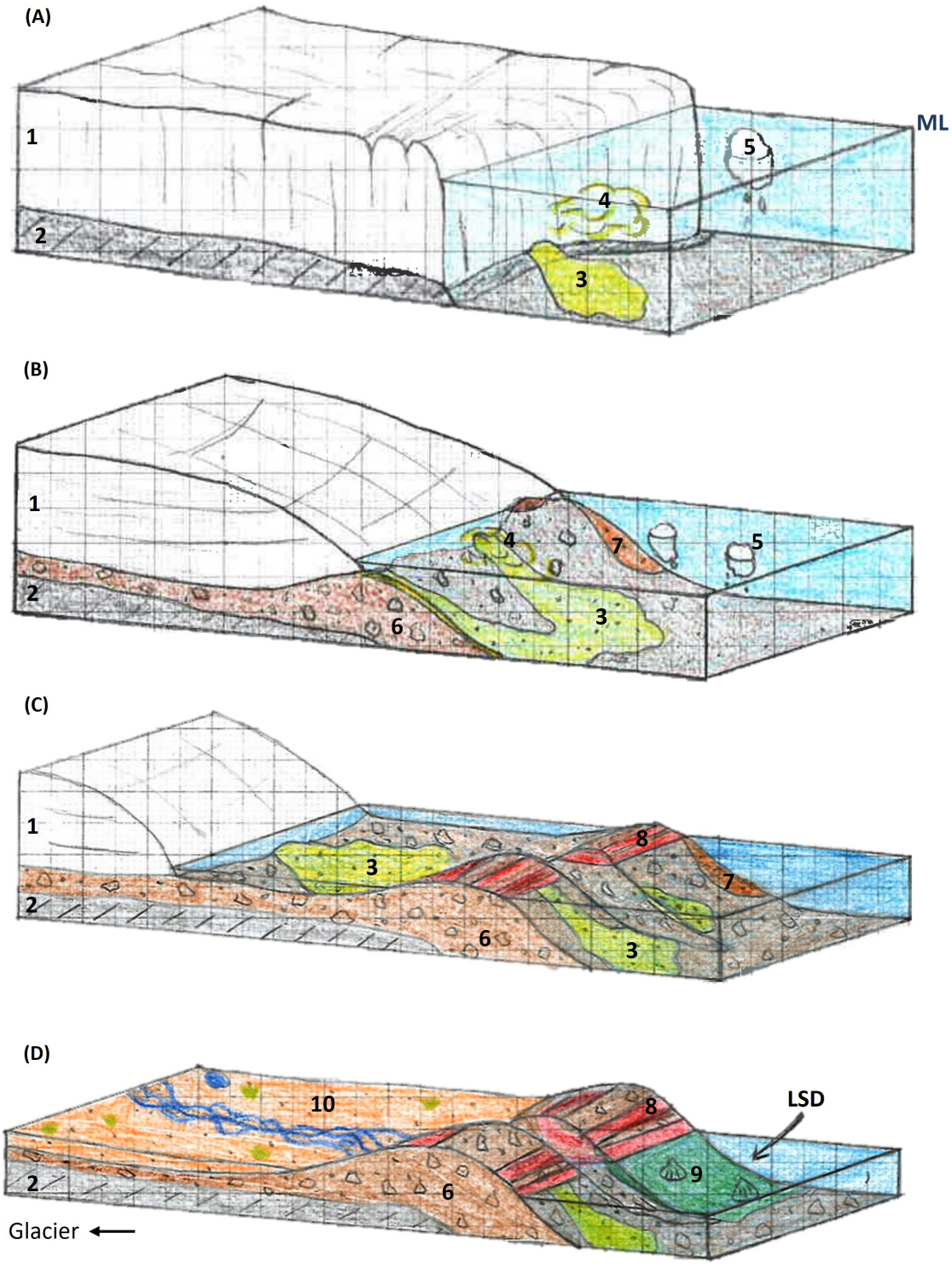

Figure 5.1: Conceptual model of the Synndalen valley-mouth. (A) Synndalen glacier after unsuturing from Colesdalen trunk glacier (subsection 5.2.1); (B) Stabilisation of ice in Synndalen and construction of the Synndalen valley end moraine (subsection 5.2.2.); (C) Retreat of Synndalen ice and formation of lagoon system behind the moraine (subsection 5.2.3); (D) Formation of the longshore drift deposit and deposition of the reworked shells (subsection 5.2.4). Sea level drops continuously over time. ML: marine limit; 1: Synndalen glacier; 2: Bedrock; 3: Ice-proximal glacio-marine deposits; 4: melt-water plume; 5: icebergs transporting IRD; 6: moraine, constituted of till; 7: lateral melt-water channel deposits; 8: beach deposits; 9: longshore drift deposits including shells; 10: floodplain deposits; LSD: Longshore drift. Not to scale.

5.2.1 Deglaciation of Colesdalen trunk glacier

As the trunk glacier that was flowing through Colesdalen during the Late Pleistocene retreated, the sea entered Colesdalen, a fjord at this time. When the Colesdalen glacier retreated back far enough, the Synndalen glacial system and the Colesdalen glacial system disconnected (Fig. 5.1.A). The moment of unsuturing must have been contemporaneous with the marine limit at the entrance of Synndalen, as relative sea level fall has been continuous throughout the Late Pleistocene and Early Holocene in Svalbard (Forman et al., 2004). After the glaciers unsutured, a calving front retreated further into inner Colesdalen, and the Synndalen glacier was at its maximum position, in contact with the sea.

5.2.2 Construction of Synndalen end moraine

After the disconnection with the Colesdalen glacial system, the end moraine at the mouth of Synndalen formed (Fig. 5.1.B). This moraine must have formed either while the glacier had stabilized at the end of the valley, or during a minor retreat and advance cycle, for which potential driving factors are discussed in subsection 5.2.6. As a glacial retreat would imply that the sea would have entered Synndalen, and as there are no signs of reworked or overridden marine deposits, such as shells, within the till constituting the moraine, this retreat cannot have been of significant magnitude. More likely is that, even though the glacier was in stable position, the flowing rate of this polythermal or warm-based glacier was significant enough to transport sediments and deposit the end moraine. The moraine must have formed subaquously, as marine deposits have been distinguished on different elevations on the moraine and sea level is known to have fallen continuously throughout this time, without any transgressions (Forman et al., 2004). As the highest sea level in the valley occurred simultaneous with the Colesdalen glacier retreat, before the formation of the Synndalen end moraine, the beach deposits on the end moraine do not represent the local marine limit.

While the Synndalen glacier was at its maximum extent, glaciomarine sediments were deposited within the shallow marine environment on the outer flanks of the moraine. Fine grained sediments settled down from meltwater plumes while larger clasts melted out of icebergs. On the eastern side, but likely also on the western side, a lateral meltwater channel drained around the emergent margins of the moraine into the Colesdalen fjord, building out submarine fans.

5.2.3 Glacial retreat

The location of the Synndalen glacier front cannot have been at the Synndalen valley entrance for a prolonged period. The sea level is known to have fallen rapidly during the Early Holocene, as a result of significant glacio-isostatic rebound during fast deglaciation (Fig. 2.2). If the end moraine would have still been actively forming during times of sea level fall, this would have distorted the preservation of the beach deposits on top of the moraine, reworking these deposits. Hence, as these deposits have been preserved, it can be inferred that the glacier must have retreated away from the moraine before significant sea level fall. The inside of the moraine has been wave-washed. Therefore, following the glacier retreat into the valley, either the sea must have entered through the incised moraine, forming a lagoon, or a pro-glacial lake must have formed. The highest wave-washed deposit on the inside of the moraine was found at 58 m elevation, just under the location of Camp 1 (Fig. 4.7.C). Fig. 5.2.A shows the extent of the 58 m contour line into the modern valley. As only small parts of the (modern) moraine are higher than 58 m, it is deduced that the option of a tidal lagoon is more likely than that of the formation of a pro-glacial lake; the water behind the moraine is assumed to have been in contact with the sea (Fig. 5.1.C). As the moraine must have provided some shelter, the conditions were likely relatively calm in the lagoon. Furthermore, the lagoon sheltered the area outside of the moraine from the influx of glacial sediments. The sediment assemblages that must have been deposited within the

pro-glacial lagoon environment have not been observed and have either not been preserved, or have been covered or reworked by more recent processes, such as fluvial infill or solifluction. As the lagoon must have formed simultaneously with glacier retreat, the glacier must have terminated in the lagoon for some period in time. It is unknown how fast and far the glacier retreated during the existence of the lagoon, but over time, with continuous retreat and continuous sea level fall, the glacier must have gradually evolved into a land terminating glacier. While the glacier retreated, it may have stabilised at the steep bedrock steps halfway up the valley, as these contain a till deposit that potentially is a retreat moraine and in geometrical respect form a logical place for the glacier front to stabilize for some time.

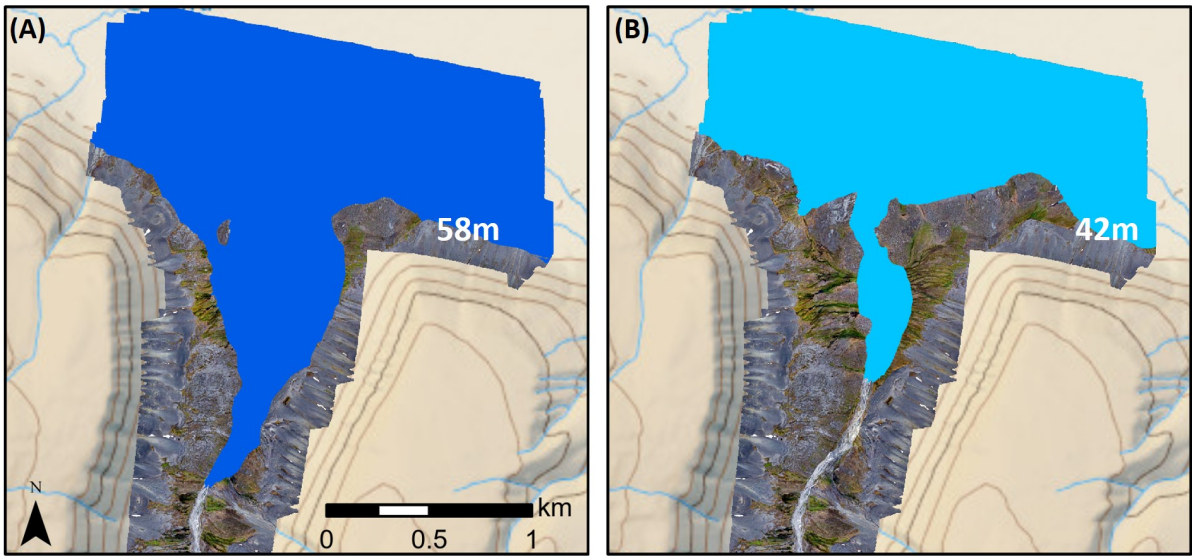

Figure 5.2: Contour line on Ortho_Camp1 of (A) 58 m a.s.l. and (B) 41 m a.s.l.

5.2.4 Longshore drift

The highest elevation where the longshore drift deposits have been found is at 42 m a.s.l.. The blue polygon on Fig. 5.2.B marks all the elevations below the 42 m isoline and shows that the previously described lagoon would have diminished in size drastically with sea level fall, to a tidally-influenced river outlet. Synndalen was thus above sea level and must have been covered by a large floodplain (Fig. 5.1.D). The sedimentary sequence that contained the longshore drift facies was capped by beach deposit and can therefore be said to have been preserved unimpaired. The absence of ice rafted debris in the longshore drift deposit is in line with the previous retreat of the glacier into Synndalen.

5.2.5 Temporal constraints

As became clear from the reconstruction presented above, the ages from the mollusc fragments within the sandy gravel longshore drift deposit (11.3 - 11.7 cal. ka BP) provide a minimum-limiting age constrain for the glacial retreat at the mouth of Synndalen. As the longshore drift deposits potentially only have been deposited centuries after the actual glacial retreat, it is unknown how tightly the ages from these raised marine sediments constrain the deglaciation ages. Ideally, more geochronological data would be available to better constrain marked events of the deglaciation of Synndalen. As these constraints are lacking, it is attempted to place the events in a temporal context based on described cross-cutting relationships and field and geochronological data of the Isfjorden region accumulated in published literature.

Firstly, the beach ridges on the inside of the end moraine constrain the minimum age of glacial retreat tighter

than the longshore drift deposits. No direct age of these beach-deposits has been obtained, as they were barren of shells. However, the elevation of the beaches at 58 m a.s.l. is instructive. The elevation of the beach deposit on top of the longshore drift deposit at the location where the shells were sampled is 41 m a.s.l.. Hence, the difference in elevation between the minimum height of the sea level on the inner side of the moraine and that of the dated shell deposit is 58 m - 41 m = 17 m.

While there is a large amount of variability, the Late Pleistocene and Early Holocene exhibit the fastest rates of recorded isostatic uplift (Farnsworth et al., 2022; Forman et al., 2004). Minimum uplift rates from raised marine shorelines have been derived from various locations and have been suggested to range between 1.0 - 2.5 m of uplift per 100 years during the Early Holocene on Svalbard (Farnsworth et al., 2020; Forman et al., 2004; Salvigsen and Osterholm, 1982). On western Svalbard however, relative sea level curves generally suggest lower rates of Late Glacial emergence, around 0.5 m per 100 years (Forman, 1990; Forman et al., 2004; Farnsworth et al., 2022). Nevertheless, Farnsworth et al. (2022) presents Late Glacial emergence rates that range between 1.5 - 4.5 m per 100 years, and likely on the order of 3 m per 100 years. This rate is based on a combination of dated shell fragments and well-defined Vedde Ash ages in Heftyevatnet, a small lake in inner Grønfjorden, only 24 km away from the shell sample location of this study. Due to this relatively short distance, this rate is assessed as the most viable for Synndalen.

Although the emergence pattern typically approximates an exponential curve and is thus non-linear, these emergence rates can serve as a rough approximation of the emergence rates at Synndalen during the Late Glacial and Early Holocene. Here, as a rough estimation, the rate is assumed to have been between 1 - 3 m per 100 years. When taking the 17 m of isostatic uplift between the different beach deposits into account, the difference between deposition times can be roughly estimated to range between 600 to 1700 years. This would imply the age of the highest beach deposits on the inside of the moraine, at 58 m and constraining the minimum age of glacier retreat, is between 11.9 and 13.4 ka BP. It is acknowledged that this extrapolation of very sparse data potentially serves as an over-interpretation of limited knowledge, nevertheless, it is interesting to note that this entire age range falls outside of the Early Holocene and would constrain the glacial retreat to the YD, or even the pre-YD.

By extension, the same line of reasoning could be used to constrain the maximum age of the end moraine. The separation of the Colesdalen and Synndalen glacial systems occurred contemporaneous with the marine limit at the mouth of Synndalen and coincided with the initiation of the development of the end moraine at the mouth of the valley. Nearby local marine limits range between 62 to 70 m (mouth of Bolterdalen: 62 m, mouth of Endalen: 63 m, Isdammen: 65 m, mouth of Adventdalen: 70 m (Lønne, 2005); mouth of Grønfjorden: 70 m (Farnsworth et al., 2022), see Lønne (2005) for map of named locations within Adventdalen). From these locations, Synndalen's location is most comparable to Isdammen's location; approximately 9 km away from the mouth of the fjord. Therefore, when assuming a marine limit of 65 m and the same emergence rates of 1 to 3 m / 100 years, the isostatic rebound of 24 m between marine limit and deposition of the shells is roughly estimated to have occurred in 800 to 2400 years and dates to 12.1 - 14.1 ka BP. With a more conservative approach, the level of the marine limit could be assumed to have had an elevation of 70 m, resulting in a maximum constraining age of the moraine of 12.3 - 14.7 ka BP.

5.2.6 Glacier dynamics

Based on a series of glacial advances in inner St. Johnsfjorden, Farnsworth et al. (2017) developed a conceptual model that explains small advances of tributary glaciers (Fig. 5.3). This model provides a potential explanation to the formation of the end moraine at the Synndalen valley-mouth. The concept is that small advances can occur due to unbalanced glaciodynamic conditions, and not in direct response to climate. First, the tributary glacier, the Synndalen glacier in this case, is at equilibrium and has a stable profile given the

back-stress caused by the primary trunk glacier, here the Colesdalen glacier. Retreat of this trunk glacier perturbs the balance of the tributary. This leads to a re-organization of the over-steepened glacier profile, which is glaciodynamically expressed as an advance. Therefore, after unsuturing of the Colesdalen and Synndalen glacier, the Synndalen glacier likely advanced until it reached a new dynamic equilibrium state that was marked by a new quasi-stable marginal position due to the lack of back-stress (Wuite et al., 2015). This shedding of accumulated mass is what potentially resulted in the deposition of the end moraine at the Synndalen valley-mouth. Farnsworth et al. (2017) chose to exclude a sea level component in the conceptual model but emphasizes that this response might be amplified in the marine environment. As the Synndalen end moraine has been formed subaquously, a sea level component might indeed have been of importance.

This conceptual model provides a potential explanation to the numerous descriptions of glacier advances on Svalbard that occurred during periods of unfavourable climate conditions for glacier growth (Lønne, 2005; van der Bilt et al., 2015). Furthermore, this model explains why the Synndalen glacier was not at its maximum extent for a prolonged time period, as the advance was unsustainable and lead to an unbalanced glacier profile.

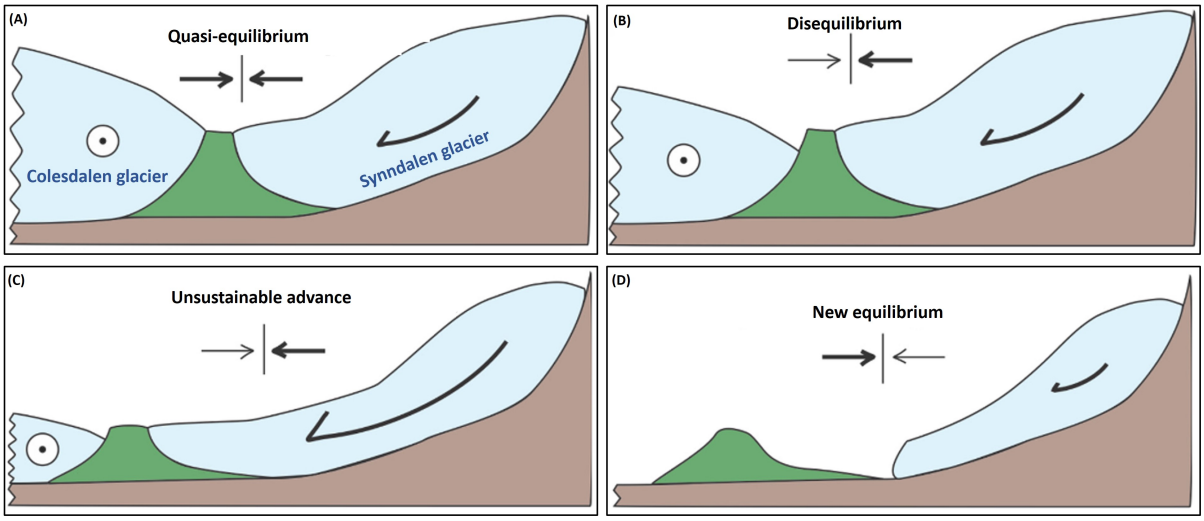

Figure 5.3: Conceptual model for a dynamic glacier advance of the Synndalen glacier, resulting in the formation of the end moraine in the valley-mouth and resulting from unbalanced equilibrium. (A) The Colesdalen trunk glacier is in balance and the Synndalen tributary glacier is in equilibrum with the back-stress of the trunk glacier. (B) Retreat of the Colesdalen trunk glacier created an unbalanced system. (C) The tributary Synndalen glacier re-organized its over-steepened surface profile in response to the release of back-stress, which resulted in an unsustainable advance of the ice-front. (D) The Synndalen glacier retreated back to an equilibrium state in balance with the new conditions and pursues a new balanced profile. Figure modified from Farnsworth et al. (2017).

5.3 Glacial readvance in inner Synndalen

As the attempt to beryllium date the boulders on the moraine has unfortunately been unsuccessful, no absolute time constrains are available to date the glacial events at the valley-head. Lab results attempting to obtain chlorine ages of the rock samples and radiocarbon ages of lacustrine organic materials are still in process and will hopefully provide more decisive information in the future. Despite the lack of absolute temporal constraints, the most likely scenario are hypothesized below based on morphology and valley geometry.

5.3.1 Formation of the moraine

The moraine in inner Synndalen is interpreted to have been formed due to a glacial readvance of past Passfjellbreen. This is in line with the deducted flow direction from S-S-W direction. Passfjellbreen's main drainage

valley is Istjørndalen, so this readvance must have been significant enough for the ice to 'spill-over' into Synndalen (Fig. 5.4). The existence of a smaller glacier on the eastern valley side next to the lake around the same time could explain the formation of the small E-W trending moraine. The confluence of this small glacier and Passfjellbreen could have resulted in a locally altered flow direction, resulting in the differently trending part of the moraine. The existence of a small glacier here is in line with the slope geomorphology and with the formation of the protalus rampart right next to this assumed glacier. Not enough data is available to determine the driving factors of this glacial readvance. Since no trunk glacier was involved, a dynamic advance as depicted in Fig. 5.3 is ruled out. No characteristics of a past surge, such as crevasse squeezed ridges or flutes (Benn and Evans, 2014), have been distinguished in either Synndalen, Istjørndalen or Hollenderdalen. Nevertheless, these characteristics have potentially not been preserved, so internal dynamic driving forces cannot be excluded. As Passfjellbreen does not show signs it has ever experienced another surge, and surges are often quasi-periodic, this scenario is considered less likely than a climatically driven readvance.

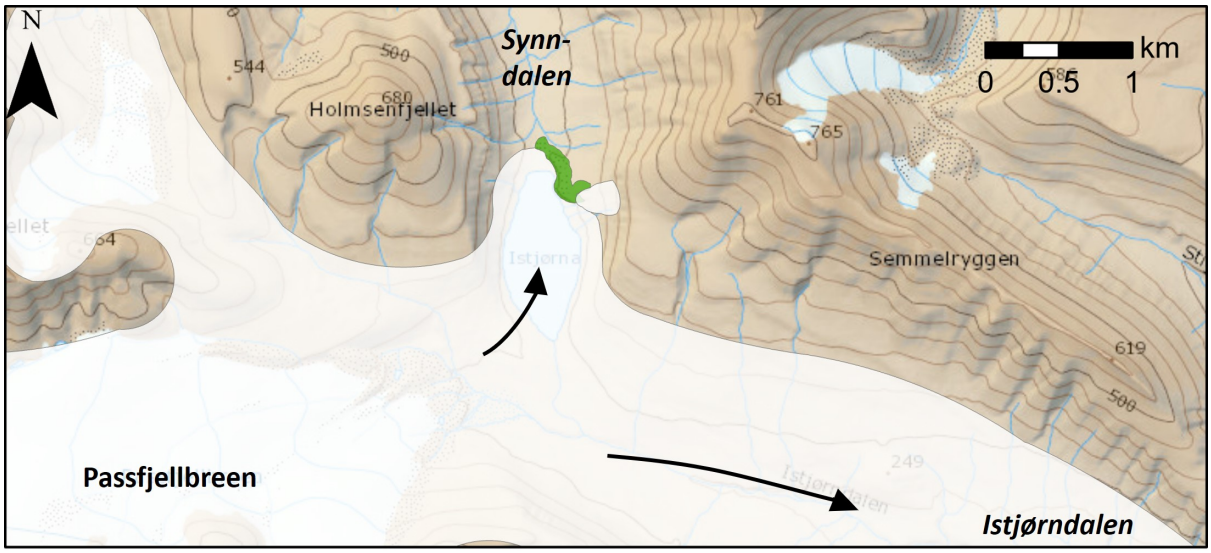

Figure 5.4: Readvance of Passfjellbreen, arrows depict ice flow direction. The ice mainly drains through Istjørndalen but also spills-over into Synndalen to form the moraine. The existence of a small glacier on the slope above the moraine could explain the formation of the E-W trending part of the moraine. Basemap (Institute, 2014)

5.3.2 Alternative hypotheses

An alternative hypothesis is that the glacier that formed this moraine was not Passfjellbreen, but a small, local glacier on the valley slope to the north of the moraine. There seems to be enough space on the valley for a small glacier to form and also nowadays there is a relatively high amount of snow still present in summer, compared to other parts of the slope. However, this supposed glacier would have really had to fan out, in up-stream direction, to form this moraine. Furthermore, no till or other glacial landforms which would trace the supposed glacier margin are observed to the north of the moraine. Therefore, all in all, this hypothesis is considered highly unlikely.

5.3.3 Temporal framework

Despite the absence of absolute chronological data, a hypothetical timeframe is nevertheless presented here. As discussed, it is assumed that the moraine has formed as a result of a glacial readvance of Synndalen, and that this readvance was climatically driven. Based on the literature available on Svalbard's Holocene glacial history (Section 2.3), glacial readvances are expected to have either occurred during the Early Holocene

(11.7-8.2 ka BP) or during the Neoglacial period and Little Ice Age (4.0 ka BP – 1900 AD). Passfjellbreen has a very clearly distinguished Little Ice Age moraine system several hundred metres away from the modern glacier extent. When comparing this system with the moraine system in inner Synndalen, it is obvious that the Synndalen system is much older. The moraine is much more subdued and buried ice has had the time to melt out. The Synndalen moraine is extensively covered by lichens and other vegetation, as are many other areas in both Synndalen and Istjørndalen. The western part of the Synndalen moraine has not been preserved and in general, only sparse till covers are still distinguishable on the surface. The Neoglacial is not known for large advances of valley-glaciers (Farnsworth et al., 2020), but even if this readvance would have occurred right at the beginning of the Neoglacial, approximately 4 ka BP, these landforms would be expected to look fresher than they do now. Also, apart from the moraine, more distinct traces of this glacial advance would be expected to be preserved until this day, around the lake, but also in Istjørndalen. Therefore, the readvance is expected to not have happened during the Neoglacial and is interpreted as a Late Glacial or Early Holocene glacial readvance. In the case that the readvance was the result of a surge-event, the same reasoning in age can be followed. Since the dated longshore drift deposit do not constrain the minimum-limiting age of the valley-mouth deglaciation tightly, it is not impossible that this inner-valley readvance had already occurred before deposition of the dated shells. Therefore, in the context of the conceptual model of the deglaciation of the valley-mouth (Fig. 5.1), the readvance in the inner-valley could have occurred either before or after the stage in Fig. 5.1. Hopefully, future cosmogenic nuclide results will help to better constrain the age of this moraine.

5.4 Synndalen's deglaciation in a Late Quaternary - Holocene context

5.4.1 The deglaciation of the valley-mouth

According to Farnsworth et al. (2022), the Heftyebreen moraine, with a deposition age ranging between 12.8 to 12.5 cal. ka BP, is the first and (as of yet) only glacier margin constrained to the YD chronozone in Svalbard. While numerous other moraines have been constrained to the Late Glacial - Early Holocene transition, these were all not completely constrained to within the YD chronozone (Mangerud et al., 1992; Lønne, 2005; Larsen et al., 2018; Farnsworth et al., 2018). Therefore, the results of the approximate calculations presented in subsection 5.2.5, which constrain the end moraine at the mouth of Synndalen to the YD, are especially interesting. The small readvance at the mouth of Synndalen, which is interpreted to have been of dynamic origin, implies that the Colesdalen trunk glacier already retreated far into the valley before or during the YD. This would mean deglaciation of the main valley occurred earlier than generally stated in the literature (Farnsworth et al., 2020). These results could therefore potentially be of importance. It is however important to realise that both the presented calculations and the obtained calibrated radiocarbon ages are met with significant uncertainties. Hence, better time constraints are necessary and the need for further research is emphasized.

5.4.2 Passfjellbreen's readvance

Until recently, the deglaciation of Svalbard was considered as being continuous with uninterrupted retreat, partly due to the apparent absence of moraines or other ice-marginal landforms dating to the YD or Early Holocene (Forwick and Vorren, 2009; Hormes et al., 2013). Recently however, an increasing number of ice-marginal landforms deposited by glacier readvances during the Late Glacial-Early Holocene have been identified around Svalbard, showing that tributary ice margins (from cirques, valleys and outlet glaciers) exhibited readvances after the Svalbard fjord systems became ice-free and during overall warm climatic con-

ditions (section 2.3). For example, at least six readvances during the Late Glacial and Early Holocene have been identified at the west coast of Spitsbergen, ranging from between 10 to 12.8 cal. ka BP. The oldest glacial readvance is constrained by the previously discussed Heftyebreen Moraine during the YD (Farnsworth et al., 2022). Salvigsen et al. (1990) described a glacial readvance of Esmarkbreen shortly after 10.3 cal. ka BP, where Lønne (2005) identified another brief glacial readvance in Bolterdalen during roughly the same period. This readvance is believed to have been climatically driven, lasted for several decades (from 10.4 - 10.9 cal. ka BP) and the maximum ice-front position reached around 7 km further than the present ice margin. Larsen et al. (2018) identified two glacial readvances in tributary valleys to van Mijenfjorden, both well outside the LIA margins. One of these readvances is interpreted to have been a dynamic response to regional deglaciation of the main fjord, whereas the other occurred roughly 1.5 ka later during a relatively warm period, which may have been characterized by increased moisture availability. A thrust moraine in central Tempelfjorden has also been linked to a glacial readvance during the Late Glacial (Forwick and Vorren, 2010). Additionally, multiple readvances have been identified in north-west Spitsbergen (Henriksen et al., 2014; van der Bilt et al., 2015) and the east coast (Farnsworth et al., 2018; Flink et al., 2018).

For the majority of these Late Glacial and Early Holocene glacial readvances, an ice margin position has been identified that extended well beyond the maximum LIA extent. These results correlate with the findings of this study of a glacial readvance in Synndalen during the Late Glacial or Early Holocene and confirm that glacier margins were more complex and dynamic during the Late Glacial than previously thought. Despite an increasing number of these dated ice margins with enhanced chronological constraint, no clear synchronicity among Late Glacial - Early Holocene glacier fluctuations has yet been identified and it can often not be validated if readvances are controlled by internal glacier dynamics or by regional mass balance trends. In general however, the highest frequency of Early Holocene glacier readvances occurred between 11-10 cal. ka BP (Farnsworth et al., 2020). Despite the generally unfavourable conditions for glacier growth, with summer temperatures reaching up to 7°C warmer than today, warmer ocean bottom waters and rising summer insolation (van der Bilt et al., 2016; Farnsworth et al., 2020; Mangerud and Svendsen, 2018, section 2.3), different explanations and suggestions for climatic readvances have been proposed. For example, increase in ocean temperature may have resulted in enhanced moisture supply (Larsen et al., 2018).

5.5 Post-glacial evolution of Synndalen

After deglaciation, landforms in Synndalen formed or evolved further, often greatly impacted by permafrost and periglacial processes. Many different slope processes are at play in the valley and the pronounced, active, rock glaciers are characteristic for the prevalent mountain periglacial landscape. To obtain a better understanding of the post-glacial evolution of Synndalen, it would be interesting to obtain ages on the two different generations of these rock glaciers. As the upper layer on all rock glaciers is basically uncovered by vegetation and has very steep slopes of up to 40°, they are interpreted to be young, most likely originating from the LIA. The lower layers, with significantly more vegetation cover and slightly more subdued slopes (around 34°-36°), are interpreted to be an older and less active rock glacier generation. Based on the available data, it is currently impossible to determine their age, although it is known that these rock glaciers must be younger than the deglaciation ages of the valley-mouth, as inner Synndalen was still ice-filled by this time. If the chlorine dating in inner Synndalen proves to be successful, it could potentially also be performed on a talus-derived rock glacier to obtain formation ages (Amschwand et al., 2021; Hippolyte et al., 2009). Furthermore, rock glaciers contain massive ice that may be useful in paleoclimate studies, and interpretation of geochemical ice-core records from one of the rock glaciers may present further information on Synndalen's post-glacial evolution (Konrad et al., 1999).

5.6 Potential and pitfalls of geomorphological mapping

Geomorphological mapping is a well-established method for examining landscape evolution and earth surface processes in different environmental contexts. It can provide essential geomorphological frameworks for establishing glacial chronologies and serve as a helpful tool for reconstructions of the extent, dimensions and dynamics of former (or formerly more extensive) ice masses (Chandler et al., 2018). Furthermore, it can provide parameters to constrain and test numerical simulations. Nevertheless, it has to be acknowledged that the geomorphological mapping process is to some extend subjective and depends on the author. Mapping styles and interpretations may highly differ and can depend on skill, philosophy and experience of the mapper, which can significantly impact the outcome. As geomorphological mapping often forms the basis of a wide range of interpretations, any errors and uncertainties incorporated in landform interpretations and the geomorphological map may propagate into subsequent glacial reconstructions (Chandler et al., 2018). Therefore, mapping errors and uncertainties should be explicitly reported, acknowledged and of course minimized. Below, different approaches that have been used to ensure the robust assimilation of data are discussed.

To start with, one way to minimize subjectivity as much as possible, is the incorporation of established standard guidelines. An example is the rock glacier inventory guideline (RGIK, 2022) that is used in this study. Furthermore, to gain a wider range of perspectives and to prevent tunnel vision, the mapping process was enriched by discussions with several geomorphologists, sedimentologists and cartographers. A great approach to minimize subjectivity and individual perceptions would be to have multiple authors map the same area and compare results. Unfortunately, this is a time and money intensive approach that is often, for example in the current study, unrealistic.

Geomorphology often adopts an inductive approach, where collected observations are used to argue towards a particular conclusion. This is a valid approach, although it can also be misleading; the explanation of a certain set of observations can appear very persuasive or self-evident, but there may be other scenarios that are also consistent with the same observations (Popper, 1972; Chandler et al., 2018). A better approach is an inductive-deductive approach, where after the first data collection, preliminary interpretations are used to predict the outcome of new observations, which can subsequently be used to test and refine the interpretation (Chandler et al., 2018). An example of the use of an inductive-deductive approach in the current study is that, after geomorphological mapping and sedimentological analysis around Camp 1 on the west side of the moraine, hypothesis were formulated anticipating the existence of certain landforms on the east side of the moraine. Observations on the east side indeed confirmed these hypothesis and therefore allowed for testing of achieved understanding.

Of course, a large factor reflecting the accuracy and precision of a map is the detectability of landforms and the complexity of morphologies. The reconstruction of glacial histories is especially difficult due to the time transgressive nature of ice sheet growth and decay and the superimposition and partial to total reworking of the evidence of previous events (Benn and Evans, 2014). As the preservation of landforms can vary strongly, mapping and landform interpretations are often biased to the youngest process. Often, definitive interpretations of glacial landforms, and glacial landscapes as a whole, cannot be made on the basis of surface morphology alone. Additional field evidence may be highly relevant. Combining the mapping process with detailed sedimentological investigations can aid the inductive-deductive process and help to avoid issues related to equifinality, whilst obtaining more robust chronological data can be fundamental for glacial reconstructions (Chandler et al., 2018). In general, a multi-proxy, holistic approach will lead to more reliable interpretations and has therefore been pursued in the current study, by combining surface morphological interpretations with sedimentological investigations, remote analysis, radiocarbon age determinations of organic material and the attempt of cosmogenic nuclide dating. However, there is room for improvement, especially to obtain a better temporal framework. Therefore, different methods that could be incorporated within the multi-proxy

approach in the future are discussed in the following section.

To conclude, mapping is ideally an iterative process that involves several consultations of field mapping, remotely sensed data and field checking. The quality of the map and associated interpretations could have been improved by an extra fieldtrip to Synndalen to verify interpretations based on remote sensing analysis and to clarify uncertainties. This would also have allowed the acquisition of more drone imagery to obtain a more complete remote sensing dataset. Nevertheless, notwithstanding the battery issues during the droning campaign, the wide array of remotely-sensed datasets used within this study accurately enabled remote sensing interpretations. Lastly, mapping has been conducted in a GIS software to facilitate georeferencing and an easy transfer between users.

5.7 Recommendations for further studies

The current study has provided new insights into the Late Pleistocene and Holocene glacial history of Synndalen. The presented glacial history is still fragmented however, and uncertainties remain. Here, different proxies and methods are discussed that could improve knowledge on outstanding uncertainties.

First and foremost, better age constraints are necessary, on both moraines, but particularly the moraine next to the lake, to allow for a better quantification of the timing and length of the Early Holocene readvance in inner Synndalen. Hopefully, chlorine dating of the rock samples at the University of New Hampshire will be successful. Chlorine dating is a form of cosmogenic nuclide dating and involves the measurement of ^{36}Cl isotopes, which build-up in rock minerals predictably over time when rocks are exposed to sunlight, due to bombardment of the upper few metres of the earth's surface by cosmic rays (Darvill, 2013). If successful, this method can date the length of time the sampled boulders have been exposed to sunlight, and thus when the moraine has formed and the glacier retreated.

Additionally, the boulders that were sampled on top of the moraine were extensively covered by lichens, hence, lichonometry, a method for dating Holocene rock surfaces, could be useful. Lichonometry uses the size of the largest lichen to provide a minimal age of the originally fresh rock surface that it colonised, hence dating the time since the freshly deposited rock became stable. Growth rates can be obtained by comparing with a suitable calibration curve, based on maximum lichen sizes on substrates of known ages (Bradley, 1999; McCarthy, 2002). Lichenometric dating is highly critisized however, especially due to the, often unjust, assumption that the largest lichen(s) colonized soon after deposition and will survive indefenitely (Osborn et al., 2015; Rosenwinkel et al., 2015). Nevertheless, lichonometry might have potential for confirming the hypothesis that the moraine has been formed during the Early Holocene, as opposed to the Neoglacial period, as for this, no precise dates are necessary. Added advantages are that this method is straightforward and inexpensive.

A third method that has the potential to obtain age constraints on the glacial readvance is to obtain a longer lacustrine core from Istjørna. If this core would be deep enough, it would likely include valuable information on the glacial readvance, as this readvance must have completely covered Istjørna. During the glacier's retreat, Istjørna must have been a pro-glacial lake, until Passfjellbreen continued to only drain into Istjørndalen again. (Glacio-)lacustrine deposits of these events, especially if they contain organic material, would therefore be extremely beneficial to constraining the age of the readvance of the glacier,

Ground penetrating radar (GPR) could be used to assess internal structures of the moraine complexes, or for example the landslide-connected rock glacier. Subsurface profiles of these landform could allow for the distinction of ice cores or internal deformation structures. Furthermore, GPR could also be used to determine Istjørna's bathymetry, and even the nature of its bottom sediments (Sambuelli and Bava, 2012).

At the mouth of Synndalen, it would be helpful to have a better constrained sea level curve and a better estimation of the marine limit. To achieve this, different locations within Colesdalen or its tributary valleys could be assessed, mapped and sampled. In general, a geomorphological assessment of the surrounding valleys would be of great added value to better understand the deglaciation of Synndalen, but also to better place this deglaciation in a spatial context, and achieve a better understanding of driving factors. Especially the geomorphological mapping of Istjørndalen and Hollenderdalen would be intriguing, as these valleys are both connected to Passfjellbreen and should therefore contain fingerprints of the same glacial-deglacial advance cycles.

The application of numerical models could serve as a more quantitative approach. Glacio-isostatic models, based on empirical reconstructions as boundary conditions, have the potential to improve the local sea level curve, which could in turn help to better constrain the temporal framework presented in section 5.2.5. In the South of Synndalen, the valley dimensions could serve as boundary conditions to create a numerical glaciological model to quantify how big an ice advance of Passfjellbreen has to be to not only flow through Istjørndalen, but also through Synndalen. If advanced further, such a model could even have the potential to simulate moraine formation as to better understand the processes that have been at play.

6 | Summary and conclusions

This study has reconstructed the Late Glacial and Holocene deglacial history of Synndalen by unravelling its geomorphological evolution. The main conclusions of this study are as follows:

- The radiocarbon ages of three marine bivalve molluscs, derived from the longshore drift deposit on the NW side of the valley-mouth end moraine, range between 10251 and 10532 ^{14}C yrs BP. Despite uncertainties associated with high-latitude marine radiocarbon age calibration, these radiocarbon ages have been calibrated to 11.3-11.7 cal. ka BP. These ages provide a minimum-limiting age constrain for the glacial retreat at the mouth of Synndalen.
- The deglacial history of Synndalen is characterised by the following stages:
    1. Disconnection from the Colesdalen trunk glacier: As the Colesdalen trunk glacier retreated, the Synndalen and Colesdalen glacial systems disconnected. The Synndalen glacier now terminated into the sea at the valley-mouth, contemporaneous with the marine limit.
    2. Minor readvance constructing the moraine: A minor retreat and advance cycle formed the end moraine at the valley-mouth, subaquously. This readvance is considered to have been mainly dynamically driven.
    3. Glacial retreat: While the glacier retreated into the valley, a pro-glacial lagoon developed between the moraine and the glacier front.
    4. Further retreat: Glacier retreat continued. The shoreline retreated due to progressive sea-level fall and a flood-plain developed in the Synndalen glacial forefield. Sediments and shells transported by longshore drift were deposited on the north-west of the moraine and have been dated to 11.3-11.7 cal. ka BP.
    5. Early Holocene glacial readvance: After further retreat, the glacier readvanced during the Early Holocene and formed the moraine at the valley-head.
    6. Post glacial evolution: After deglaciation, the valley has greatly been impacted by periglacial processes and landforms related to permafrost are widespread.
- It has been inferred that the Synndalen glacier must have been a polythermal valley glacier during the Late Glacial and Early Holocene.
- Based on very approximate age constraints, the formation of the moraine is constrained to the YD. This would imply that the deglaciation of Colesdalen already occurred earlier than generally considered. As of yet, the Heftyebreen moraine is the only glacier margin on Svalbard that has been constrained to the YD chronozone (Farnsworth et al., 2022). Better age constraints are needed and the need for further research is emphasized.
- The inner-valley readvance adds to an increasing number of identified Late Glacial - Early Holocene readvances on Svalbard. No clear synchronicity has yet been identified and driving forces are still unclear.

Bibliography

Aagaard, K., Foldvik, A., and Hillman, S. (1987). The west spitsbergen current: disposition and water mass transformation. *Journal of Geophysical Research: Oceans*, 92(C4):3778–3784.

Ahlmann, H. W. S. (1933). Scientific results of the swedish-norwegian arctic expedition in the summer of 1931. part viii. glaciology. *Geografiska Annaler*, 15(2-3):161–216.

Allaart, L., Müller, J., Schomacker, A., Rydningen, T. A., Håkansson, L., Kjellman, S. E., Mollenhauer, G., and Forwick, M. (2020). Late quaternary glacier and sea-ice history of northern wijdefjorden, svalbard. *Boreas*, 49(3):417–437.

Allen, M. J. (2017). *Molluscs in archaeology: Methods, approaches and applications*, volume 3. Oxbow Books.

Amschwand, D., Ivy-Ochs, S., Frehner, M., Steinemann, O., Christl, M., and Vockenhuber, C. (2021). Deciphering the evolution of the bleis marscha rock glacier (val d'err, eastern switzerland) with cosmogenic nuclide exposure dating, aerial image correlation, and finite element modeling. *The Cryosphere*, 15(4):2057–2081.

Arnold, J. R. and Libby, W. F. (1949). Age determinations by radiocarbon content: checks with samples of known age. *Science*, 110(2869):678–680.

Arnold, J. R. and Libby, W. F. (1951). Radiocarbon dates. *Science*, 113(2927):111–120.

Ballantyne, C. K. (2018). *Periglacial geomorphology*. John Wiley & Sons.

Bard, E. (1988). Correction of accelerator mass spectrometry 14c ages measured in planktonic foraminifera: Paleoceanographic implications. *Paleoceanography*, 3(6):635–645.

Bartels, M., Titschack, J., Fahl, K., Stein, R., and Hebbeln, D. (2018). Wahlenbergfjord, eastern svalbard: a glacier-surrounded fjord reflecting regional hydrographic variability during the holocene? *Boreas*, 47(4):1003–1021.

Benn, D. I. and Evans, D. J. (2014). *Glaciers & glaciation*. Routledge.

Berger, A. and Loutre, M.-F. (1991). Insolation values for the climate of the last 10 million years. *Quaternary Science Reviews*, 10(4):297–317.

Bergstrøm, B., Reite, A., Sveian, H., and Olsen, L. (2001). Feltrutiner, kartleggingsprinsipper og standarder for kvartærgeologisk kartlegging/løsmassekartlegging ved ngu. *Norges geologiske undersøkelse. Intern rapport 2001.018*.

Bianchi, G. G. and McCave, I. N. (1999). Holocene periodicity in north atlantic climate and deep-ocean flow south of iceland. *Nature*, 397(6719):515–517.

Blake Jr, W. (1989). Radiocarbon dating by accelerator mass spectrometry; a contribution to the chronology of holocene events in nordaustlandet, svalbard. *Geografiska Annaler: Series A, Physical Geography*, 71(1-2):59–74.

Bowman, S. (1990). *Radiocarbon dating*, volume 1. Univ of California Press.

Bradley, R. S. (1999). *Paleoclimatology: reconstructing climates of the Quaternary*. Elsevier.

Bradley, R. S. and Bakke, J. (2019). Is there evidence for a 4.2 ka bp event in the northern north atlantic region? *Climate of the Past*, 15(5):1665–1676.

Butzin, M., Köhler, P., and Lohmann, G. (2017). Marine radiocarbon reservoir age simulations for the past 50,000 years. *Geophysical Research Letters*, 44(16):8473–8480.

Chandler, B. M., Lovell, H., Boston, C. M., Lukas, S., Barr, I. D., Benediktsson, Í. Ö., Benn, D. I., Clark, C. D., Darvill, C. M., Evans, D. J., et al. (2018). Glacial geomorphological mapping: A review of approaches and frameworks for best practice. *Earth-Science Reviews*, 185:806–846.

Christiansen, H. H., Etzelmüller, B., Isaksen, K., Juliussen, H., Farbrot, H., Humlum, O., Johansson, M., Ingeman-Nielsen, T., Kristensen, L., Hjort, J., et al. (2010). The thermal state of permafrost in the nordic area during the international polar year 2007–2009. *Permafrost and Periglacial Processes*, 21(2):156–181.

Dallmann, W. K. (2015). *Geoscience atlas of Svalbard*. Norsk polarinstitutt.

Darvill, C. (2013). Cosmogenic nuclide analysis. In *Geomorphological techniques*, pages 1–25. British Society for Geomorphology.

de Kluijver, M., Ingalsuo, S., and de Bruyne, R. (2018). Mollusca of the north sea. marine species identification portal, 2018, accessed: 14.09.2022 `http://species-identification.org/index.php`.

de Vries, H. (1958). Variation in concentration of radiocarbon with time and location on earth. *Proc. Koninkl. Nederl. Akad. Wetenschappen, B*, 61:1–9.

Dzierzek, J., Nitychoruk, J., and Rzetkowska, A. (1990). Geological-geomorphological analysis and 14c dating of submoraine organogenic deposits within the renardbreen outer margin, wedel jarlsberg land, spitsbergen. *Polar Research*, 8(2):275–281.

Ebbesen, H., Hald, M., and Eplet, T. H. (2007). Lateglacial and early holocene climatic oscillations on the western svalbard margin, european arctic. *Quaternary Science Reviews*, 26(15-16):1999–2011.

Eckerstorfer, M., Christiansen, H., Rubensdotter, L., and Vogel, S. (2013). The geomorphological effect of cornice fall avalanches in the longyeardalen valley, svalbard. *The Cryosphere*, 7(5):1361–1374.

Eckerstorfer, M. and Christiansen, H. H. (2011). The "high arctic maritime snow climate" in central svalbard. *Arctic, Antarctic, and Alpine Research*, 43(1):11–21.

Eckerstorfer, M., Rubensdotter, L., Stalsberg, K., Christiansen, H., and Trøyen, P. (2015). Landforms and sediments in todalen and upper gangdalen and bødalen, svalbard. scale 1: 25 000.

Farnsworth, W. R., Allaart, L., Ingólfsson, Ó., Alexanderson, H., Forwick, M., Noormets, R., Retelle, M., and Schomacker, A. (2020). Holocene glacial history of svalbard: Status, perspectives and challenges. *Earth-Science Reviews*, 208:103249.

Farnsworth, W. R., Ingólfsson, Ó., Mannerfelt, E. S., Kalliokoski, M. H., Guðmundsdóttir, E. R., Retelle, M., Allaart, L., Brynjólfsson, S., Furze, M. F., Hancock, H. J., et al. (2022). Vedde ash constrains younger dryas glacier re-advance and rapid glacio-isostatic rebound on svalbard. *Quaternary Science Advances*, 5:100041.

Farnsworth, W. R., Ingólfsson, Ó., Noormets, R., Allaart, L., Alexanderson, H., Henriksen, M., and Schomacker, A. (2017). Dynamic holocene glacial history of st. jonsfjorden, svalbard. *Boreas*, 46(3):585–603.

Farnsworth, W. R., Ingólfsson, Ó., Retelle, M., Allaart, L., Håkansson, L. M., and Schomacker, A. (2018). Svalbard glaciers re-advanced during the pleistocene–holocene transition. *Boreas*, 47(4):1022–1032.

Farnsworth, W. R., Ingólfsson, Ó., Retelle, M., and Schomacker, A. (2016). Over 400 previously undocumented svalbard surge-type glaciers identified. *Geomorphology*, 264:52–60.

Fjeldskaar, W., Bondevik, S., and Amantov, A. (2018). Glaciers on svalbard survived the holocene thermal optimum. *Quaternary Science Reviews*, 199:18–29.

Flink, A. E., Hill, P., Noormets, R., and Kirchner, N. (2018). Holocene glacial evolution of mohnbukta in eastern spitsbergen. *Boreas*, 47(2):390–409.

Førland, E. J., Benestad, R., Hanssen-Bauer, I., Haugen, J. E., and Skaugen, T. E. (2011). Temperature and precipitation development at svalbard 1900–2100. *Advances in Meteorology*, 2011.

Forman, S., Lubinski, D., Ingólfsson, Ó., Zeeberg, J., Snyder, J., Siegert, M., and Matishov, G. (2004). A review of postglacial emergence on svalbard, franz josef land and novaya zemlya, northern eurasia. *Quaternary Science Reviews*, 23(11-13):1391–1434.

Forman, S., Lubinski, D., Miller, G., Matishov, G., Korsun, S., Snyder, J., Herlihy, F., Weihe, R., and Myslivets, V. (1996). Postglacial emergence of western franz josef land, russian, and retreat of the barents sea ice sheet. *Quaternary Science Reviews*, 15(1):77–90.

Forman, S. L. (1990). Post-glacial relative sea-level history of northwestern spitsbergen, svalbard. *Geological Society of America Bulletin*, 102(11):1580–1590.

Forwick, M. and Vorren, T. O. (2009). Late weichselian and holocene sedimentary environments and ice rafting in isfjorden, spitsbergen. *Palaeogeography, Palaeoclimatology, Palaeoecology*, 280(1-2):258–274.

Forwick, M. and Vorren, T. O. (2010). Stratigraphy and deglaciation of the isfjorden area, spitsbergen. *Norwegian Journal of Geology/Norsk Geologisk Forening*, 90(4).

Furrer, G., Stapfer, A., and Glaser, U. (1991). Zur nacheiszeitlichen gletschergeschichte des liefdefjords (spitzbergen)(ergebnisse der geowissenschaftlichen spitzbergenexpedition 1990). *Geographica helvetica*, 46(4):147–155.

Gjermundsen, E. F., Briner, J. P., Akçar, N., Salvigsen, O., Kubik, P., Gantert, N., and Hormes, A. (2013). Late weichselian local ice dome configuration and chronology in northwestern svalbard: early thinning, late retreat. *Quaternary Science Reviews*, 72:112–127.

Godwin, H. (1962). Half-life of radiocarbon. *Nature*, 195(4845):984–984.

Golledge, N. R., Hubbard, A., and Sugden, D. E. (2008). High-resolution numerical simulation of younger dryas glaciation in scotland. *Quaternary Science Reviews*, 27(9-10):888–904.

Hagen, J. O., Liestøl, O., Roland, E., and Jørgensen, T. (1993). *Glacier atlas of Svalbard and jan mayen*, volume 129. Norsk Polarinstitutt Oslo.

Hald, M., Ebbesen, H., Forwick, M., Godtliebsen, F., Khomenko, L., Korsun, S., Olsen, L. R., and Vorren, T. O. (2004). Holocene paleoceanography and glacial history of the west spitsbergen area, euro-arctic margin. *Quaternary Science Reviews*, 23(20-22):2075–2088.

Hald, M. and Korsun, S. (2008). The 8200 cal. yr bp event reflected in the arctic fjord, van mijenfjorden, svalbard. *The Holocene*, 18(6):981–990.

Hanssen-Bauer, I., Førland, E., Hisdal, H., Mayer, S., Sandø, A., and Sorteberg, A. (2019). Climate in svalbard 2100. *A knowledge base for climate adaptation*.

Heaton, T. J., Köhler, P., Butzin, M., Bard, E., Reimer, R. W., Austin, W. E., Ramsey, C. B., Grootes, P. M., Hughen, K. A., Kromer, B., et al. (2020). Marine20—the marine radiocarbon age calibration curve (0–55,000 cal bp). *Radiocarbon*, 62(4):779–820.

Hegerl, G., Zwiers, F., Braconnot, P., Gillett, N. P., Luo, Y. M., Orsini, J. M., Nicholls, N., Penner, J. E., and Stott, P. A. (2007). Understanding and attributing climate change.

Henriksen, M., Alexanderson, H., Landvik, J. Y., Linge, H., and Peterson, G. (2014). Dynamics and retreat of the late weichselian kongsfjorden ice stream, nw svalbard. *Quaternary Science Reviews*, 92:235–245.

Hippolyte, J.-C., Bourlès, D., Braucher, R., Carcaillet, J., Léanni, L., Arnold, M., and Aumaitre, G. (2009). Cosmogenic 10be dating of a sackung and its faulted rock glaciers, in the alps of savoy (france). *Geomorphology*, 108(3-4):312–320.

Holmgren, S. U., Bigler, C., Ingólfsson, O., and Wolfe, A. P. (2010). The holocene–anthropocene transition in lakes of western spitsbergen, svalbard (norwegian high arctic): climate change and nitrogen deposition. *Journal of Paleolimnology*, 43(2):393–412.

Hormes, A., Gjermundsen, E. F., and Rasmussen, T. L. (2013). From mountain top to the deep sea–deglaciation in 4d of the northwestern barents sea ice sheet. *Quaternary Science Reviews*, 75:78–99.

Hughes, A. L., Gyllencreutz, R., Lohne, Ø. S., Mangerud, J., and Svendsen, J. I. (2016). The last eurasian ice sheets–a chronological database and time-slice reconstruction, dated-1. *Boreas*, 45(1):1–45.

Humlum, O. (2002). Modelling late 20th-century precipitation in nordenskiold land, svalbard, by geomorphic means. *Norsk Geografisk Tidsskrift-Norwegian Journal of Geography*, 56(2):96–103.

Humlum, O. (2005). Holocene permafrost aggradation in svalbard. *Geological Society, London, Special Publications*, 242(1):119–129.

Humlum, O., Christiansen, H. H., and Juliussen, H. (2007). Avalanche-derived rock glaciers in svalbard. *Permafrost and Periglacial Processes*, 18(1):75–88.

Humlum, O., Instanes, A., and Sollid, J. L. (2003). Permafrost in svalbard: a review of research history, climatic background and engineering challenges. *Polar research*, 22(2):191–215.

Ingólfsson, Ó. (2011). Fingerprints of quaternary glaciations on svalbard. *Geological Society, London, Special Publications*, 354(1):15–31.

Ingólfsson, Ó. and Landvik, J. Y. (2013). The svalbard–barents sea ice-sheet–historical, current and future perspectives. *Quaternary Science Reviews*, 64:33–60.

Institute, N. P. (2014). Kartdata svalbard 1:250 000 (s250 kartdata).

IPCC (2013). *Climate Change 2013: The Physical Science Basis. Contribution of Working Group I to the Fifth Assessment Report of the Intergovernmental Panel on Climate Change*. Cambridge University Press, Cambridge, United Kingdom and New York, NY, USA.

Irvine-Fynn, T. D., Hodson, A. J., Moorman, B. J., Vatne, G., and Hubbard, A. L. (2011). Polythermal glacier hydrology: A review. *Reviews of Geophysics*, 49(4).

Jessen, S. P., Rasmussen, T. L., Nielsen, T., and Solheim, A. (2010). A new late weichselian and holocene marine chronology for the western svalbard slope 30,000–0 cal years bp. *Quaternary Science Reviews*, 29(9-10):1301–1312.

Jiskoot, H., Boyle, P., and Murray, T. (1998). The incidence of glacier surging in svalbard: evidence from multivariate statistics. *Computers & Geosciences*, 24(4):387–399.

Key, R. M., Kozyr, A., Sabine, C. L., Lee, K., Wanninkhof, R., Bullister, J. L., Feely, R. A., Millero, F. J., Mordy, C., and Peng, T.-H. (2004). A global ocean carbon climatology: Results from global data analysis project (glodap). *Global biogeochemical cycles*, 18(4).

Knies, J., Matthiessen, J., Vogt, C., Laberg, J. S., Hjelstuen, B. O., Smelror, M., Larsen, E., Andreassen, K., Eidvin, T., and Vorren, T. O. (2009). The plio-pleistocene glaciation of the barents sea–svalbard region: a new model based on revised chronostratigraphy. *Quaternary Science Reviews*, 28(9-10):812–829.

Knies, J., Matthießen, J., Vogt, C., and Stein, R. (2002). Evidence of 'mid-pliocene (3 ma) global warmth'in the eastern arctic ocean and implications for the svalbard/barents sea ice sheet during the late pliocene and early pleistocene (3–1.7 ma). *Boreas*, 31(1):82–93.

Konrad, S., Humphrey, N., Steig, E., Clark, D., Potter Jr, N., and Pfeffer, W. (1999). Rock glacier dynamics and paleoclimatic implications. *Geology*, 27(12):1131–1134.

Krylov, A. A., Andreeva, I. A., Vogt, C., Backman, J., Krupskaya, V. V., Grikurov, G. E., Moran, K., and Shoji, H. (2008). A shift in heavy and clay mineral provenance indicates a middle miocene onset of a perennial sea ice cover in the arctic ocean. *Paleoceanography*, 23(1).

Landvik, J. Y., Alexanderson, H., Henriksen, M., and Ingólfsson, Ó. (2014). Landscape imprints of changing glacial regimes during ice-sheet build-up and decay: a conceptual model from svalbard. *Quaternary Science Reviews*, 92:258–268.

Landvik, J. Y., Brook, E. J., Gualtieri, L., Linge, H., Raisbeck, G., Salvigsen, O., and Yiou, F. (2013). 10 b e exposure age constraints on the l ate w eichselian ice-sheet geometry and dynamics in inter-ice-stream areas, western s valbard. *Boreas*, 42(1):43–56.

Landvik, J. Y., Ingolfsson, O., Mienert, J., Lehman, S. J., Solheim, A., Elverhøi, A., and Ottesen, D. (2005). Rethinking late weichselian ice-sheet dynamics in coastal nw svalbard. *Boreas*, 34(1):7–24.

Larsen, E., Lysså, A., Rubensdotter, L., Farnsworth, W. R., Jensen, M., Nadeau, M. J., and Ottesen, D. (2018). Lateglacial and holocene glacier activity in the van mijenfjorden area, western svalbard. *arktos*, 4(1):1–21.

Lartaud, F., Emmanuel, L., De Rafélis, M., Pouvreau, S., and Renard, M. (2010). Influence of food supply on the δ13c signature of mollusc shells: implications for palaeoenvironmental reconstitutions. *Geo-Marine Letters*, 30(1):23–34.

Laskar, J., Correia, A., Gastineau, M., Joutel, F., Levrard, B., and Robutel, P. (2004). Long term evolution and chaotic diffusion of the insolation quantities of mars. *Icarus*, 170(2):343–364.

Lefauconnier, B. and Hagen, J. O. (1991). *Surging and calving glaciers in eastern Svalbard*. Norsk Polarinstitutt.

Libby, W. F. (1946). Atmospheric helium three and radiocarbon from cosmic radiation. *Physical Review*, 69(11-12):671.

Linick, T., Damon, P., Donahue, D., and Jull, A. T. (1989). Accelerator mass spectrometry: the new revolution in radiocarbon dating. *Quaternary International*, 1:1–6.

Lønne, I. (2005). Faint traces of high arctic glaciations: an early holocene ice-front fluctuation in bolterdalen, svalbard. *Boreas*, 34(3):308–323.

Lovell, H., Benn, D. I., Lukas, S., Ottesen, D., Luckman, A., Hardiman, M., Barr, I. D., Boston, C. M., and Sevestre, H. (2018). Multiple late holocene surges of a high-arctic tidewater glacier system in svalbard. *Quaternary Science Reviews*, 201:162–185.

Major, H., Haremo, P., Dallmann, W., and Andresen, A. (2000, webmap 2020). Geological map of svalbard 1: 100 000, sheet c9g adventdalen, temakart nr. 31, `https://geokart.npolar.no/geologi/GeoSvalbard/#11/78.0466/15.1691`. *Norsk Polarinstitutt, Tromsø, Norway*.

Major, H. and Nagy, J. (1972). Geology of the adventdalen map area: with a geological map, svalbard c9g 1:100 000. *Norsk Polarinstitutt Skrifter*, (138):1–62.

Mangerud, J., Bolstad, M., Elgersma, A., Helliksen, D., Landvik, J. Y., Lønne, I., Lycke, A. K., Salvigsen, O., Sandahl, T., and Svendsen, J. I. (1992). The last glacial maximum on spitsbergen, svalbard. *Quaternary Research*, 38(1):1–31.

Mangerud, J., Bondevik, S., Gulliksen, S., Hufthammer, A. K., and Høisæter, T. (2006). Marine 14c reservoir ages for 19th century whales and molluscs from the north atlantic. *Quaternary Science Reviews*, 25(23-24):3228–3245.

Mangerud, J. and Landvik, J. Y. (2007). Younger dryas cirque glaciers in western spitsbergen: smaller than during the little ice age. *Boreas*, 36(3):278–285.

Mangerud, J. and Svendsen, J. I. (2017). The svalbard climate transformed rapidly from younger dryas climate to warmer-than-present by 11.0 cal ka bp. In *EGU General Assembly Conference Abstracts*, page 2179.

Mangerud, J. and Svendsen, J. I. (2018). The holocene thermal maximum around svalbard, arctic north atlantic; molluscs show early and exceptional warmth. *The Holocene*, 28(1):65–83.

McCarthy, D. (2002). Lichenometry. In *Monitoring with Lichens—Monitoring Lichens*, pages 379–383. Springer.

MeteorologiskInstitutt (2020). Ny normal i klimaforskningen, date: 16.12.2020, last changed: 18.01.2021, accessed: 04.02.2022, `https://www.met.no/vaer-og-klima/ny-normal-i-klimaforskningen`,.

Müller, R. D. and Spielhagen, R. F. (1990). Evolution of the central tertiary basin of spitsbergen: towards a synthesis of sediment and plate tectonic history. *Palaeogeography, Palaeoclimatology, Palaeoecology*, 80(2):153–172.

Nesje, A., Dahl, S. O., and Bakke, J. (2004). Were abrupt lateglacial and early-holocene climatic changes in northwest europe linked to freshwater outbursts to the north atlantic and arctic oceans? *The Holocene*, 14(2):299–310.

Nesje, A., Jansen, E., Birks, H. J. B., Bjune, A. E., Bakke, J., Andersson, C., Dahl, S. O., Kristensen, D. K., Lauritzen, S., Lie, O., et al. (2005). Holocene climate variability in the northern north atlantic region: a review of terrestrial and marine evidence. *Geophysical Monograph-American Geophysical Union*, 158:289.

Nordli, Ø., Przybylak, R., Ogilvie, A. E., and Isaksen, K. (2014). Long-term temperature trends and variability on spitsbergen: the extended svalbard airport temperature series, 1898–2012. *Polar research*, 33(1):21349.

Nordli, Ø., Wyszyński, P., Gjelten, H., Isaksen, K., Łupikasza, E., Niedźwiedź, T., and Przybylak, R. (2020). Revisiting the extended svalbard airport monthly temperature series, and the compiled corresponding daily series 1898–2018.

NPI (1990). S100 topographic raster data for svalbard, norwegian polar institute (1990). retrieved from: `https://doi.org/10.21334/npolar.1990.44ca8c2a` on 07.09.2022.

NPI (2011). Orthophotos based on aerial photographs; np_ortofoto-svalbard_wmts-25833 layer: Gsd20_nordenskioeldlandvest_2011.tif (id: 3), norwegian polar institute (2011). retrieved from `https://geodata.npolar.no/arcgis/rest/services/Basisdata/NP_Ortofoto_Svalbard_WMTS_25833/MapServer/WMTS/1.0.0/WMTSCapabilities.xml` on 07.09.2022.

NPI (2014). Toposvalbard. np_basiskart_svalbard_wmts_25833, norwegian polar institute (2014). retrieved from: `https://geodata.npolar.no/arcgis/rest/services/Basisdata/NP_Basiskart_Svalbard_WMTS_25833/MapServer/WMTS/1.0.0/WMTSCapabilities.xml` on 07.09.2022.

NPI (2020). Satelite map, np_satellitt_svalbard_wmts_25833. satellite imagery mosaic of copernicus sentinel-data, prepared by norwegian polar institute (2020). retrieved from: `https://doi.org/10.21334/npolar.2014.a23acc28on04.02.2022`.

Nuth, C., Kohler, J., König, M., Von Deschwanden, A., Hagen, J., Kääb, A., Moholdt, G., and Pettersson, R. (2013). Decadal changes from a multi-temporal glacier inventory of svalbard. *The Cryosphere*, 7(5):1603–1621.

Oerlemans, J. (2005). Extracting a climate signal from 169 glacier records. *science*, 308(5722):675–677.

Osborn, G., McCarthy, D., LaBrie, A., and Burke, R. (2015). Lichenometric dating: science or pseudo-science? *Quaternary Research*, 83(1):1–12.

Ottesen, D., Dowdeswell, J. A., Landvik, J. Y., and Mienert, J. (2007). Dynamics of the late weichselian ice sheet on svalbard inferred from high-resolution sea-floor morphology. *Boreas*, 36(3):286–306.

Philipps, W., Briner, J., Gislefoss, L., Linge, H., Koffman, T., Fabel, D., Xu, S., and Hormes, A. (2017). Late holocene glacier activity at inner hornsund and scottbreen, southern svalbard. *Journal of Quaternary Science*, 32(4):501–515.

Pieńkowski, A. J., Husum, K., Furze, M. F., Missana, A. F., Irvalı, N., Divine, D. V., and Eilertsen, V. T. (2022). Revised δr values for the barents sea and its archipelagos as a pre-requisite for accurate and robust marine-based 14c chronologies. *Quaternary Geochronology*, 68:101244.

Popper, K. R. (1972). *Objective knowledge*, volume 360. Oxford University Press Oxford.

Porter, C., Morin, P., Howat, I., Noh, M., Bates, B., Peterman, K., Keesey, S., Schlenk, M., Gardiner, J., et al. (2018). Arctic dem, polar geospatial center. *Harvard Dataverse, V1*, 1.

Ramsey, C. B. (2009). Bayesian analysis of radiocarbon dates. *Radiocarbon*, 51(1):337–360.

Rasmussen, T. L., Forwick, M., and Mackensen, A. (2012). Reconstruction of inflow of atlantic water to isfjorden, svalbard during the holocene: Correlation to climate and seasonality. *Marine Micropaleontology*, 94:80–90.

Rasmussen, T. L. and Thomsen, E. (2014). Brine formation in relation to climate changes and ice retreat during the last 15,000 years in storfjorden, svalbard, 76–78 n. *Paleoceanography*, 29(10):911–929.

Reimer, P. J., Austin, W. E., Bard, E., Bayliss, A., Blackwell, P. G., Ramsey, C. B., Butzin, M., Cheng, H., Edwards, R. L., Friedrich, M., et al. (2020). The intcal20 northern hemisphere radiocarbon age calibration curve (0–55 cal kbp). *Radiocarbon*, 62(4):725–757.

Reimer, P. J., Bard, E., Bayliss, A., Beck, J. W., Blackwell, P. G., Ramsey, C. B., Buck, C. E., Cheng, H., Edwards, R. L., Friedrich, M., et al. (2013). Intcal13 and marine13 radiocarbon age calibration curves 0–50,000 years cal bp. *radiocarbon*, 55(4):1869–1887.

Reusche, M., Winsor, K., Carlson, A. E., Marcott, S. A., Rood, D. H., Novak, A., Roof, S., Retelle, M., Werner, A., Caffee, M., et al. (2014). 10be surface exposure ages on the late-pleistocene and holocene history of linnébreen on svalbard. *Quaternary Science Reviews*, 89:5–12.

RGIK (2022). Delaloye, r and echelard, t. ipa action group rock glacier inventories and kinematics: Towards standard guidelines for inventorying rock glaciers: Baseline concepts (version 4.2.2.

Rogers, J. C., Yang, L., and Li, L. (2005). The role of fram strait winter cyclones on sea ice flux and on spitsbergen air temperatures. *Geophysical Research Letters*, 32(6).

Rohling, E. J. and Pälike, H. (2005). Centennial-scale climate cooling with a sudden cold event around 8,200 years ago. *nature*, 434(7036):975–979.

Rosenwinkel, S., Korup, O., Landgraf, A., and Dzhumabaeva, A. (2015). Limits to lichenometry. *Quaternary Science Reviews*, 129:229–238.

Røthe, T. O., Bakke, J., Vasskog, K., Gjerde, M., D'Andrea, W. J., and Bradley, R. S. (2015). Arctic holocene glacier fluctuations reconstructed from lake sediments at mitrahalvøya, spitsbergen. *Quaternary Science Reviews*, 109:111–125.

Rubensdotter, L., Christiansen, H., Farnsworth, W., and Romundset, A. (2015). Landforms and sediments in bjørndalen-vestpynten, svalbard. quaternary geological map 1: 10 000.

Salvigsen, O. and Elgersma, A. (1993). Radiocarbon dating of deglaciation and raised beaches in north-western sorkapp land, spitsbergen, svalbard. *Zeszyty Naukowe Uniwersytetu Jagiellońskiego. Prace Geograficzne*, pages 39–48.

Salvigsen, O., Elgersma, A., Hjort, C., Lagerlund, E., Liestøl, O., and Svensson, N.-O. (1990). Glacial history and shoreline displacement on erdmannflya and bohemanflya, spitsbergen, svalbard. *Polar Research*, 8(2):261–273.

Salvigsen, O. and Osterholm, H. (1982). Radiocarbon dated raised beaches and glacial history of the northern coast of spitsbergen, svalbard. *Polar Research*, 1982(1):97–115.

Sambuelli, L. and Bava, S. (2012). Case study: A gpr survey on a morainic lake in northern italy for bathymetry, water volume and sediment characterization. *Journal of Applied Geophysics*, 81:48–56.

Sarnthein, M., Küssner, K., Grootes, P. M., Ausin, B., Eglinton, T., Muglia, J., Muscheler, R., and Schlolaut, G. (2020). Plateaus and jumps in the atmospheric radiocarbon record–potential origin and value as global age markers for glacial-to-deglacial paleoceanography, a synthesis. *Climate of the Past*, 16(6):2547–2571.

Schlitzer, R. (2015). Ocean data view.

Schomacker, A. and Kjær, K. H. (2008). Quantification of dead-ice melting in ice-cored moraines at the high-arctic glacier holmströmbreen, svalbard. *Boreas*, 37(2):211–225.

Seguinot, J., Ivy-Ochs, S., Jouvet, G., Huss, M., Funk, M., and Preusser, F. (2018). Modelling last glacial cycle ice dynamics in the alps. *The Cryosphere*, 12(10):3265–3285.

Sejrup, H. P., Hjelstuen, B. O., Dahlgren, K. T., Haflidason, H., Kuijpers, A., Nygård, A., Praeg, D., Stoker, M. S., and Vorren, T. O. (2005). Pleistocene glacial history of the nw european continental margin. *Marine and Petroleum Geology*, 22(9-10):1111–1129.

Senger, K., Betlem, P., Birchall, T., Horota, R. K., and Smyrak-Sikora, A. (2021). Svalbox: an interactive geoscientific portal for svalbard.

Ślubowska-Woldengen, M., Rasmussen, T. L., Koc, N., Klitgaard-Kristensen, D., Nilsen, F., and Solheim, A. (2007). Advection of atlantic water to the western and northern svalbard shelf since 17,500 cal yr bp. *Quaternary Science Reviews*, 26(3-4):463–478.

Smith, M., Rose, J., and Booth, S. (2006). Geomorphological mapping of glacial landforms from remotely sensed data: an evaluation of the principal data sources and an assessment of their quality. *Geomorphology*, 76(1-2):148–165.

Snyder, J., Werner, A., and Miller, G. (2000). Holocene cirque glacier activity in western spitsbergen, svalbard: sediment records from proglacial linnévatnet. *The Holocene*, 10(5):555–563.

Solheim, A., Andersen, E., Elverhøi, A., and Fiedler, A. (1996). Late cenozoic depositional history of the western svalbard continental shelf, controlled by subsidence and climate. *Global and Planetary Change*, 12(1-4):135–148.

Solheim, A., Faleide, J. I., Andersen, E. S., Elverhøi, A., Forsberg, C. F., Vanneste, K., Uenzelmann-Neben, G., and Channell, J. E. (1998). Late cenozoic seismic stratigraphy and glacial geological development of the east greenland and svalbard–barents sea continental margins. *Quaternary Science Reviews*, 17(1-3):155–184.

Sollid, J. L. and Sørbel, L. (1992). Rock glaciers in svalbard and norway. *Permafrost and Periglacial Processes*, 3(3):215–220.

Starr, C. (1993). Atmospheric co2 residence time and the carbon cycle. *Energy*, 18(12):1297–1310.

Stuiver, M., Pearson, G. W., and Braziunas, T. (1986). Radiocarbon age calibration of marine samples back to 9000 cal yr bp. *Radiocarbon*, 28(2B):980–1021.

Stuiver, M. and Reimer, P. J. (1993). Extended 14c data base and revised calib 3.0 14c age calibration program. *Radiocarbon*, 35(1):215–230.

Sund, M. (2006). A surge of skobreen, svalbard. *Polar Research*, 25(2):115–122.

Svendsen, J. I., Alexanderson, H., Astakhov, V. I., Demidov, I., Dowdeswell, J. A., Funder, S., Gataullin, V., Henriksen, M., Hjort, C., Houmark-Nielsen, M., et al. (2004). Late quaternary ice sheet history of northern eurasia. *Quaternary Science Reviews*, 23(11-13):1229–1271.

Svendsen, J. I. and Mangerud, J. (1997). Holocene glacial and climatic variations on spitsbergen, svalbard. *The Holocene*, 7(1):45–57.

Teshebaeva, K., Echtler, H., Bookhagen, B., and Strecker, M. (2019). Deep-seated gravitational slope deformation (dsgsd) and slow-moving landslides in the southern tien shan mountains: new insights from insar, tectonic and geomorphic analysis. *Earth surface processes and landforms*, 44(12):2333–2348.

Thrower, N. J. and Jensen, J. R. (1976). The orthophoto and orthophotomap: characteristics, development and application. *The American Cartographer*, 3(1):39–56.

Törnqvist, T. E., Rosenheim, B. E., Hu, P., and Fernandez, A. B. (2015). Radiocarbon dating and calibration. *Handbook of Sea-Level Research, edited by: Shennan, I., Long, AJ, and Horton, BP*, pages 349–360.

van der Bilt, W., Bakke, J., Vasskog, K., DAndrea, W., Bradley, R., and Olafsdottir, S. (2016). Holocene record of glacier variability from lake sediments reveals tripartite climate history for svalbard. pages EPSC2016–14340.

van der Bilt, W. G., Bakke, J., Vasskog, K., D'Andrea, W. J., Bradley, R. S., and Ólafsdóttir, S. (2015). Reconstruction of glacier variability from lake sediments reveals dynamic holocene climate in svalbard. *Quaternary Science Reviews*, 126:201–218.

Waelbroeck, C., Duplessy, J.-C., Michel, E., Labeyrie, L., Paillard, D., and Duprat, J. (2001). The timing of the last deglaciation in north atlantic climate records. *Nature*, 412(6848):724–727.

Wanner, H., Beer, J., Bütikofer, J., Crowley, T. J., Cubasch, U., Flückiger, J., Goosse, H., Grosjean, M., Joos, F., Kaplan, J. O., et al. (2008). Mid-to late holocene climate change: an overview. *Quaternary Science Reviews*, 27(19-20):1791–1828.

Werner, A. (1993). Holocene moraine chronology, spitsbergen, svalbard: lichenometric evidence for multiple neoglacial advances in the arctic. *The Holocene*, 3(2):128–137.

Wuite, J., Rott, H., Hetzenecker, M., Floricioiu, D., De Rydt, J., Gudmundsson, G., Nagler, T., and Kern, M. (2015). Evolution of surface velocities and ice discharge of larsen b outlet glaciers from 1995 to 2013. *The Cryosphere*, 9(3):957–969.

A | Field log

Table A.1: Fieldwork logbook

Date	Description of field day
22-07-2022	- Transport Longyearbyen - Colesbukta - Hike in all gear through Colesdalen to Camp 1 in two shifts, set-up camp - First exploration of moraine area on west side of river, found first shells
23-07-2022	- Acquire all drone imagery of Ortho_Camp1 - Sample two shells, map moraine area west of river
24-07-2022	- Pack-up camp, transport gear to Camp 2, set up camp - Map moraine area east side of river - Map valley between Camp 1 and Camp 2
25-07-2022	- Map moraine area around Camp 2 - Map area around Istjørna, Istjørndalen and Passfjellbreen forefield - Acquire all drone imagery Ortho_Camp2
26-07-2022	- Sample 3 boulders on moraine next to Camp 2 - Sample 3 boulders on rock glacier halfway up the valley
27-07-2022	- Pack up camp, hike back to location Camp 1, set up camp - Log shell section, sample three more shells
28-07-2022	- Carry first round of gear back to Colesbukta - Pass by mouth of Lailadalen to compare valley-mouth landforms
29-07-2022	- Pack up camp, carry gear back to Colesbukta - Pick up, transport Colesbukta - Longyearbyen

B | Sample inventory

Table B.1: Shell sample inventory

Sample ID	Sample type	Latitude	Longitude	Elevation
Synn-1-S1	Shell fragment	78.077342	15.099599	39
Synn-1-S2	2 Shells	78.077468	15.098083	35
Synn-1-S3	Shell fragment	78.077342	15.099599	40.5
Synn-1-S4	Shell fragment	78.077333	15.099426	39.5
Synn-1-S5	Shell fragment	78.077333	15.099426	40

Table B.2: Rock sample inventory

Sample ID	Sample location	Lithology	Latitude	Longitude	Elevation	Shielding
Synn-2-R1	Moraine rocksample	Siltstone	78.03314	15.12326	219	0.996780
Synn-2-R2	Moraine rocksample	Siltstone	78.03165	15.12445	257	0.995831
Synn-2-R3	Moraine rocksample	Siltstone	78.03188	15.12571	265	0.996560
Synn-2-R4	Rock glacier	Siltstone	78.05538	15.09834	121	-
Synn-2-R5	Rock glacier	Siltstone	78.05573	15.09843	123	-
Synn-2-R6a	Rock glacier	Siltstone	78.05590	15.09825	121	-
Synn-2-R6b	Rock glacier	Siltstone	78.05590	15.09825	121	-

Table B.3: Istjørna lacustrine core sample inventory. Core coordinates: N 78.026701°, E 15.118102°, 239 a.s.l.. Core retrieved by Joseph Buckby and Mark Furze in April 2021.

SampleID	Depth (cm)	Description	Weight (mg)
Ist-R-1-21-1	146	Organic material	549.6
Ist-R-1-21-2	155	Organic material	18.48
Ist-R-1-21-3	165	Organic material	2.72